

Electronic Skin: Recent Progress and Future Prospects for Skin-Attachable Devices for Health Monitoring, Robotics, and Prosthetics

Jun Chang Yang, Jaewan Mun, Se Young Kwon, Seongjun Park, Zhenan Bao,* and Steve Park*

Recent progress in electronic skin or e-skin research is broadly reviewed, focusing on technologies needed in three main applications: skin-attachable electronics, robotics, and prosthetics. First, since e-skin will be exposed to prolonged stresses of various kinds and needs to be conformally adhered to irregularly shaped surfaces, materials with intrinsic stretchability and self-healing properties are of great importance. Second, tactile sensing capability such as the detection of pressure, strain, slip, force vector, and temperature are important for health monitoring in skin attachable devices, and to enable object manipulation and detection of surrounding environment for robotics and prosthetics. For skin attachable devices, chemical and electrophysiological sensing and wireless signal communication are of high significance to fully gauge the state of health of users and to ensure user comfort. For robotics and prosthetics, large-area integration on 3D surfaces in a facile and scalable manner is critical. Furthermore, new signal processing strategies using neuromorphic devices are needed to efficiently process tactile information in a parallel and low power manner. For prosthetics, neural interfacing electrodes are of high importance. These topics are discussed, focusing on progress, current challenges, and future prospects.

1. Introduction

Skin is the largest organ in the human body and has a wide variety of interesting properties such as stretchability, self-healing ability, high mechanical toughness, and tactile sensing capability. Devices that mimic such properties of human skin along with additional features are commonly referred to as electronic skin or e-skin. The applications of e-skin vary widely, however, the key application areas are in the wearable or skin attachable devices, robotics, and prosthetics. This article will review the recent progress in the field of e-skin, focusing on the latest research results over the past 6 years since our last review paper,^[1] and on the necessary technologies to enable the aforementioned three applications. The topics to be discussed in this review will generally apply to all three applications, while the importance of the topics to each application will vary. This is a broad review covering a wide variety of topics. Our purpose is to introduce the key concepts and key papers for each topic. For

a more focused review, we guide the reader to review papers referenced in each of the topics. Figure 1 summarizes the on-going research in the three application areas. Table 1 lists the requirements and their relative importance in each of the three applications. Below, we briefly summarize the contents of this review with the motivation underlying the discussion of each topic.

When e-skin is attached to human skin or is functioning as skin in robotics or prosthetics, first, they need to be well adhered to moving surfaces. For instance, at the joints, the surface will undergo lateral tension, compression, and twisting. In order for the e-skin to be adhered to the body under such conditions, stretchability is of critical matter. Without stretchability, the e-skin is likely to be delaminated from the surface. Here we note that the conformal contact to a given surface is also dependent on geometrical factors of the device and the strength of the adhesive layers. Furthermore, for skin-attachable applications, since stretchable materials can stretch along with the surface of the skin, the user will experience higher comfort. In addition, stretchability is needed to provide the necessary mechanical degrees of freedom to prevent the breakage of e-skin during

J. C. Yang, S. Y. Kwon, Prof. Steve Park
 Department of Materials Science and Engineering
 Korea Advanced Institute of Science and Technology (KAIST)
 Daejeon 34141, Republic of Korea
 E-mail: stevepark@kaist.ac.kr

J. Mun, Prof. Z. Bao
 Department of Chemical Engineering
 Stanford University
 Stanford, CA 94305-5025, USA
 E-mail: zbao@stanford.edu

Prof. Seongjun Park
 Department of Bio and Brain Engineering
 Korea Advanced Institute of Science and Technology (KAIST)
 Daejeon 34141, Republic of Korea

Prof. Seongjun Park
 KAIST Institute for Health Science and Technology
 Korea Advanced Institute of Science and Technology (KAIST)
 Daejeon 34141, Republic of Korea

 The ORCID identification number(s) for the author(s) of this article can be found under <https://doi.org/10.1002/adma.201904765>.

DOI: 10.1002/adma.201904765

usage. When e-skin is attached to human skin or is replacing skin in prosthetics, the daily human motion will generate strain values up to 30%.^[2] Hence, without stretchability, the e-skin will likely undergo serious damage. In the case of robotics, stretchability of e-skin will enable the robot to take on a variety of shapes and enable high degrees of freedom in movement. Section 2.1 will discuss the recent progress in the fabrication of stretchable devices, and intrinsically stretchable materials and devices. Even with the necessary mechanical properties, since e-skin will be exposed to repeated and prolonged mechanical stresses. Hence, e-skin may experience wear and tear over time, which significantly limits its long-term durability. In this regard, self-healing ability is important. Section 2.2 will hence discuss self-healable materials and devices. Furthermore, since e-skin will interact closely with humans, biocompatibility is also critical. In Section 2.3, biocompatibility of e-skin materials will be discussed.

Tactile sensing is also necessary to enable skin-like functionality. Broadly speaking, tactile sensing refers to the detection of temperature and physical stimuli such as pressure, strain, shear, and slip. In skin attachable devices, these sensors can be used to detect human motion, and vital signs such as heart rate, respiration, and body temperature for health monitoring. For robotics and prosthetics, tactile sensors will enable critical functions such as object manipulation. Various types and current challenges of tactile sensors will be covered in Section 3. Other types of sensors such as chemical and electrophysiological sensors are particularly important for health monitoring in skin attachable devices. These sensors will be covered in Section 4.

The development of materials and the fabrication of individual sensors and devices must be accompanied by their large-area fabrication and integration. First, enabling spatial tactile sensing is important. Also, particularly for robotics and prosthetics, large-area fabrication of e-skin on 3D surfaces is critical. Sections 5.1 and 5.2 will discuss these aspects, focusing mainly on solution-based processing. For skin-attachable devices, wireless communication is of high importance to enable portability and user comfort. Section 5.3 will discuss the recent progress in wireless tactile signal communication. To enable human-like tactile sensing in robotics and prosthetics, signal coming from a large number of sensors needs to be processed. This becomes a serious challenge as the number of sensors increases, due to various issues such as complex wiring, high power consumption, and time delay of external read-out circuitry. In this regard, neuromorphic computing based on artificial synaptic devices offers a promising solution as it can potentially enable low power parallel signal processing, with added features such as learning-based noise elimination and classification. Section 5.4 will address the recent progress in tactile sensors integrated with artificial synaptic devices. For prosthetic applications, the tactile signal needs to be transmitted to neurons. Therefore, electrodes for neural interface are of high importance. Section 5.5 will discuss the recent progress in this area. Finally in Section 6, summary and future prospect of e-skin will be discussed.

2. Mimicking the Mechanical and Chemical Properties of Human Skin

Human skin has several unique properties that distinguish it from conventional electronics. For example, skin can



Zhenan Bao is a K.K. Lee Professor of Chemical Engineering at Stanford University. Prior to joining Stanford in 2004, she was a Distinguished Member of Technical Staff in Bell Labs, Lucent Technologies from 1995 to 2004. She received her Ph.D. in chemistry from the University of Chicago in 1995. She pioneered a

number of design concepts for organic electronic materials. Her work has enabled flexible electronic circuits and displays. Recently, she developed skin-inspired organic electronic materials, resulting in unprecedented performance in medical devices, energy storage, and environmental applications. Bao is a member of the National Academy of Engineering and the National Academy of Inventors.



Steve Park is a professor in the Materials Science and Engineering Department at Korea Advanced Institute of Science and Technology. He received his bachelor's degree at the University of Illinois at Urbana-Champaign in materials science and engineering, his Ph.D. at Stanford University in materials science and engineering, and conducted his postdoctoral research at Columbia University in the Electrical Engineering Department. Park focuses on the use of organic and carbon-based materials for electronic skin, biosensing, 3D printing, and thin-film crystallization for large-area printed electronics.

be stretched up to strain values of tens of percent without permanent deformation, which enables the free movement of the human body.^[3] In addition, skin is capable of repairing itself (autonomous self-healing), drastically increasing its durability and lifetime. The aforementioned properties of human skin should be mimicked in e-skin devices to properly apply them in skin attachable devices, prosthetics, and robotics. This section summarizes the recent advances in stretchable and self-healing materials and devices.

2.1. Stretchable Materials and Devices

As mentioned above, e-skin will be exposed to a variety of mechanical stresses, causing strains in various directions. It is hence imperative that the e-skin maintains their functionality under such strains. In this regard, research on stretchable



Figure 1. Overview of electronic skin (e-skin) component and technological requirements. Stretchable materials: Reproduced with permission.^[20] Copyright 2017, AAAS. Stretchable transistors: Reproduced with permission.^[99] Copyright 2018, Macmillan Publishing Ltd. Self-healing materials: Reproduced with permission.^[111] Copyright 2012, Macmillan Publishing Ltd. Tactile sensors (left): Reproduced with permission.^[209] Copyright 2018, American Chemical Society. Tactile sensors (right): Reproduced with permission.^[168] Copyright 2018, AAAS. Chemical sensors: Reproduced with permission.^[246] Copyright 2016, Macmillan Publishing Ltd. Electrophysiological sensors: Reproduced with permission.^[10] Copyright 2011, AAAS. Spatial tactile sensing: Reproduced with permission.^[295] Copyright 2017, Macmillan Publishing Ltd. Solution-based large-area fabrication: Schematic of 3D printing to generate e-skin on 3D surfaces. Wireless communication: Reproduced with permission.^[326] Copyright 2017, Macmillan Publishing Ltd. Neuromorphic devices for biological signal processing: Reproduced with permission.^[437] Copyright 2018, Wiley-VCH. Electrodes for neural interfaces: Reproduced with permission.^[437] Copyright 2018, Wiley-VCH.

electronic materials and devices has been intensively investigated, and huge improvements have been witnessed over the past few years. In this section, several strategies to achieve stretchability, materials with intrinsic stretchability, and stretchable e-skin devices will be reviewed.

2.1.1. Approaches to Stretchable Devices

Two approaches have been mainly studied to endow stretchability to e-skin devices. On the one hand, conventional brittle materials (such as Si) employed in conventional electronics can be geometrically engineered to withstand strain. On the other hand, intrinsically stretchable organic materials can be used to build e-skin devices.

Geometric Engineering: Brittle electronic materials can be geometrically designed and patterned to endow stretchability. First, certain geometries such as serpentine, kirigami, and horseshoe-shaped structures allow brittle conductors to

be stretched out, because these configurations effectively reduce the actual stress applied on the materials.^[4–6] For example, it was shown that serpentine-shaped copper interconnects embedded in polyimide exhibited stretchability up to 300%.^[6] Second, when devices are placed on “rigid islands,” which are embedded in relatively softer elastomeric substrate, the stress applied on the devices can be minimized. In this approach, devices are connected by either geometrically engineered or intrinsically stretchable interconnects. Because of the large difference in the modulus of the rigid islands and the substrate, stress is mostly applied on the interconnects, which prevents the active components from being mechanically damaged. This “rigid island” approach has been successfully used for both organic- and inorganic-based devices.^[7–10] For example, Lacour and co-workers fabricated stretchable organic thin-film transistors using soft and stiff elastomeric substrates.^[7] Rogers and co-workers utilized a rigid island structure to incorporate conventional electronic components for the fabrication of stretchable displays.^[8] However, strain

Table 1. Overview of key e-skin technologies and their relative importance to the three applications discussed in this review (H: High, M: Medium, L: Low).

| Key technology | | Skin-attachable devices | Robotics | Prosthetics |
|-------------------------------|---|-------------------------|----------|-------------|
| Material and transistor | Intrinsically stretchable materials | H | H | H |
| | Intrinsically stretchable transistors | M | H | H |
| | Self-healing materials | H | H | H |
| | Biocompatibility | H | M | H |
| Tactile sensor | Pressure sensor | H | H | H |
| | Strain sensor | H | H | H |
| | Temperature sensor | H | H | H |
| | Slip sensor (force vector) | L | H | H |
| | Multifunctional sensors | M | H | H |
| Sensors for health monitoring | Chemical sensor | H | L | M |
| | Electrophysiological sensor | H | L | M |
| Fabrication & integration | Spatial tactile sensing | L | H | H |
| | Solution-based large-area fabrication | M | H | H |
| | Wireless communication | H | M | M |
| | Neuromorphic devices for biological signal processing | L | H | H |
| | Electrodes for neural interfaces | L | L | H |

localization at the edges of the rigid islands (i.e., at the interface between rigid and soft material) may cause device failure. Lastly, depositing active components onto prestrained elastomers may lead to stretchability up to the prestrain level. Once prestrain is released, high-modulus active components are wrinkled in the out of plane direction. Then, the buckled structures can endure strain by changing the curvature of the buckles. In a pioneering study conducted by Rogers and co-workers, stretchable and foldable silicon integrated circuits were demonstrated by transferring the circuits on the prestretched elastomer.^[11] Although the use of these geometric engineering strategies may afford high-performance electronic devices, it may compromise device density and require additional photolithography processes (e.g., development and etching). For more detailed reviews, readers may consult the following recent review articles.^[12–15]

Intrinsic Stretchability: In contrast to geometrically engineered devices, some organic materials offer the benefits of low-cost solution processability and intrinsic stretchability through which high degree of durability, conformability can be achieved. Stretchable organic materials, however, exhibit relatively poor electrical performance compared to that of inorganic materials. Such limitation is currently being researched upon, and significant improvement in electrical performance has been achieved in recent years. In the following sections, some of the recent advances in the development of intrinsically stretchable organic materials and devices will be explored, with a focus on transistors.

2.1.2. Stretchable Insulators

Elastomeric polymers such as polydimethylsiloxane (PDMS), polyurethane (PU), and polystyrene-block-poly(ethylene-random-butylene)-block-polystyrene (SEBS) are widely used as stretchable dielectrics^[1,16–20] due to their commercial availability and

ease of processability. These elastomers exhibit low dielectric constants ($k < 3$), which require the corresponding devices to be operated at high voltages.^[1,21,22] Consequently, several approaches have been developed to realize high-k dielectrics, and thus allow operation at low voltages.

For instance, the incorporation of ceramic powders (e.g., TiO₂ and BaTiO₃) into polymer matrices^[23–25] allows one to combine the advantages of inorganic fillers (high dielectric constant) with those of the organic matrix (high breakdown strength and high stretchability),^[22] although such hybrid dielectrics may lose stretchability at high filler concentrations. Additionally, the introduction of conductive fillers such as carbon nanotubes (CNTs), conductive polymers, metal particles, and liquid metals^[26–30] increases the effective electrode area and facilitates polarization, which results in higher k values.^[1] However, at high concentrations of conductive fillers, the leakage current may become significantly high to adversely influence the device performance. Finally, elastomeric polymers engineered at a molecular level to have high polarizability (e.g., via the incorporation of polarizable moieties such as N, O, and F atoms) can also be used. For example, the dielectric constant of conventional PU was increased by the incorporation of highly polarizable poly(ethylene glycol) units through copolymerization.^[31]

In addition to elastomeric materials, ion gels have also been used to fabricate stretchable dielectrics.^[32–36] Unlike conventional polymeric materials, ion gels form an electric double layer (EDL) under bias^[37,38] and are therefore expected to be insensitive to thickness and strain, which makes them suitable for use in stretchable devices. Additionally, the high capacitance of ion gels allows for operation at low voltages.^[39] However, the introduction of ion gels into devices may result in disadvantages such as large frequency dependence, active layer doping, and operational hysteresis^[32,37,38,40,41] that should be overcome for the efficient application of ion gels.

Advances in the field of stretchable dielectric materials necessitate the development of suitable characterization techniques. Bao and co-workers showed that the capacitance of dielectrics forming an EDL can be easily underestimated and suggested a universal protocol for accurate capacitance measurement.^[37,38] Here, the authors demonstrated that although all examined samples exhibited consistent capacitance values at high frequencies, the presence of trace amounts of mobile ions in elastomers led to significant changes in capacitance at low frequencies (<10 Hz). Therefore, the capacitance of ionic species-containing elastomers may be easily underestimated when measured using regular LCR meters, which ultimately results in an overestimation of semiconductor mobilities. Therefore, EDL-forming dielectrics should instead be characterized using a resistor–capacitor circuit.

2.1.3. Stretchable Conductors

Stretchable conductors are most commonly realized by embedding conductive fillers into or placing them on elastomeric polymer substrates. Thin metal films,^[42–44] metal nanowires (NWs),^[45–49] CNTs,^[50–53] conductive polymers,^[54–57] and metal nanoparticles (NPs),^[58,59] which are often used as conductive fillers, should ideally maintain their percolation network under strain to retain their conductivity (**Table 2**). High-aspect-ratio

conductors such as NWs and CNTs are preferentially used because of their ability to form percolation junctions at relatively low concentrations.^[60] Although pristine conductive fillers are fractured at low strain, those supported by elastomers maintain a high level of conductivity under strain. In these composites, conductive fillers slide against each other instead of getting fractured, which preserves some of the percolation pathways. Resistance of these stretchable conductors under strain can be “programmed” by the first cycle of strain and release.^[52] In the subsequent cycles of strain, resistance change is reversible up to the first strain level. This reversibility arises from buckling of the conductive fillers, once the first strain is released. Some studies utilized systems with hybrid materials to further improve the conductivity of the electrodes under strain,^[45,61–64] e.g., when Ag NPs and NWs were used as conductive fillers (**Figure 2a**), NWs bridged NPs to maintain percolation paths under strain.^[63] It should be noted that the mechanical and electrical properties of the conductive composites strongly depend on the concentration of conductive fillers, i.e., high concentration of conductors may improve conductivity at the cost of compromised stretchability.

Poly(3,4-ethylenedioxythiophene):polystyrene sulfonate (PEDOT:PSS), engineered to exhibit intrinsic stretchability in the absence of elastomers, is widely used as a conductor because of its high conductivity.^[54,55,65] The stretchability of PEDOT:PSS can be significantly improved by the addition of nonvolatile plasticizers,^[65] which render this polymer

Table 2. Summary of stretchable conductors. Stretchability and performance values are given only if exact numbers are available.

| Materials | Stretchability | Performance without strain | Performance under strain ^{a)} | Refs. |
|--------------------------------------|----------------|----------------------------|--|-------------------------------|
| Ag NWs | 460% | 9–70 Ω sq ⁻¹ | – | Ko et al. ^[46] |
| Ag–Au NWs | 266% | 41 850 S cm ⁻¹ | – | Kim et al. ^[49] |
| Ag NPs | 140% | 5400 S cm ⁻¹ | 2200 S cm ⁻¹ (@100%) | Kim et al. ^[58] |
| Au NPs | 115% | 11 000 S cm ⁻¹ | 2400 S cm ⁻¹ (@110%) | Kotov et al. ^[59] |
| Ag flakes | 215% | 738 S cm ⁻¹ | 182 S cm ⁻¹ (@215%) | Someya et al. ^[75] |
| Ag flakes | 400% | >4000 S cm ⁻¹ | 935 S cm ⁻¹ (@400%) | Someya et al. ^[76] |
| Ag flakes | 450% | 0.06 Ω sq ⁻¹ | – | Someya et al. ^[78] |
| CNTs | 134% | 57 S cm ⁻¹ | 6 S cm ⁻¹ (@134%) | Someya et al. ^[50] |
| CNTs | 150% | 1100 S cm ⁻¹ | 2200 S cm ⁻¹ (@150%) | Bao et al. ^[52] |
| CNTs | 60% | 2000 S cm ⁻¹ | – | Xie et al. ^[53] |
| PEDOT:PSS | 800% | 3100 S cm ⁻¹ | 4100 S cm ⁻¹ (@100%) | Bao et al. ^[54] |
| PEDOT:PSS | 75% | 0.38 S cm ⁻¹ | – | Noh et al. ^[57] |
| PEDOT:PSS | 57% | 16 Ω sq ⁻¹ | – | Jeong et al. ^[65] |
| PEDOT:PSS | 180% | 1280 S cm ⁻¹ | – | Lee et al. ^[66] |
| PEDOT:PSS | – | 46 Ω sq ⁻¹ | – | Bao et al. ^[74] |
| Liquid metal (AuGa ₂ /Ga) | – | <1 Ω sq ⁻¹ | – | Lacour et al. ^[67] |
| Liquid metal (Galinstan) | – | 105 S cm ⁻¹ | – | Majidi et al. ^[69] |
| Ag NPs/CNTs/Ag flakes | 140% | 5710 S cm ⁻¹ | 20 S cm ⁻¹ (@140%) | Baik et al. ^[45] |
| Graphene/metal nanotrough | 80% | 1 Ω sq ⁻¹ | – | Park et al. ^[61] |
| Ag NWs/CNTs | 460% | 24–27 Ω sq ⁻¹ | – | Ko et al. ^[62] |
| Ag NPs/Ag NWs | 900% | 2450 S cm ⁻¹ | – | Lee et al. ^[63] |
| Graphenes/AgNWs | 100% | 33 Ω sq ⁻¹ | – | Park et al. ^[73] |

^{a)}Strain level is in parenthesis.

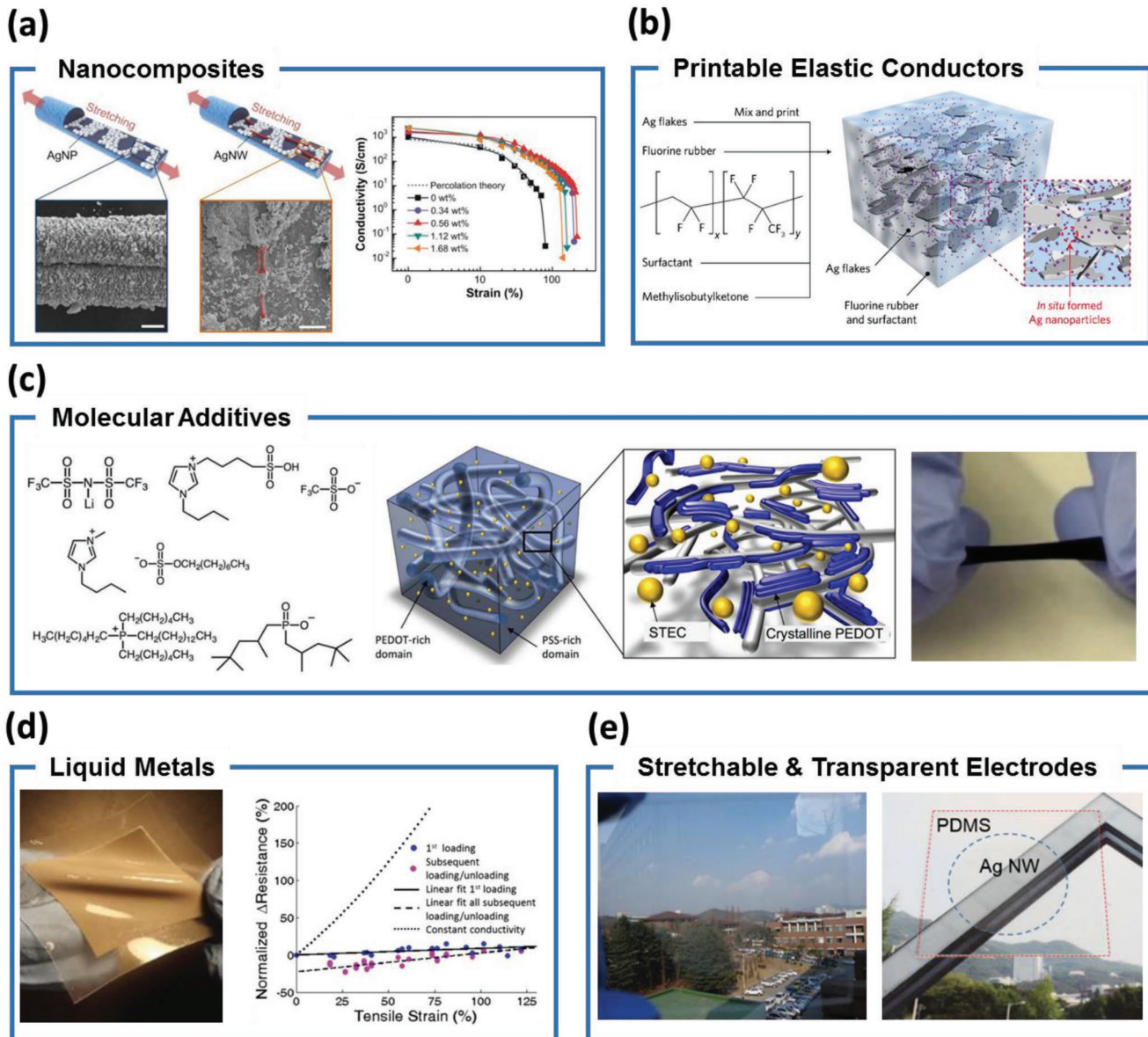


Figure 2. a) Stretchable conductors using silver nanoparticles and silver nanowires. Small fraction of silver nanowires connected silver nanoparticles to maintain conductive pathways under strain. Reproduced with permission.^[63] Copyright 2012, Wiley-VCH. b) Printable elastic conductors containing in situ formed silver nanoparticles. In situ formation of the nanoparticles led to high conductivity. Reproduced with permission.^[76] Copyright 2017, Macmillan Publishing Ltd. c) Ionic additives improved stretchability and conductivity of PEDOT:PSS. Reproduced with permission.^[54] Copyright 2017, AAAS. d) Galinstan embedded in an elastomeric matrix. This conductive composite showed stable resistance under strain. Reproduced with permission.^[69] Copyright 2015, Wiley-VCH. e) Stretchable and transparent electrodes using CNTs/Ag NWs nanocomposites (left) and Ag NWs (right). Reproduced with permission.^[62] Copyright 2014, Wiley-VCH. Reproduced with permission.^[48] Copyright 2015, Wiley-VCH.

viscoelastic and consequently improves its elongation at break. Also, ionic additives^[54,66] (Figure 2c) soften PSS domains while increasing the crystallinity of PEDOT domains, allowing one to realize exceptionally high conductivities of up to 4100 S cm^{-1} at 100% strain.^[54]

Finally, liquid metals such as the eutectic gallium–indium alloy (EGaIn) are conductors with an intrinsic stretchability, high conductivity, and very small piezoresistivity; therefore, they can be used as stretchable electrodes and interconnects in stretchable electronics.^[17] However, the presence of liquid

components limits the reliability of stretchable devices. In this regard, embedding liquid metals into elastomers is a good alternative (Figure 2d), although patterning liquid metal still remains challenging because of the high surface tension and the spontaneous oxide formation on the surface of the material. Microfluidics can be used to pattern liquid metal; however, it offers limited resolution over large surfaces.^[67] Several techniques have been developed to address these challenges, allowing the use of liquid metals in stretchable devices.^[67–72]

Some applications such as stretchable displays and photovoltaics require the use of highly transparent stretchable electrodes, which can be realized by employing Ag NWs,^[48,62,73] graphene,^[64,73] CNTs,^[51–53,62] and PEDOT:PSS (Figure 2e).^[54,74] The major challenge of realizing such conductors is the inevitable trade-off between conductivity and transparency, the extent of which depends on conductive filler concentration. Therefore, the optimization of these two parameters is a task of high practical significance. The performance of transparent electrodes can be quantified in terms of σ_{dc}/σ_{op} , where σ_{dc} and σ_{op} are dc and optical conductivities, respectively,^[74] with higher σ_{dc}/σ_{op} values indicating higher conductivity at a given transparency.

Printable stretchable conductors are particularly advantageous for the production of large-area electronics, where these conductors can be used as durable interconnects and electrodes. However, as mentioned above, simultaneous realization of high stretchability and high conductivity remains challenging. Among the materials investigated for the fabrication of highly stretchable and conductive inks,^[45,50,54,65,75–77] elastic conductors comprising Ag flakes blended with an elastomeric fluorine-containing polymer, a fluorine-containing surfactant, and an organic solvent demonstrated extraordinarily high conductivity and stretchability (Figure 2b).^[45,75–78] The in situ formation of Ag NPs from Ag flakes was shown to improve conductivity, while the use of an elastomeric polymer enhanced stretchability,^[76] and thus the obtained elastic conductors demonstrated only a small conductivity decrease (from 6168 to 935 S cm⁻¹) at 400% strain.

2.1.4. Stretchable Semiconductors

Polymeric semiconductors are typically used as active layers in e-skin because of their softness. The greatest challenge of developing stretchable polymer semiconductors is the trade-off between electrical mobility and stretchability. Semiconducting polymer films form semicrystalline structures with both amorphous and crystalline domains. The amorphous domains can dissipate applied stress, which makes them desirable for high stretchability, while the crystalline domains are preferred for efficient charge transport. Therefore, to achieve high-performance stretchable semiconductors, the above trade-off should be avoided.

Early studies of stretchable semiconductors were performed with polythiophene derivatives. O'Connor et al. systematically studied the mechanical and electrical properties of polythiophenes,^[79] comparing the properties of poly(3-hexylthiophene) (P3HT) with those of poly(2,5-bis(3-alkylthiophene-2-yl)thieno[3,2-b]thiophene) (PBTTT) and revealing that PBTTT films had higher crystallinity than P3HT. As a result, the P3HT films showed lower modulus, higher crack onset strain, but poorer mobility. Considering the significantly high crack onset strain of 150% achieved for P3HT films, the same authors tested P3HT as a stretchable active layer for organic field-effect transistors (OFETs).^[80,81] Under uniaxial strain, mobilities above 0.01 cm² V⁻¹ s⁻¹ under 100% strain were observed in directions parallel and perpendicular to the strain. Mobility parallel to the strain direction was one order

of magnitude higher than that of the perpendicular direction because of the chain alignment effect, which could be mitigated by biaxial stretching of polymer films. Kim et al. investigated how the regioregularity of P3HT affects its mechanical properties,^[82] demonstrating that the degree of crystallinity linearly increased with increasing regioregularity and that P3HT films with a higher degree of crystallinity exhibited higher mobility, larger modulus, and lower elongation at break.

As mentioned above, pristine P3HT seems to suffer from the same trade-off between electrical and mechanical properties, which has inspired the chemical or physical bonding of rubbery components to preserve the intrinsic stretchability of P3HT without compromising mobility. In a pioneering work, Stigelin-Stutzmann and co-workers synthesized diblock copolymers containing P3HT and polyethylene (PE) as the building blocks (Figure 3a).^[83] At a 90 wt% loading of insulating PE blocks, fracture strains as high as 600% were achieved without any mobility decrease. In another work on triblock copolymer structures, the use of a high (65 wt%) rubbery block loading did not result in any mobility degradation and allowed one to realize an elongation at break of 140%.^[84] Moreover, P3HT nanofibers were also physically embedded in an elastomeric matrix.^[85,86] In these studies, the semiconducting fibers gained high stretchability because of the copresence of supporting elastomers and active layers containing elastomeric components.

Although P3HT-based active layers can exhibit high stretchability, the research focus has now shifted from polythiophene derivatives to donor–acceptor-type polymer semiconductors, mainly because of their relatively high mobilities (above 5 cm² V⁻¹ s⁻¹),^[87–89] and the fact that some donor–acceptor semiconductors with seemingly amorphous microstructures demonstrate relatively high mobility.^[90,91] Therefore, the use of near-amorphous microstructures of donor–acceptor polymer semiconductors can help to achieve a high degree of stretchability while maintaining high mobility. For example, the backbone twist-induced low crystallinity of an indacenodithiophene-based donor–acceptor semiconductor results in a crack onset strain greater than 100% with mobility of 0.06 cm² V⁻¹ s⁻¹.^[92]

To further increase the stretchability of donor–acceptor semiconductors, additional engineering strategies have been implemented. For example, semiconducting polymers have been rendered highly stretchable via several strategies such as side-chain engineering,^[93] the use of soft crosslinkers,^[94] conjugation-break spacers,^[19,95] dynamic bonding,^[18] and nanoconfinement.^[20] These chemical and physical engineering strategies allow one to realize a high degree of stretchability without significantly compromising mobility. For instance, investigations of side-chain branching effect on the mechanical properties of conjugated polymers^[93] showed that branched side chains are preferred for lowering elastic modulus and improving crack onset strain, since they can increase the content of amorphous domains. Moreover, crack onset strain exceeding 100% strain was reported for diketopyrrolopyrrole-based (DPP-based) polymer semiconductors crosslinked with a soft poly(dimethylsiloxane) oligomer through semiconductor side chains (Figure 3b).^[94] Despite being cross-linked, the semiconducting films exhibited lower moduli than their non-crosslinked counterparts because of cross-linker softness. Furthermore, these cross-linked samples maintained elastic behavior under strain.

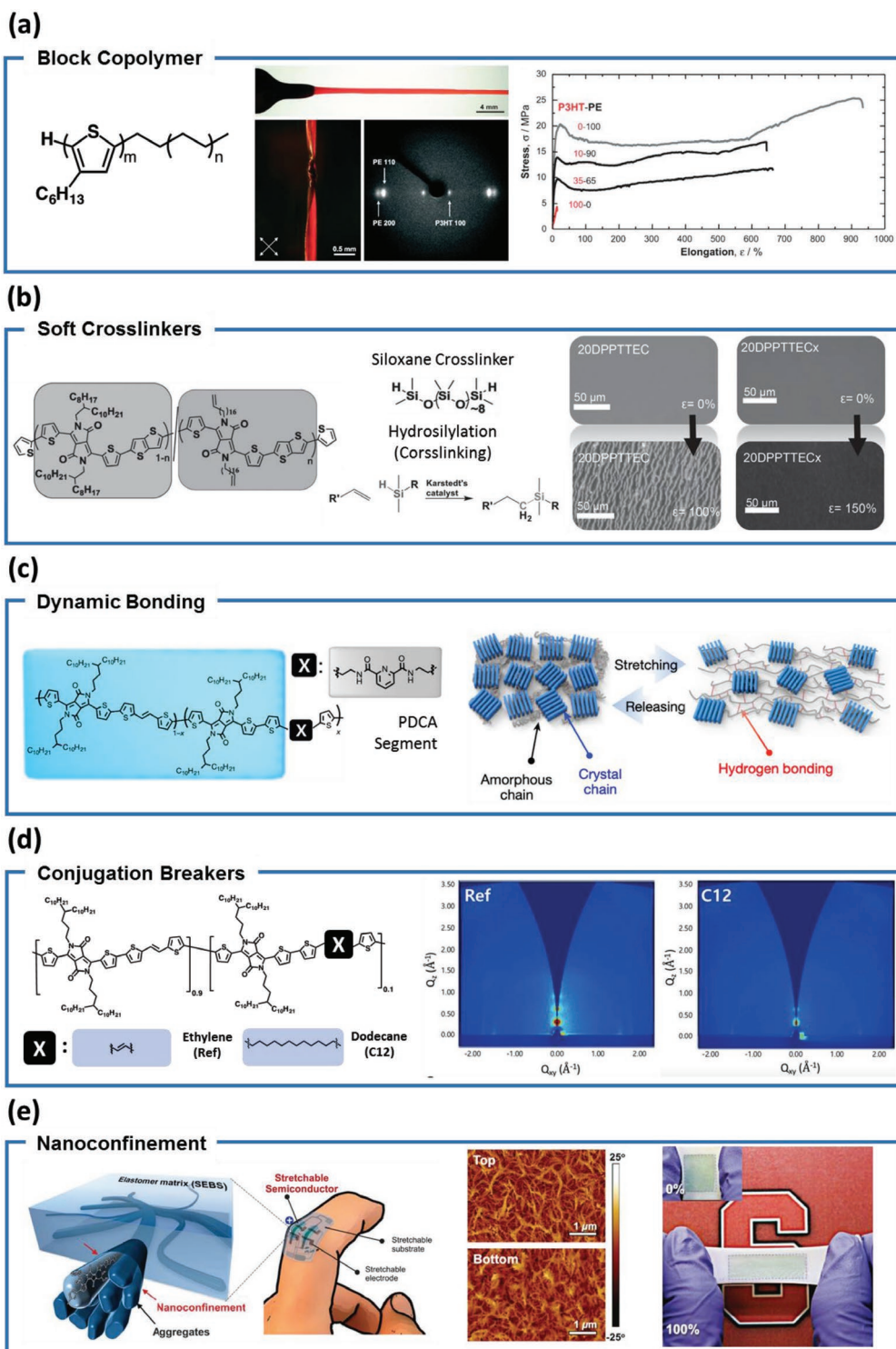


Figure 3. a) Stretchable semiconducting diblock copolymers containing P3HT and PE as building blocks. The semiconductors showed high elongation at break. Reproduced with permission.^[83] Copyright 2007 Wiley-VCH. b) DPP-based stretchable semiconductors using soft crosslinkers. Crosslinked semiconductors showed high crack onset strain of 150%, while the reference sample showed severe crack formation at lower strain. Reproduced with permission.^[94] Copyright 2016, Wiley-VCH. c) Stretchable semiconductors capable of energy dissipation. Rupturing of hydrogen bonds dissipated applied stress, which prohibited crack formation. Reproduced with permission.^[18] Copyright 2016, Macmillan Publishing Ltd. d) Conjugation breakers for stretchable semiconductors. 10 mol% incorporation of dodecyl spacers significantly reduced crystallinity, and improved stretchability. Reproduced with permission.^[19] Copyright 2018, Wiley-VCH. e) Nanoconfined semiconductors in an elastomer matrix. Nanoconfinement tuned dynamics of polymer chains and improved stretchability. Reproduced with permission.^[20] Copyright 2017, AAAS.

Recently, DPP-based semiconducting polymers with conjugation breakers were tested for applications such as stretchable transistors. Early studies on conjugation-break spacers presented strategies of effectively improving the stretchability of conjugated polymers; however, this improvement was associated with a large compromise in mobility.^[95,96] Significant advancement in this area was achieved by the introduction of 2,6-pyridine dicarboxamide (PDCA) moieties as nonconjugated spacers (Figure 3c)^[18] capable of forming hydrogen bonds (dynamic bond) to realize energy dissipation upon stretching. This energy dissipation effect allows DPP-based semiconductors to be stretchable up to 100% strain while exhibiting a modulus one order of magnitude lower than that of their fully conjugated counterparts. Moreover, the incorporation of dodecyl spacers (10 mol%) was shown to increase crack onset strain from 25% to 100% without any significant compromise in mobility (Figure 3d).^[19] Such high degree of stretchability was ascribed to the formation of highly amorphous microstructures induced by dodecyl spacers.

Finally, the chain dynamics and properties of conjugated polymers have been modified using the nanoconfinement approach (Figure 3e),^[20] e.g., polymer chains became more dynamic under nanoconfinement conditions, as confirmed by the decrease of glass transition temperature. Nanoconfined semiconductors were shown to exhibit crack onset strains above 100% and maintained mobilities above $1 \text{ cm}^2 \text{ V}^{-1} \text{ s}^{-1}$ under 100% strain. More importantly, the mobilities of the nanoconfined stretchable semiconducting films were further improved up to $5 \text{ cm}^2 \text{ V}^{-1} \text{ s}^{-1}$ through solution shearing.^[97]

2.1.5. Intrinsically Stretchable Transistors

Intrinsically Stretchable Transistors: Electronic devices require transistors as key elements for their functioning; therefore, stretchable transistors are essential for the realization of electronic skin.^[18,19] Conventional rigid transistors can become stretchable using rigid island structures, but they may require additional fabrication processes. In this regard, intrinsically stretchable counterparts are preferable for e-skin applications. Since all components of an intrinsically stretchable transistor must be stretchable, and all components must be adhered to each other under strain, such transistors have not been extensively explored. This section summarizes the materials used to fabricate intrinsically stretchable transistors and their performance.

Intrinsically stretchable transistors have been fabricated using P3HT as the semiconductor.^[17] In particular, the presence of microcracked P3HT embedded between two PU layers enabled transistors to function even at 265% strain in the direction perpendicular to the strain. However, the mobilities of pristine and stretched films were on the order of $10^{-2} \text{ cm}^2 \text{ V}^{-1} \text{ s}^{-1}$ because of the limited performance of P3HT. The use of CNTs as both an active layer and electrodes allowed the fabrication of mechanically durable and fully stretchable transistors^[98] that exhibited an initial mobility of $0.18 \text{ cm}^2 \text{ V}^{-1} \text{ s}^{-1}$, and maintained 50% of the initial on-current under 100% strain. Intrinsically stretchable transistors containing donor–acceptor semiconductors with broken conjugation^[18,19] were demonstrated to feature relatively

high initial mobilities of $\approx 0.5 \text{ cm}^2 \text{ V}^{-1} \text{ s}^{-1}$ and maintained moderate mobilities of $\approx 0.1 \text{ cm}^2 \text{ V}^{-1} \text{ s}^{-1}$ under 100% strain. Some of the best performing stretchable transistors were fabricated using nanoconfined semiconductors^[20] and exhibited high initial mobilities of $\approx 0.5 \text{ cm}^2 \text{ V}^{-1} \text{ s}^{-1}$. Under 100% strain, no mobility decrease was observed in the strained direction, while mobilities above $0.1 \text{ cm}^2 \text{ V}^{-1} \text{ s}^{-1}$ were still maintained in the strain-perpendicular direction. More importantly, these transistors experienced only a small mobility decrease after 1000 cycles of 100% strain because of the appropriate encapsulation and mechanical robustness of nanoconfined semiconductors. These mobility values were further improved when the nanoconfined semiconductors were aligned through solution-shearing.^[97] Specifically, initial mobilities as high as $1.0 \text{ cm}^2 \text{ V}^{-1} \text{ s}^{-1}$ were obtained, which decreased to $0.8 \text{ cm}^2 \text{ V}^{-1} \text{ s}^{-1}$ in the strain direction under 100% strain. In the strain-perpendicular direction, mobilities greater than $0.3 \text{ cm}^2 \text{ V}^{-1} \text{ s}^{-1}$ were maintained under 100% strain.

Finally, several studies employed ion gels as dielectrics in fully stretchable transistors,^[34–36] and EDL formation helped these transistors to operate at low voltages and resulted in exceptionally high mobilities ($\approx 10 \text{ cm}^2 \text{ V}^{-1} \text{ s}^{-1}$) even under strain. However, as mentioned above, it is difficult to compare the mobilities of polymer dielectric- and ion gel-based transistors because of the differences in their working mechanisms.

Scalable Fabrication of Stretchable Active-Matrix Transistor Arrays: Despite the significant progress made in the design of stretchable electronic materials and the fabrication of intrinsically stretchable transistors, the mass production of these devices and their integration into an active-matrix array is still a challenge,^[99] mainly because intrinsically stretchable transistors are generally produced by transfer printing, an unreliable technique that can potentially generate interfacial issues. This problem can be mitigated by the use of standard lithographic fabrication methods, which, however, are generally unsuitable for organic electronics because of the susceptibility of these devices to damage by organic solvents and ultraviolet radiation. Therefore, the development of new scalable fabrication schemes for the production of intrinsically stretchable transistors is urgently required.

Recently, Bao and co-workers reported a universal fabrication platform for intrinsically stretchable transistors (Figure 4a)^[99] that includes patterning of dielectric and semiconducting layers by azide cross-linking and protective copper coating, respectively. The thus produced intrinsically stretchable transistor arrays exhibited small sample-to-sample variations and stable mobilities under strain (Figure 4b,c). More importantly, the above study demonstrated the suitability of this approach to the production of complex stretchable electronic devices and circuits such as an active-matrix transistor array, an inverter with pseudo-CMOS design, a tactile sensor, a NAND gate, and an amplifier (Figure 4d).

2.1.6. Challenges and Outlook

The field of stretchable organic electronics has witnessed significant progress in both materials and devices. However, several challenges should still be overcome to achieve stretchable and high-performance devices. As described above, novel

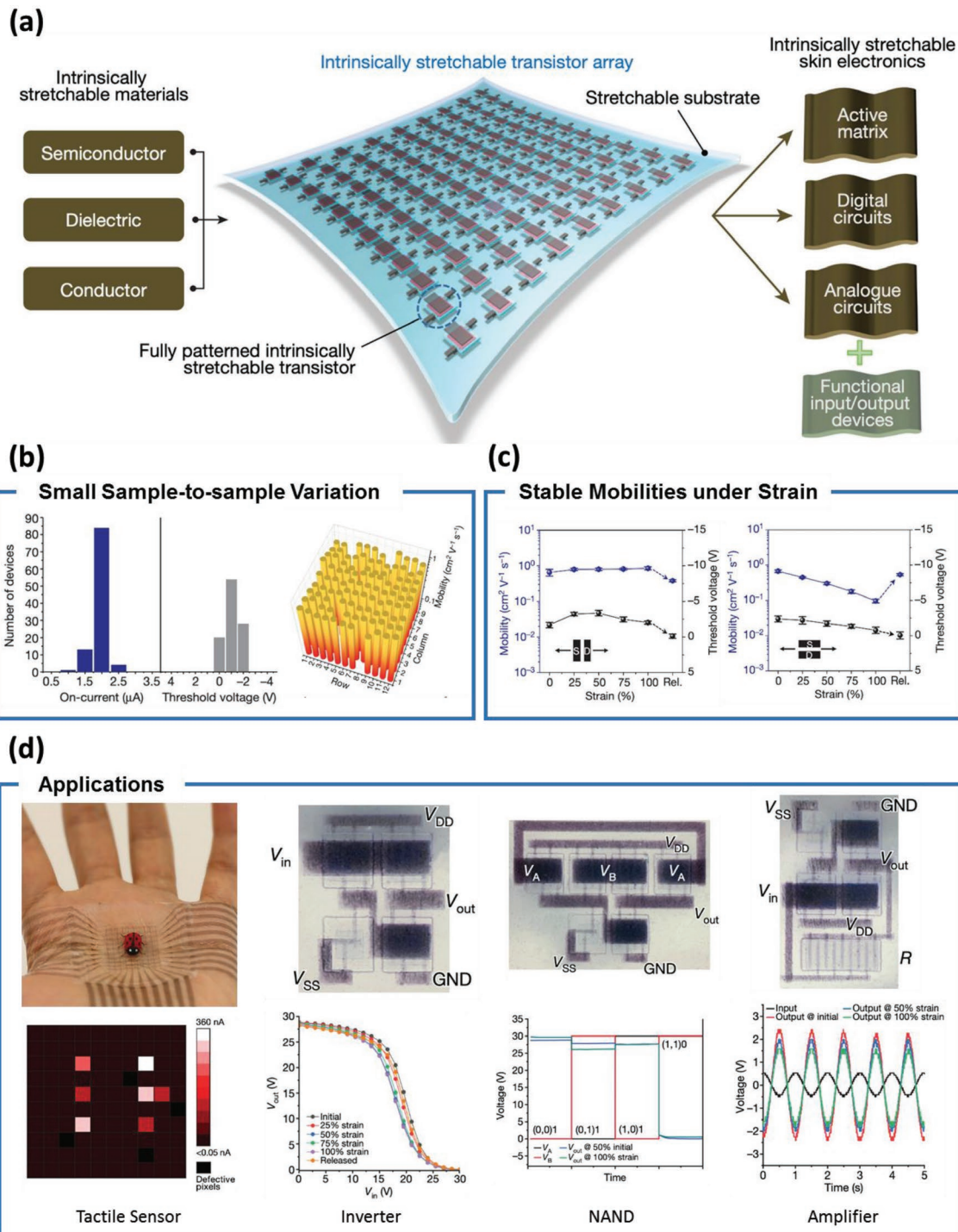


Figure 4. a) An intrinsically stretchable transistor array for skin-electronics. b) The transistor array showed small sample-to-sample variation. c) Mobilities of the intrinsically stretchable transistor array under strain. d) Scalable fabrication of an intrinsically stretchable transistor array enabled various applications. Reproduced with permission.^[99] Copyright 2018, Macmillan Publishing Ltd.

strategies have been developed for the scalable fabrication of stretchable devices, although further investigations of reliable fabrication processes are needed to utilize stretchable materials in micro- and nanoelectronics. In addition, stretchable devices need to be integrated into a single platform, and

communication between stretchable and external devices should be investigated. For example, currently employed stretchable devices need wiring for data acquisition, which highlights the need to develop stretchable devices with wireless communication. Wireless communication is especially important in that it

may significantly improve e-skin users' convenience. Although stretchable conductors, dielectrics, and semiconductors were studied separately, their interfaces in a single device have not been fully considered yet. Since interface issues such as contact resistance, delamination, and defects may strongly affect device performance, especially under strain, they should be further studied to improve the robustness of fully stretchable devices. To date, stretchable organic semiconductors exclusively utilize p-type semiconductors, as n-type semiconductors often exhibit poor performance and environmental stability. Thus, the development of stable and stretchable n-type semiconductors may expand the application scope of stretchable organic electronics.

2.2. Self-Healing Materials

The long-term use of e-skin devices may result in unexpected mechanical damage over time. Self-healing ability endows e-skin with advantages such as long-term robustness and reliability.^[100] Ideally, for practical applications, self-healing should occur at room temperature without any external stimuli; such behavior is called "autonomous self-healing."^[101,102] This section summarizes the design principles of self-healing materials and their applications to soft electronics. For a more focused review, please refer to the following review articles.^[100,103–107]

2.2.1. Mechanisms of Self-Healing

Self-healing polymers can be categorized into two groups based on the healing mechanism. Materials of the first group contain self-healing agents inside microcapsules.^[108] Upon mechanical damage, these agents are released, and polymerization at the damaged regions restores initial material properties. However, this self-healing mechanism is unsuitable for e-skin applications, since such self-healing is limited to single or few occurrences of mechanical damage.^[100,109] The second method, which is more preferable for e-skin applications, relies on the use of dynamic bonds and realizes self-healing in a two-step process. Once polymeric samples are mechanically damaged, polymer chains diffuse into the damaged area (mobile chains with low glass transition temperature facilitates diffusion), and the reformation of dynamic bonds restores the original polymer properties. Such dynamic bonds include hydrogen bonds,^[18,110–119] metal-ligand coordination bonds,^[117,120,121] ionic interactions,^[122,123] disulfide bonds,^[124] and π - π interactions.^[101,102] In subsequent sections, we mainly discuss self-healing based on dynamic bond formation.

2.2.2. Self-Healable Insulators

The current research in self-healing materials is mainly centered on the development of stretchable and self-healing polymeric materials that can potentially be used as dielectrics in electronics. For self-healing materials, the recovery of mechanical properties is most commonly discussed in terms of "healing efficiency." Several property values such as fracture

strain and fracture energy can be used to calculate healing efficiency, which is defined as follows^[103]

$$\text{Healing efficiency} = \frac{\text{Property value (healed)}}{\text{Property value (pristine)}} \times 100\% \quad (1)$$

Healing efficiencies of different materials should be compared with caution, since this parameter excludes the influences of time span and external stimuli such as temperature and solvent exposure.

Self-healing polymers based on noncovalent dynamic bond formation may exhibit autonomous healing, high healing efficiency, and toughness. Bao et al. investigated self-healing polymers containing hierarchical hydrogen bonds (Figure 5a),^[116,118] demonstrating that these materials feature high healing efficiency at room temperature. In addition, energy dissipation through reversible hydrogen bond formation/rupture allows such materials to exhibit high strain at fracture, high fracture energy, and notch-insensitive stretching behavior (Figure 5b–d).^[116] The notch-insensitiveness is especially interesting because it enables devices to function even when mechanically damaged.

Several studies have tested several self-healing polymers as dielectrics.^[114,116,119–121] For example, PDMS-based polymers with metal-ligand coordination have been used in fully stretchable organic field-effect transistors (Figure 5e,f) that did not suffer from gate leakage current or large hysteresis (Figure 5g).^[120] Furthermore, high dielectric constants were achieved because of the high polarizability of metals and ligands.

2.2.3. Self-Healable Conductors

Bielawski et al. prepared intrinsically conductive and self-healing conductors using N-heterocyclic carbenes and transition metals.^[125] These polymer networks were severed by a razor blade, and mechanical damage was healed by heating at 150 °C in the presence of dimethyl sulfoxide (DMSO) vapor. However, these materials could not be used in practice because of major limitations such as low conductivity and nonautonomous self-healing.

Another (more common) approach relies on the use of composite systems. In this approach, conductive fillers are incorporated into a self-healing polymer matrix, which has advantages such as relatively high conductivity and ease of fabrication. Several organic and inorganic materials such as metal particles,^[111,117] CNTs,^[112,115,126,127] Ag NWs,^[109,115,128,129] and liquid metals^[116,130,131] have been used as conductive fillers. Interestingly, although the above conductive fillers are not self-healable, the mechanical and electrical properties of the corresponding composites were recovered after mechanical damage. Bao and co-workers developed a self-healing conductive composite using nanostructured nickel microparticles in a polymer matrix capable of forming hydrogen bonds (Figure 6a),^[111] revealing that nanostructuring results in homogeneity and high conductivity of the composite. Specifically, the above composite featured a conductivity of 40 S cm⁻¹, which was several orders of magnitude higher than that of the nonnanostructured sample. The composite regained its initial conductivity even after bifurcation followed by reconnection (Figure 6b). A recent systematic investigation

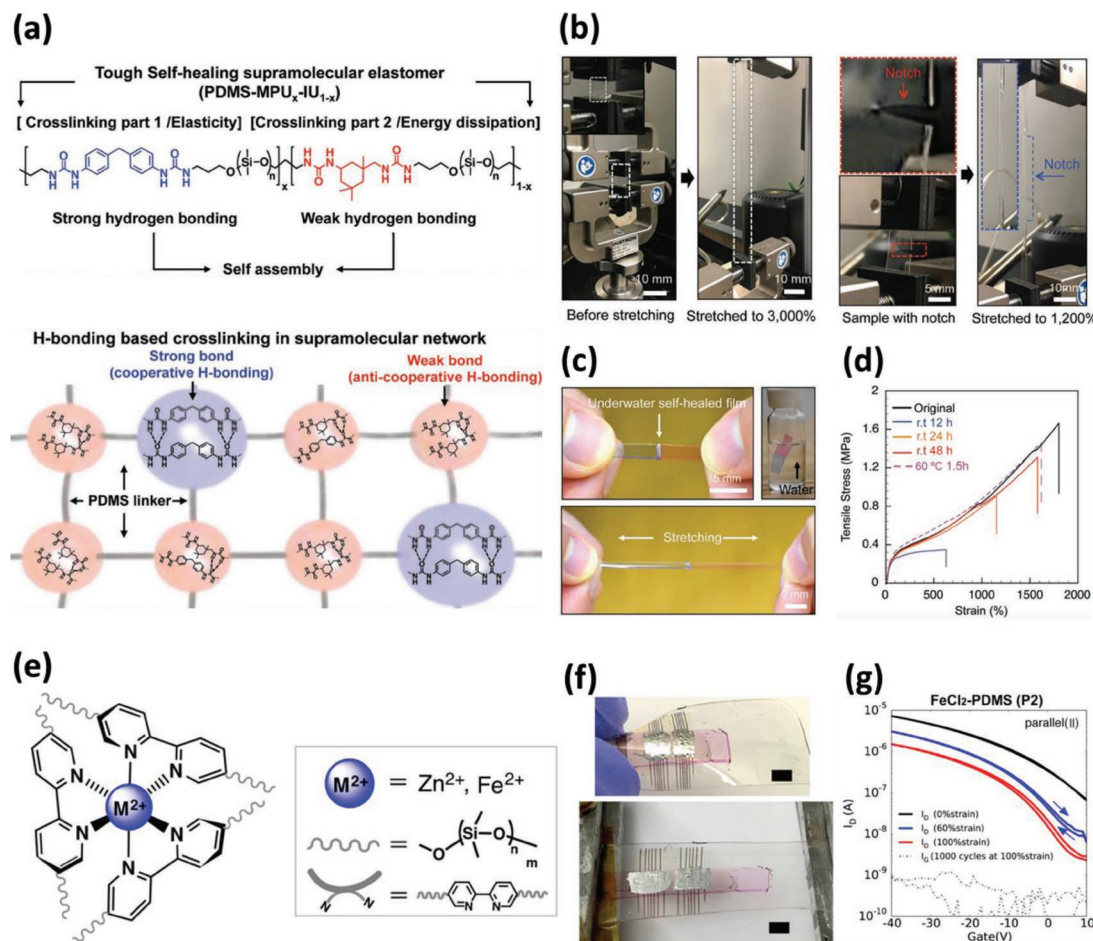


Figure 5. a) Design of a highly tough and self-healable supramolecular elastomer. High toughness and self-healability were achieved using hierarchical hydrogen bonds. b) The elastomer exhibited high stretchability and notch-insensitiveness. c) The elastomer was self-healed in water. d) Stress–strain curves of self-healed elastomers. Mechanical properties were mostly recovered after self-healing at room temperature. Reproduced with permission.^[116] Copyright 2018, Wiley-VCH. e) Design of a self-healing elastomer based on metal–ligand interactions. f) Fully stretchable transistors fabricated using the self-healable elastomer. g) Transfer curves of the fully stretchable transistors under various strains. All samples showed typical transfer curves without significant gate leakage. Reproduced with permission.^[120] Copyright 2016, American Chemical Society.

of the dynamic reconstruction process of a conducting network (Figure 6c)^[115] showed that conductive fillers embedded in a self-healing matrix follow the dynamic behavior of the self-healing polymer, which ultimately results in the recovery of conductivity and mechanical properties of the entire network.

Unlike other conductive fillers, liquid metals are of great interest, because disconnected liquid metal components can easily recover conductivity once reconnected. For example, an autonomously and electrically self-healing liquid metal–elastomer composite was demonstrated using EGaIn droplets dispersed in PDMS.^[131] Once mechanical damages were introduced to the self-healing composite, EGaIn droplets ruptured to form a new conductive pathway among the droplets, which allowed for electrical self-healing without any external stimuli.

2.2.4. Self-Healable Semiconductors

Reports on self-healable semiconductors are scarce, possibly because achieving both high performance and self-healability

is challenging. Bao et al. reported self-healing semiconductors based on hydrogen bonds,^[18] showing that exposure to solvent vapor and heat allowed semiconductor mobilities to be recovered and caused the disappearance of nanocracks. Mei and co-workers investigated the self-healing of melt-processable semiconductors,^[132] which contained flexible conjugation-break spacers to achieve low melting temperatures. Once these semiconductors were blended with their fully conjugated counterparts, the blend exhibited moderate mobility and melt processability. For example, mechanically damaged semiconducting blend films of this type could be healed upon heating at 160 °C.

2.2.5. Applications of Self-Healable Materials in Electronics

White et al. realized the self-recovery of electrical circuits using microcapsulated EGaIn.^[133] Mechanical damage led to the rupture of EGaIn capsules, which consequently formed conductive pathways. However, the single-use nature of this self-restoration precluded its applicability in e-skin. Since

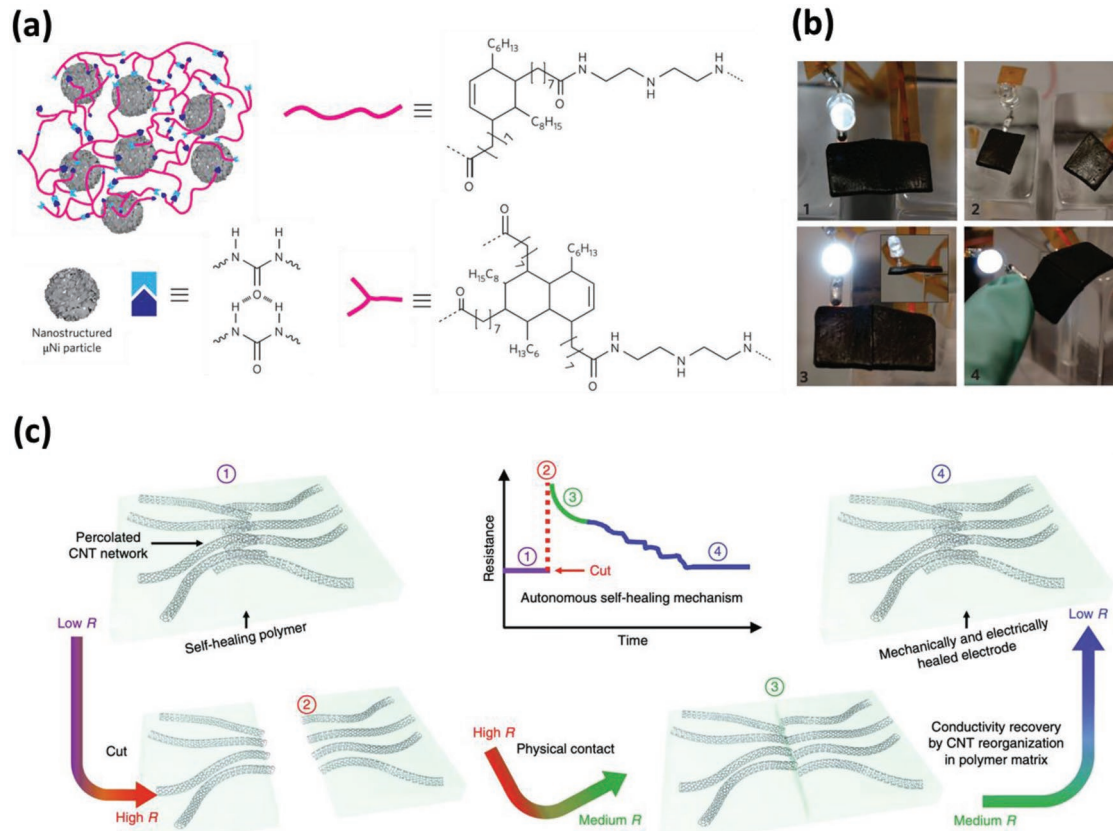


Figure 6. a) Self-healable conductors composed of μ Ni particles in a self-healing matrix. b) Light connected to the self-healable conductor was turned on after self-healing. Reproduced with permission.^[111] Copyright 2012, Macmillan Publishing Ltd. c) CNTs in a self-healing polymer matrix formed a self-healable conductor. Resistance increased abruptly after the conductor was severed. The resistance decreased gradually due to self-healing. Reproduced with permission.^[115] Copyright 2018, Macmillan Publishing Ltd.

then, a number of self-healable electronic devices based on noncovalent intermolecular interactions have been developed, e.g., tactile sensors,^[52,74,103] flexion sensors,^[111,134] strain sensors,^[115,116,126,134] humidity sensors,^[127] proximity sensors,^[127] actuators,^[121] electromyography (EMG) sensors,^[118] electrocardiography (ECG) sensors,^[115] and light-emitting electrochemical cell (LEC) displays.^[115]

Bao and co-workers developed tactile and flexion sensors using a self-healing polymer matrix with dispersed nanostructured μ Ni particles (Figure 7a),^[111] demonstrating that these sensors recognized force and bending through resistance change. The tactile and flexion sensors were then integrated with LEDs on a robot figurine, and the intensity of light emitted by the LEDs varied with applied pressure and flexion angle. In another work, EMG (electromyogram) sensors that measures signals from muscle movements were fabricated by the deposition of Au electrodes on a self-healing polymer.^[118] However, the functionality of self-healing devices was mostly tested in the absence of mechanical damage. Later, Bao and co-workers demonstrated self-healing strain sensors, ECG (electrocardiogram) sensors, and LEC (light-emitting electrochemical) displays.^[115] Specifically, Ag NWs embedded into a self-healing polymer were used in strain sensors and ECG sensors, while LEC displays utilized Cu-doped ZnS microparticles in a self-healing polymer matrix as an active layer. More

importantly, all sensors and displays maintained their functionality after being bisected into two pieces and then reconnected. Finally, multifunctional self-healing e-skin was realized by integrating strain and ECG sensors with an LEC array (Figure 7b). In this integrated device, light-emitting pixels could be turned on and off depending on heart rate and strain changes.

Finally, self-healing chemistry has been shown to enable the realization of reconfigurable electronics. Dickey and co-workers demonstrated the ability of self-healing conductors to be reconfigured into many shapes upon cutting and reconnecting (Figure 7c).^[130] Bao and co-workers further improved this concept by realizing an unprecedented stretchable modular electronic system in which each component could be exchanged by cutting and exchanging interconnects (Figure 7d). This reconfigurability led to complex 2D and 3D integration.^[135]

2.2.6. Challenges and Outlook

Despite the advances in the fabrication of highly stretchable and tough self-healing rubbery polymers, their applications in e-skin remain in their infancy. Most self-healing materials have so far been conductive composites; self-healing semiconductors

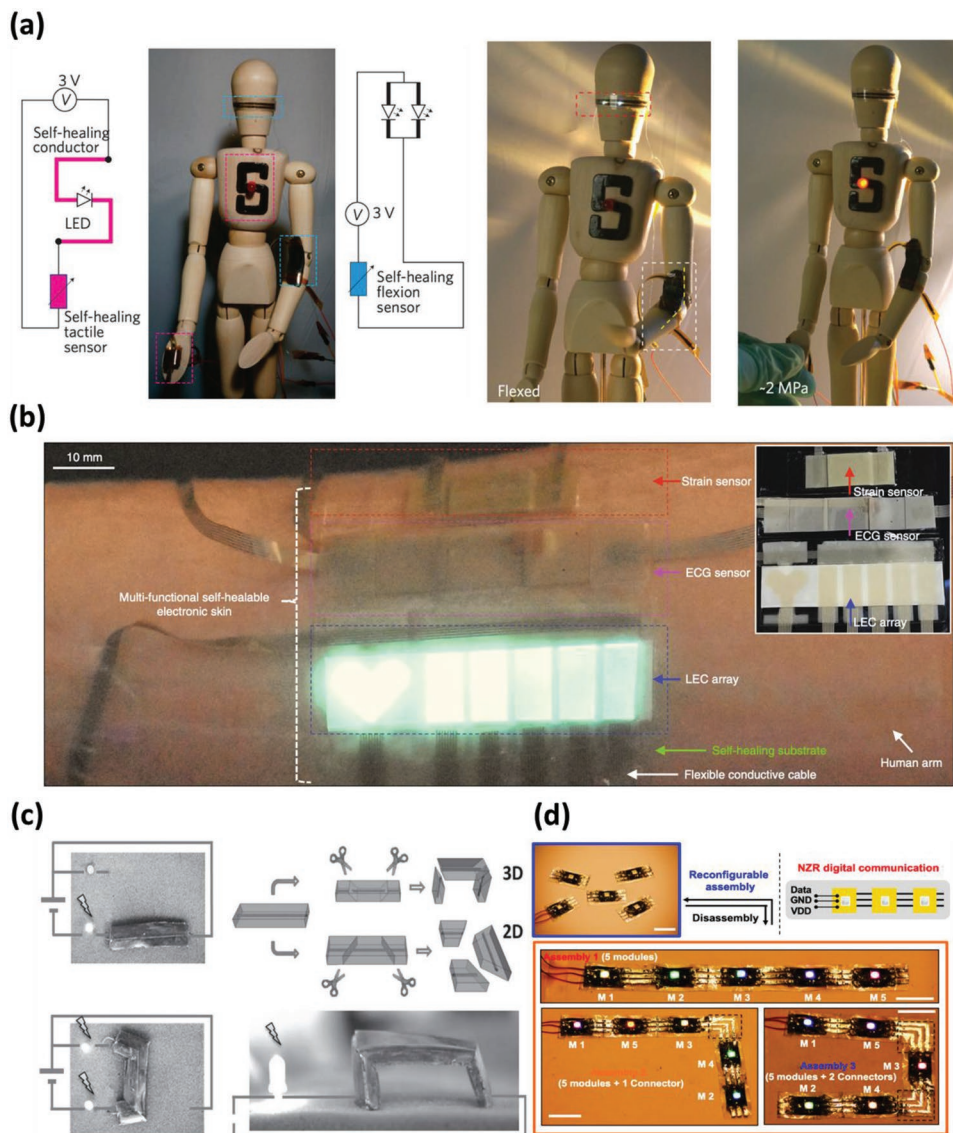


Figure 7. a) Pressure sensor and flexion sensor fabricated with a self-healing conductor. LEDs integrated onto a robot were turned on by flexion and tactile sensing. Reproduced with permission.^[111] Copyright 2012, Macmillan Publishing Ltd. b) Self-healing multifunctional e-skin containing a strain sensor, ECG sensor, and a LEC array. LEC displays were turned on and off following heart rate and strain. Reproduced with permission.^[115] Copyright 2018, Macmillan Publishing Ltd. c) Reconfigurable electrodes with 2D and 3D shapes. Self-healing of the electrodes allowed for reconfiguration. Reproduced with permission.^[130] Copyright 2013, Wiley-VCH. d) Modular electronics enabled by self-healing interconnects. Each module was reorganized through self-healing of the interconnects. Reproduced with permission.^[135] Copyright 2019, Wiley-VCH.

are currently limited in their development. When embedded in a self-healing polymer matrix, semiconductors may also exhibit autonomous self-healing capabilities, which, however, come at the expense of decreased mobility. More importantly, self-healing materials must feature autonomous repairing capabilities to be suitable for practical applications. Consequently, mechanisms of fast, repeatable, and autonomous self-healing should be further investigated.

Complex electronic circuits and devices with self-healing capabilities have not been developed yet. The self-healing devices developed thus far are at the proof-of-concept stage and are consequently far from commercial use. As initial steps toward commercialization of self-healing electronics, it

is necessary to demonstrate self-healing devices such as transistors, displays, logic circuits, and their integration. For tactile sensing applications, it is important to achieve high sensitivity, fast response time, low hysteresis, and large dynamic range (to be discussed below in Section 3). Achieving such properties with self-healing capability is currently a difficult task due to the viscous nature of self-healing materials. Novel engineering ideas are needed to solve this issue.

Finally, self-healing materials may be incompatible with the fabrication process established in the silicon industry. Therefore, scalable and reliable fabrication processes such as patterning or printing should be developed for the mass production of self-healing devices and electronics.

2.3. Biocompatible Materials

Since e-skin devices will interact closely with humans, they should be biocompatible. By definition, biocompatible materials should not negatively impact the host body (biodegradable materials (i.e., materials that decompose in the body after a certain time frame) are also by nature biocompatible; however, this topic will not be discussed in this review. The reader should refer to the following recent review articles regarding this topic).^[136–138] Biocompatible materials are application-specific; i.e., materials that are safe for use in certain applications may exhibit adverse effects when used in other applications.^[139]

Biocompatible materials may be produced from natural or nature-inspired materials. For example, paper is a cheap and lightweight seminatural material^[140] that can potentially be used as a biocompatible substrate. Transistor arrays fabricated on paper have been shown to exhibit moderate mobility of $0.2 \text{ cm}^2 \text{ V}^{-1} \text{ s}^{-1}$ with high yield of 92%.^[141] In other studies, several natural materials such as polypeptides, chicken albumen, nucleobases, and sugars were used as dielectrics of organic field-effect transistors,^[142–144] which exhibited typical transfer curves without any negative effects. Another advantage of using polypeptides as dielectrics is the ability to tune the threshold voltages by the adjustment of pH, since this parameter influences the peptide dipole moment.^[143]

Synthetic insulating materials can also be biocompatible, as exemplified by PDMS, which has been approved by the US National Heart, Lung, and Blood Institute (NHLBI) as a discriminatory tool for the evaluation of biomaterials.^[145] The excellent biocompatibility, robust dielectric behavior, and high degree of stretchability make PDMS a popular substrate and dielectric layer for electronic devices. Other synthetic polymers such as poly(ethylene glycol) (PEG) and poly(vinyl alcohol) (PVA) are also often considered to be biocompatible.^[146]

Well-known electronic materials such as P3HT,^[147–149] PEDOT:PSS,^[150,151] Phenyl-C61-butyric acid methyl ester (PCBM),^[148] N2200,^[149] and C₆₀^[152] have been shown to exhibit biocompatibility in their target applications. For example, a P3HT/N2200 blend was used to render blind rats light sensitive.^[149] The biocompatibility of this polymer blend film was tested *in vitro* for 10 d, and no adverse effects were observed. Some conductive fillers used in stretchable conductors could have application-specific compatibility issues, e.g., lung toxicity, skin irritation, and cytotoxicity are potential concerns associated with CNTs,^[153] whereas the ease of Ag oxidation accounts for some potential health issues. Consequently, such materials should be well encapsulated before use. Kim and co-workers fabricated highly stretchable conductors by embedding Ag–Au core–sheath NWs into styrene-butadiene-styrene (SBS) elastomers,^[49] revealing that the coating of Ag NWs with Au made the conductors cheap and biocompatible.

Even though materials used in a given electronic device are biocompatible, the attachment of electronic devices to skin may cause inflammation, since their long-term usage prevents skin from “breathing.” Therefore, epidermal electronics should guarantee skin breathability for long-term biocompatibility. Someya and co-workers developed a novel strategy of imparting breathability to on-skin electronics,^[154] fabricating nanomesh conductors composed of Au-coated PVA fibers and

attaching these conductors to the skin. Later, PVA fibers were removed with water to leave Au-only conductors that were inflammation-free because of their high gas permeability. In a 1 week patch test, the newly developed conductors showed significantly suppressed inflammation compared to polymer films. The conductors were further used for skin-attachable e-skin sensors that recorded touch, temperature, pressure, and electromyogram.

To the best of our knowledge, the biocompatibility of most synthetic materials has rarely been studied extensively. Moreover, the use of some additives and solvents for the fabrication of e-skin devices may result in bioincompatibility. Therefore, research on the biocompatibility of e-skin materials and devices should be carefully conducted before practical use.

3. Progress and Future Prospects of Tactile Sensors

To apply e-skin technology to skin-attachable devices, robotics, and prosthetics, tactile sensing is of critical importance. Tactile sensing includes the detection of various stimuli such as pressure, strain, temperature, shear, bending, vibration, and slip. For the three aforementioned applications, it is imperative that the tactile sensors be flexible and in many cases stretchable so that they can conformably cover irregularly shaped curvilinear surfaces and endure mechanical stress of various kinds. For skin-attachable devices, tactile sensors can be used to detect vital signs (blood pressure, respiratory rate, etc.) as well as monitor body activities and position (i.e., proprioception). Hence, skin-attachable devices can provide useful information such as fitness, posture, abnormal gait patterns, or sudden tremors in limbs.^[155] In the case of robotics and prosthesis, tactile sensors would allow a robot or an amputee to probe its physical environment, which will allow tasks such as handling and manipulation of everyday objects, and interaction with other people.^[3,156,157] For robotics, proprioception (a perception or awareness of the position and movement of its body) is an important feature for it to operate properly.^[157,158] Particularly for soft robotics, since their shape is prone to alter into various conformations when external forces are applied, monitoring proprioception is especially challenging.^[157] In addition, since soft robots generally use elastomers, they tend to have nonlinear, hysteretic, and viscoelastic properties, rendering monitoring of proprioception even more difficult. Figure 8a depicts the number of publications for various types of tactile sensors. The number of publications per year was obtained from Web of Science (2000–2018) based on the following word searches: “pressure sensor,” “strain sensor,” “temperature sensor,” and “slip sensor or sliding sensor or force vector or three-axis.” The search condition “wearable or flexible or stretchable” was set as a precondition. For pressure and strain sensors, the number of publications increased drastically starting around 2010. Relative to pressure and strain sensors, there are not as many publications on temperature and slips/force vector sensors. Particularly in regard to slip and force vectors sensors, the low number of publications suggest that there is much more research and development needed. Figure 8b depicts the some of the common issues in tactile sensors (left) and their ideal behavior (right). Tactile sensors should ideally have the following properties: high sensitivity (or gauge

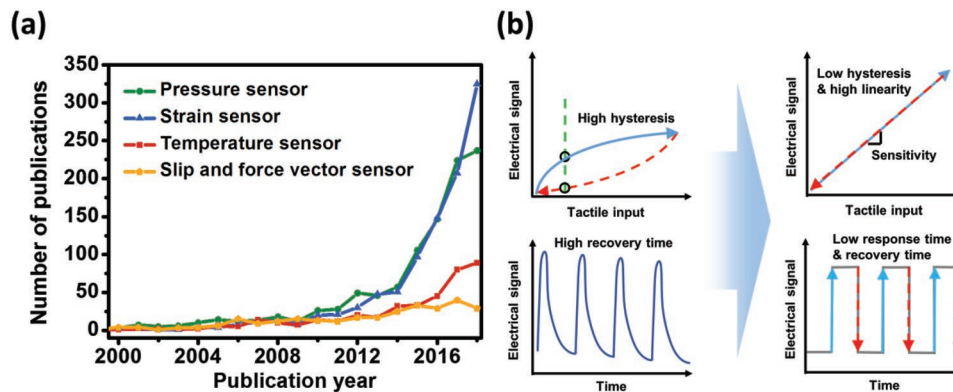


Figure 8. a) The number of publications per year on the topic “pressure sensor,” “strain sensor,” “temperature sensor,” and “slip and force vector sensor.” The search condition “wearable or flexible or stretchable” was set as a precondition. b) Typical issues (left) and ideal behavior (right) of tactile sensors with key performance indicators listed.

factor), wide dynamic range (i.e., sensing range), linearity, low hysteresis, and fast response, and recovery time. This section will review the recent progress of tactile sensors. For a more focused review on tactile sensors, the reader is encouraged to refer to the following review articles.^[3,157,159–162]

3.1. Pressure and Strain Sensors

Pressure and strain sensors detect pressure and strain through several transduction principles (e.g., capacitance, piezoresistivity, piezoelectricity, and triboelectricity). Among these sensors, piezoresistive and capacitive sensors are most commonly employed, owing to their design simplicity and the capability to detect both static and dynamic signals.^[155] A piezoresistive sensor detects pressure or strain in three different ways: 1) through the change in the percolation network of conductive materials in a polymer matrix, 2) change in contact resistance between a piezoresistive material and electrodes, and 3) change in the intrinsic resistance of the material itself (i.e., inducing a change in bandgap). Most capacitive sensors feature a dielectric layer sandwiched between two electrodes. As pressure or strain is applied, the capacitance between the electrodes changes due to geometrical deformation (i.e., change in the distance between electrodes and/or the device area), and/or the change in the effective dielectric constant of the dielectric layer. In this section, we will explain the strategies of enhancing the performance of pressure and strain sensors, focusing primarily on materials selection and architectural design.

3.1.1. Material and Structural Designs Used to Enhance Pressure Sensor Performance

Sensitivity is one of the most important performance parameters in pressure sensors. Sensitivity is defined as the slope of the relative change in electrical signal (capacitance, resistance, current, or voltage) versus applied pressure curve.^[159] Sensitivity is generally related to the compressive modulus of the sensing element (i.e., if at a given pressure higher strain is induced, larger change in electrical signal can be assumed). High sensitivity yields larger

signal-to-noise ratio (SNR) for a given difference in applied pressure, allowing the sensor to detect subtle pressure changes such as those associated with sound or artery pulse. The exact sensitivity required depends on the target application, and there is currently no concrete guideline as to what constitutes as a high or low sensitivity. Also, as implied above, the required sensitivity will also depend on the noise level of the measurement apparatus.

The most commonly used techniques to enhance sensitivity of capacitive and piezoresistive pressure sensors are to use microstructured (e.g., pyramidal, dome-like, porous, and interlocking structures) elastomer (e.g., PDMS, Ecoflex, and PU).^[163–170] For unstructured elastomers with thickness much smaller than its area (which is generally the case for many e-skin pressure sensors),^[163,167,171] decrease in thickness under pressure can be assumed to occur via intrinsic compression of the elastomer itself (i.e., free volume within the material is reduced). This phenomenon can be pictured as polymer chains being reconfigured to take on a more compact conformation. Such a way to reduce elastomer thickness requires relatively large pressure (i.e., larger compressive modulus), resulting in low sensitivity. In contrast, for microstructured elastomers, there is free space for the elastomer to expand into, hence requiring less pressure to deform the elastomer layer. Moreover, the geometry of the microstructure can be utilized to concentrate the stress to a particular region, furthermore increasing the sensitivity. For example, in a pioneering work by Bao et al., pyramidal microstructures were utilized to drastically increase sensitivity (Figure 9a).^[163,164,171] Since the tip of the pyramids have a relatively small area, the stress is locally enhanced at the tips, yielding large deformation under a given pressure.^[163] Furthermore, the effect of geometric parameters including the angle of sidewalls, the base size, the spacing of micropyramids were extensively studied using finite element modeling, and the computational results were substantiated by the experimental results to efficiently design micropyramidal structure for specific applications.^[163,172] Moreover, the above authors fabricated a piezoresistive sensor using the change of contact resistance between single-walled CNT (SWCNT)-coated pyramidal PDMS structures and electrodes (Figure 9b).^[164] The contact resistance and the threshold of resistance switching were carefully controlled by changing the height of SWCNT-film to keep the device off before applying pressure.

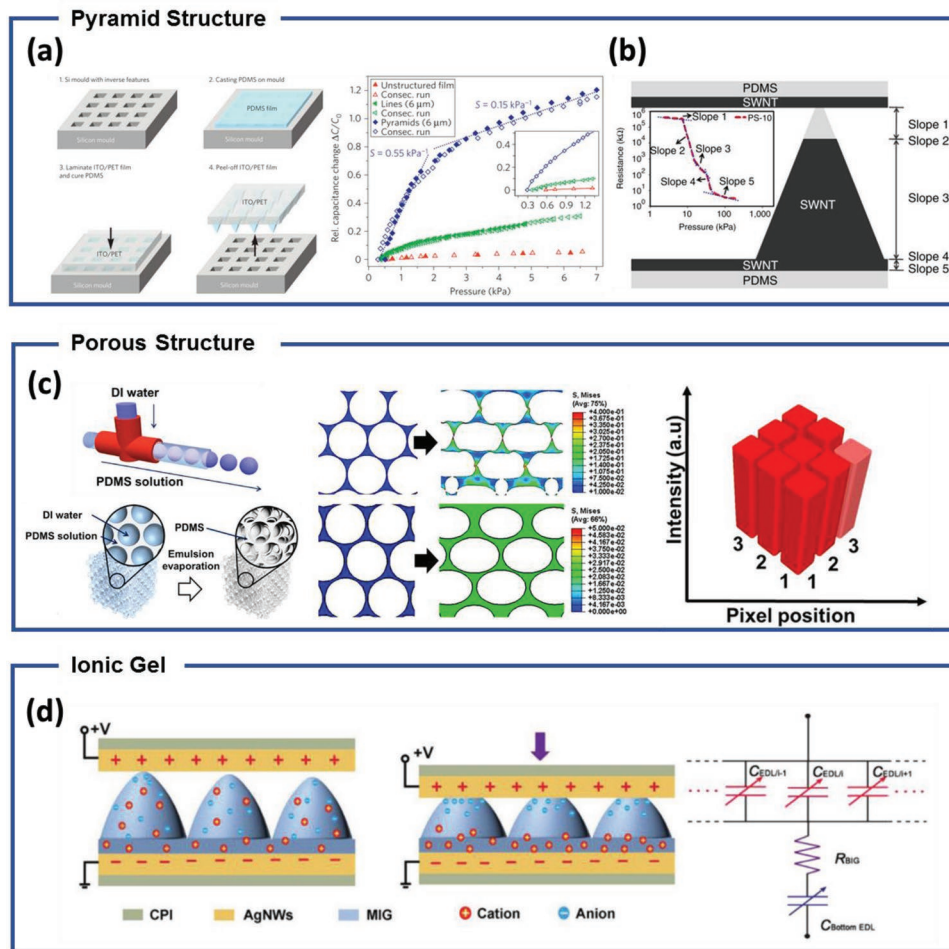


Figure 9. a) Capacitive and b) piezoresistive pressure sensor featuring a micropyramidal array, showing enhanced sensitivity compared to that of an unstructured sensor. a) Reproduced with permission.^[171] Copyright 2010, Macmillan Publishing Ltd. b) Reproduced with permission.^[164] Copyright 2014, Wiley-VCH. c) Microporous pressure sensor with uniform-sized pores showing high spatial uniformity in sensitivity. The simulated finite element model showing the stress distribution of different size pores under pressure. Reproduced with permission.^[167] Copyright 2018, American Chemical Society. d) Capacitive pressure sensor comprising microstructured ionic gel, with underlying operation principle and equivalent circuit. Reproduced with permission.^[180] Copyright 2018, Wiley-VCH.

Porous structures also generally have high sensitivity compared to that of the solid bulk counterpart since stress is concentrated at the pillars between pores, resulting in bending or buckling under pressure (i.e., less stress is required to bend or buckle the pillars). Kim et al. fabricated piezoresistive sensors based on porous CNT/PDMS composites, demonstrating that the conductive network in these composites significantly changed under a small difference in applied pressures.^[165] Park et al. fabricated microporous capacitive sensors with uniform-sized pores using a microfluidic system, exhibiting maximum sensitivity of 0.86 kPa^{-1} and excellent spatial uniformity in sensitivity (Figure 9c).^[167] Interestingly, the authors observed that the sensitivity increased with increasing pore size. This was attributed to the longer pillars between the larger pores having lower critical buckling load, decreasing the compressive modulus of the overall structure, which consequently increases the sensitivity. In a recent work by Park et al., porous pyramids were fabricated, through which ultra-high sensitive capacitive (44 kPa^{-1} to 100 Pa) pressure sensors were demonstrated.^[173]

The sensitivity of piezoresistive sensors can also be increased by changing the number of contact points or contact area between two conductive elements (i.e., typically between a sensing element and electrodes) to alter the contact resistance. These sensors are especially sensitive at low pressures.^[174–176] Zhao et al. placed carbon-decorated fabric on top of interdigitated electrode arrays, to detect the change in contact resistance with applied pressure.^[176] The above sensor showed a sensitivity of 0.244 kPa^{-1} at an applied pressure of 35 kPa and was used for continuous blood pressure monitoring. Contact resistance change can also be induced by designing two sensing elements that have an interlocking architecture.^[170,177,178] Ren et al. fabricated an epidermis microstructure-inspired pressure sensor using interlocking reduced graphene oxide (rGO)/PDMS layers.^[177] This sensor featured a high sensitivity of 25.1 kPa^{-1} at 2.5 kPa and could consequently detect low-pressure signals such as wrist pulse, normal and deep respiration of the chest, walking, running, and jumping. Recently, using porous pyramids covered with polypyrrole conductive polymer, maximum sensitivity of 449 kPa^{-1} was demonstrated.^[173]

In addition to elastomers, microstructured ionic gels are viable dielectric materials for use in capacitive pressure sensors with ultra-high sensitivity. An ionic gel comprises a polymer-matrix-trapped ionic liquid that undergoes a relatively large capacitance change with applied pressure due to the formation of an EDL.^[179] The working principle of these devices is the change in capacitance due to the increasing in contact area between the electrode and the ionic gel. Hence, also for these sensors, microstructuring enhances sensitivity (Figure 9d).^[180,181] Park and co-workers employed a micropyramidal ionic gel to fabricate a capacitive sensor with high sensitivity (41 kPa^{-1}) that could detect sound (<30 Pa), lightweight objects (4 Pa), pulse signals (2 kPa), touch (<10 kPa), and motion (<25 kPa).^[181]

Most pressure sensors with high sensitivity at low pressures exhibit small dynamic range (i.e., sensitivity decreases with increasing applied pressure). Similar to sensitivity, dynamic range depends on the target application. For instance, if the target application is measuring pulse, sensitivity above several kPa is generally not needed. On the other hand, to mimic the tactile sensing properties of human skin, a relatively large dynamic range is required (greater than 10 kPa).^[1] Hence, in this regard, a pressure sensor should ideally have high sensitivity with large dynamic range, with the same sensitivity throughout all pressures (i.e., linearity). Several approaches to achieve large dynamic range and linearity without significantly reducing sensitivity have been developed. Cho et al. fabricated a piezoresistive sensor based on bio-inspired hierarchical structure array, featuring hemispherical domes with small protuberances on their surface (Figure 10a).^[182] Compression of these domes with small protuberances resulted in a linear change in current, unlike conventional domes with a smooth surface. The sensitivity and linear working range were 8.5 kPa^{-1} and 0–12 kPa, respectively. Moreover, Cho and co-workers fabricated a capacitive sensor containing surface-wrinkled pyramidal electrodes, demonstrating that the capacitance changed with applied pressure due to the increase in electrode contact area (as opposed to the decrease in dielectric layer thickness).^[183] Since capacitance is linearly proportional with electrode area, this sensor exhibited a linear relationship between applied pressure and relative capacitance change within a specific working range (sensitivity

of 0.7 kPa^{-1} up to 25 kPa). Ko et al. fabricated a piezoresistive sensor with a multilayer interlocked microdome geometry, demonstrating that efficient stress distribution between the stacked multilayers enabled linearity over a wide sensing range (sensitivity of 47.7 kPa^{-1} from 0.0013 to 353 kPa).^[184]

Hysteresis is an important feature in pressure sensors and should be minimized for practical usability. Hysteresis is defined as the difference in the signal versus pressure curve under loading and unloading of pressure. Hence, hysteresis results in different measurements depending on whether pressure is being applied or released, the rate of increase or decrease in pressure, and the number of cycles or constant load the sensor has previously undergone. Such effects make it very difficult to accurately read out the pressure level, requiring complex compensation circuitry and signal processing. Hysteresis results from finite amount of time needed for the polymer chains to revert back to their original positions (i.e., viscoelasticity). In the case of piezoresistive composites, irreversible slippage at the interface between the conductive material and the polymer matrix may occur, which results in permanent change in baseline resistance. Despite its importance, there is currently inconsistency in reporting hysteresis in pressure sensors (also applied to strain sensors); some works do not present it at all, while many others do not quantify hysteresis. Although there is currently no standard method to quantify hysteresis, one possible method is to calculate the degree of hysteresis or DH by calculating the difference in the area underneath the signal versus pressure curves under loading and unloading. Also, since DH values can change depending on the applied pressure range and scan rate, such values should be standardized. A quantification standard such as this should be globally utilized in the field to properly compare different sensors' hysteretic performance.

To reduce hysteresis, the sensing element can be microstructured to lower its viscous properties relative to its elasticity (explained further below) and/or strengthen the bonding between polymer matrix and the conductive material. For example, patterned ionic gel of a capacitive sensor was shown to exhibit more pronounced elastic behavior than a flat ionic gel; consequently, the former showed less hysteresis behavior.^[180,181]

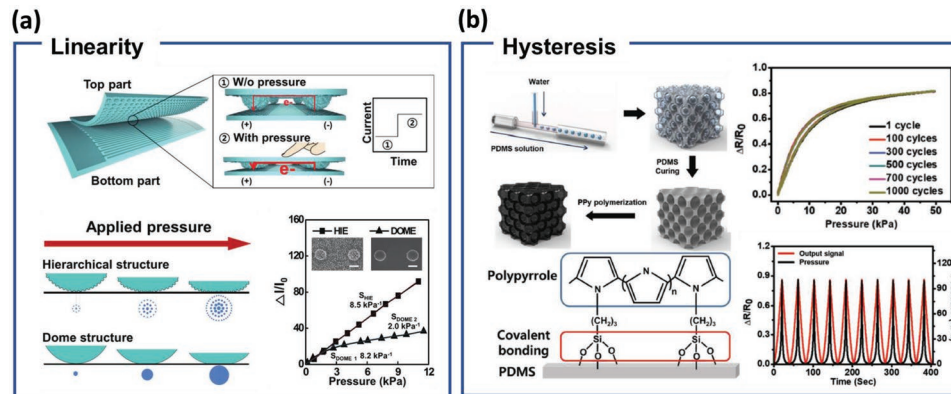


Figure 10. a) Bioinspired hierarchically structured piezoresistive pressure sensor exhibiting linear response. The hierarchically structured sensor showed linearity from 0–12 kPa, while the dome structured sensor (reference sample) showed nonlinearity. Reproduced with permission.^[182] Copyright 2016, Wiley-VCH. b) Microporous piezoresistive pressure sensor with chemically bonded conductive polymer on elastomer surface, showing reduced hysteresis. Reproduced with permission.^[185] Copyright 2019, Wiley-VCH.

In a pioneering work by Park and co-workers, polypyrrole conductive polymer was chemically grafted onto the surface of porous PDMS template (Figure 10b).^[185] Due to the strong chemical bonding between the conductive element and the elastomeric template, the devices exhibited extremely low DH of 2% up to 100 kPa.

The rate at which a sensor responds and recovers (i.e., response and recovery time) upon the application and release of load is also important. The response and recovery time is related to the viscoelasticity of the elastomer; the stronger the elastic nature of the elastomer, the lower will be the response and recovery time. Therefore, these values are related to the hysteresis. Bao and co-workers demonstrated that a capacitive pressure sensor with a micropyramidal array recovered faster than an unstructured film.^[171] For an unstructured film with thickness much smaller than its area (which is the case for most electronic skin pressure sensors), recovery is generally slower.^[171] As mentioned above, in this case, in order for the film thickness to decrease in response to applied pressure, the polymer chains likely have to undergo a large degree of displacement and reconfiguration to take on a more compact conformation. When pressure is released, longer time is required for the polymers to revert back to their original conformation. When the elastomer is microstructured, there is plenty of free volume for the elastomer to expand into; hence less displacement and reconfiguration of the polymer chains is necessary, resulting in faster recovery. Various microstructures have been used to reduce response and recovery time to tens of milliseconds, with pyramids often employed as the starting point.^[171]

Similar to that of hysteresis, there is currently a lack of standardization in attaining response and recovery time. The experimentally obtained response and recovery time depend on the level of applied pressure, the rate at which the pressure is applied and released, and the data acquisition rate of the measurement tool. Hence, it is imperative that these parameters are standardized, or at least be defined when referencing response and recovery time. In particular, if the latter two parameters are slower than the response and recovery time of the sensor itself, the attained measurements is an underestimation. Dynamic mechanical analysis, where applied pressure is varied as a sine wave and the phase difference is measured, is one possible technique to standardize the measurements.

The aforementioned design guidelines have aided the development of pressure sensors for skin-attachable devices, robotics, and prosthetics. For instance, Pan et al. fabricated an iontronic film-based capacitive sensor that can pick up pulse and muscle movements at various body regions with a clear waveform output signal.^[186] Ko et al. detected respiration, wrist pulse (1–20 kPa), and foot pressure distribution (up to 250 kPa) in humans.^[184] The monitoring of respiration and wrist pulse can help diagnose fatal diseases, while foot pressure distribution can help detect abnormal gait patterns, which are common symptoms of Parkinson's disease. Perception of skin sensation provides valuable information that allows robots to interact with their external environment. Zhao et al. constructed a robot hand with an integrated pressure sensor based on a hollow sensing element structure, and showed the output signal and tactile feedback while transporting objects.^[187] This feedback was clearer than that of a commercial flexible pressure sensor,

and in conjunction with proprioception, allowed the robot to perform dexterous motion. Lee and co-workers fabricated artificial afferent nerve based on pyramid-based piezoresistive pressure sensor, ring oscillator, and a synaptic device, emulating a biological mechanoreceptor.^[188] The artificial afferent nerves were connected to biological nerves to induce muscle movement. Thakor and co-workers fabricated prosthesis with neuromorphic multilayered e-dermis to help an amputee to perceive touch and pain by providing spike-based neuromorphic tactile information.^[156]

3.1.2. Material and Structural Designs Used to Enhance Strain Sensor Performance

The main parameters influencing the performance of a strain sensor are similar to those mentioned in the pressure sensor section above: sensitivity, dynamic range, hysteresis, linearity, and response and recovery time. The discussion regarding these topics above for pressure sensors hence applies similarly to strain sensors. Below we discuss some of the recent advances in strain sensors.

In order for a strain sensor to sensitively detect lateral and bending strains, its gauge factor (GF) must be sufficiently high. GF is a quantity analogous to sensitivity, defined as the slope of the relative change of electrical signal (capacitance or resistance change) versus applied tensile strain curve. GF determines the smallest detectable variation in strain.

For capacitive strain sensors, the GF is relatively low (<1) since the strain sensing mechanism is limited to geometrical effects.^[160] Meanwhile, piezoresistive sensors based on conductive material–elastomer composite can achieve high GFs through the change in the resistivity via modification to the conductive pathway. Strain sensors can be made either by embedding the conductive material within an elastomer matrix^[47,189] or by coating a thin film of conductive material on top of an elastomer substrate.^[190–198] As an example of the former case, Park et al. fabricated Ag NW/PDMS composites and showed that NWs were displaced inside the PDMS matrix during elongation, resulting in gradual disconnection of NW–NW junctions (Figure 11a).^[47] The corresponding sensor featured a tunable GF of 2–14 controlled by the concentration of NWs in the matrix and could be stretched up to 70%. For the latter case, conductivity of various thin films such as graphene,^[190,198] Pt,^[191] Ag NPs,^[192] Ag NWs,^[193] and CNTs^[194] has been changed via microcrack formation, yielding large resistance change at low strains (Figure 11b). One can also employ the disconnection of CNT bundles^[195,196] or overlapped graphene sheets^[197] to increase their contact resistance during strain. Shi et al. fabricated a sensor featuring a fish-scale-like overlapped graphene layer on an elastic tape.^[197] Upon stretching, the area of overlap between graphene layers was reduced, and the contact resistance consequently increased. This sensor showed a GF of 16.2–150 over a wide sensing range of 0–82% strain. Kim and co-workers fabricated a piezoresistive strain sensor comprising of highly oriented CNT bundles deposited on a prestretched Ecoflex substrate (Figure 11c).^[195] At 0–400% strain, CNTs slipped past each other, and the contact resistance gradually increased,

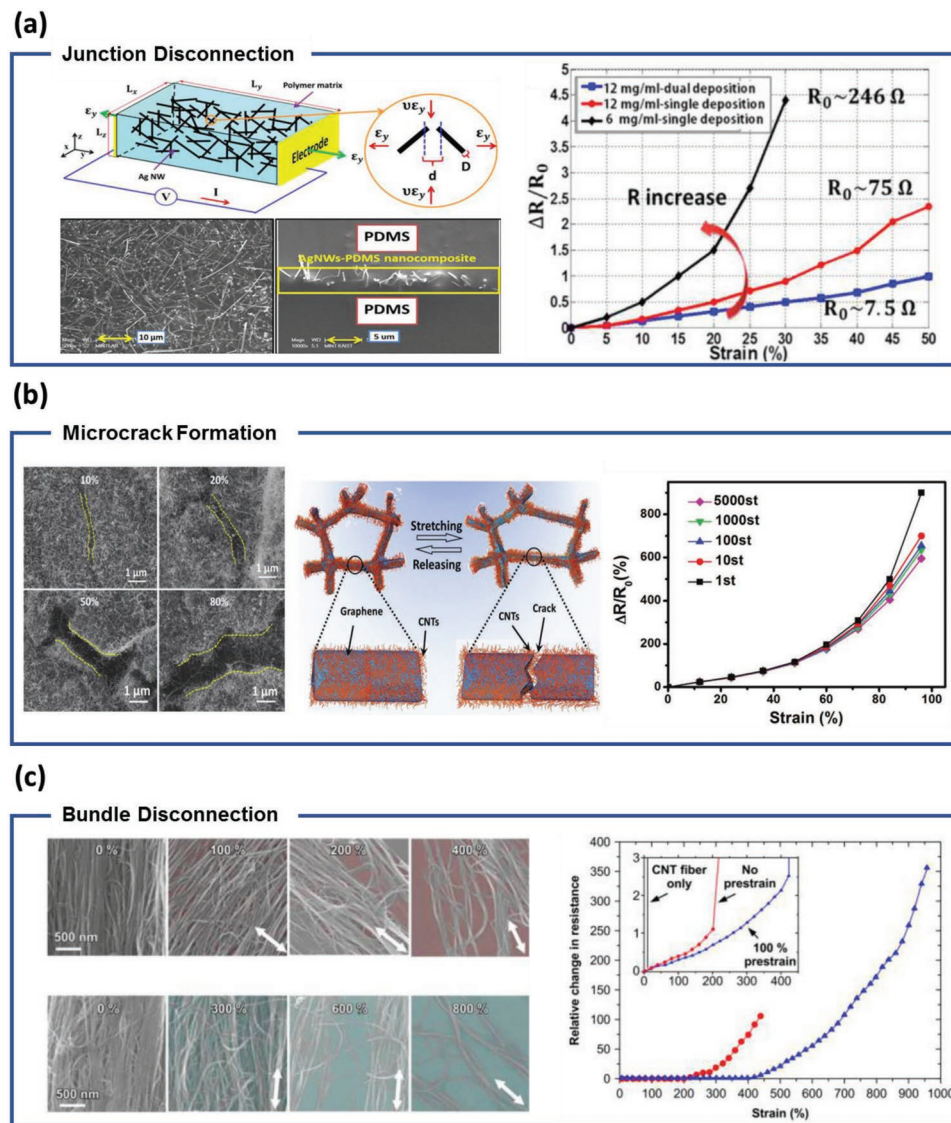


Figure 11. a) Ag NW/PDMS composite-based strain sensor with tunable GF of 2–14. Reproduced with permission.^[47] Copyright 2014, American Chemical Society. b) Strain sensor based on graphene foam–CNT conductive film, showing a GF of 35. Microcracks generated in graphene layer yielded large resistance change under stretching. Reproduced with permission.^[198] Copyright 2017, Wiley-VCH. c) Highly stretchable strain sensor with aligned CNT bundles on a prestrained Ecoflex substrate. Reproduced with permission.^[195] Copyright 2015, American Chemical Society.

which resulted in a GF of 0.54. At 400–960% strain, CNT bundles experienced abrupt disconnections, and the contact resistance consequently became very large, as reflected by a GF of 64.

The aforementioned strain sensors fabricated by combining elastomer with various conductive materials are advantageous due to their high stretchability (e.g., Ag NW–PDMS (<70%),^[47] graphene–PDMS (<110%),^[199] multiwalled CNT (MWCNT)/PEDOT:PSS–PDMS (<100%),^[200] carbon nanofiber–PDMS (<70%),^[201] P3HT nanofibrils–PDMS (<100%),^[202] carbon black–Ecoflex (<400%),^[203] and CNT–Ecoflex (<500%))^[204] along with their relatively high GF compared to that of capacitive strain sensors. Hata et al. showed that the use of aligned SWCNTs resulted in greater stretchability than that of randomly oriented SWCNTs.^[196] Upon fracture, the aligned-SWCNT film is separated into islands and gaps. However, because SWCNT bundles

bridges the gaps, the sensor exhibits high stretchability (280%) with a GF of 0.06–0.82. Kim et al. fabricated a strain sensor with a remarkably high stretchability of 900% by aligning CNT fibers on a pre-strained Ecoflex substrate with a GF of 0.54–64 (Figure 11c).^[195]

It is important to carefully define stretchability and sensing range in piezoresistive strain sensors. A strain sensor is useful only if the targeted strain range can be detected repeatedly; in other words, in defining sensing range, cycling stability should be considered.^[162] However, at maximum strain limit (i.e., maximum stretchability), the sensor's resistance may lose their ability to revert back due to irreversible slippage at the interface between the conductive material and the polymer matrix.^[159] Figure 12a is a plot of various strain sensors' stretchability (solid and dashed line), and sensing range (solid line: arbitrarily

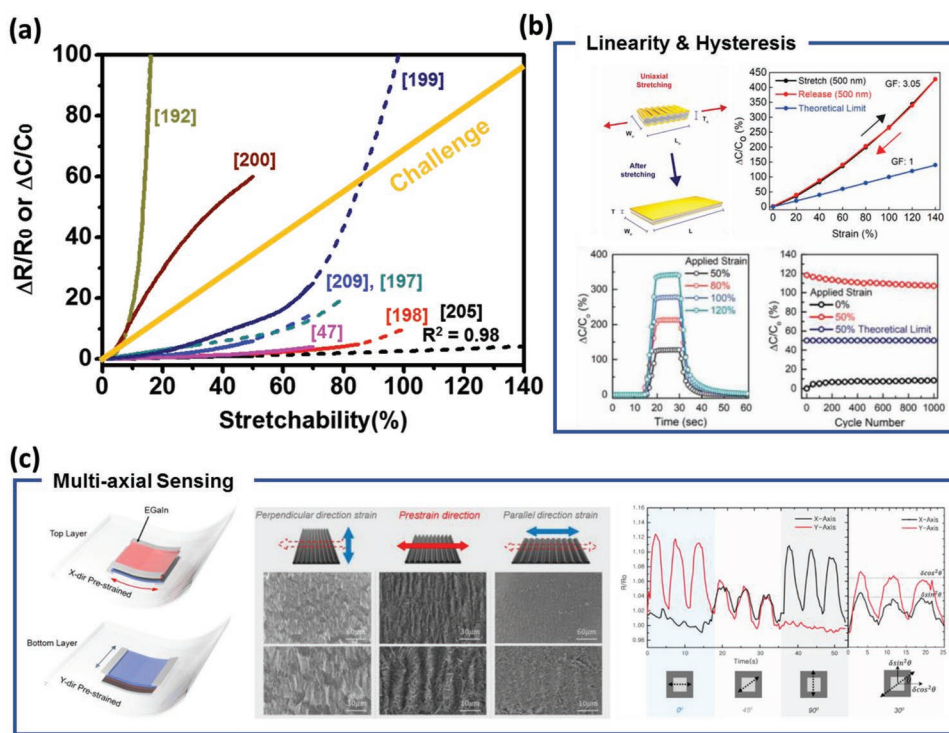


Figure 12. a) Strain sensing performance (stretchability, sensing range, gauge factor, linearity) of various previously reported strain sensors. The solid line is the sensing range and the solid/dashed line is the stretchability. b) Capacitive strain sensor containing wrinkled Au electrodes, exhibiting high linearity and low hysteresis. Reproduced with permission.^[205] Copyright 2018, American Chemical Society. c) Bilayered strain sensor with two perpendicularly oriented wrinkle structures for multiaxial sensing. Reproduced with permission.^[206] Copyright 2015, American Chemical Society.

defined as strain level to which at least five loading/unloading cycles can be measured). Evidently, the stretchability and strain range are different in many strain sensors. Hence, these values should be specifically defined to accurately gauge the performance of strain sensors. We also note that there is generally a trade-off between GF and strain sensing range. For example, although outstanding GFs are usually obtained using disconnection mechanisms such as microcrack formation, such sensors generally have low sensing range. Depending on the target application, strain sensor should hence be carefully designed.

Linearity, hysteresis, and response/recovery time are also important parameters for determining the practical applicability of strain sensors. Generally for piezoresistive strain sensors with high GFs, hysteresis and relatively long response/recovery times are observed due to the irreversibility of disconnections and crack formations, and the viscoelastic properties of the polymer matrix.^[160] Nonlinearity is also seen in these sensors as the relative proportion of disconnections in the conductive pathway changes with applied strain (i.e., for this reason, GF should be referenced with the corresponding strain range under which it was defined) (Figure 12a).^[160] These are important issues to resolve in the future; novel device concepts, and fundamental study of polymer viscoelasticity and conductive material–polymer matrix interactions are needed. Conversely, capacitive strain sensors feature relatively low GFs but generally exhibit better linearity and hysteresis. Interestingly, Someya and co-workers recently designed a capacitive strain sensor with wrinkled Au film electrodes, achieving a GF of 3.05 (ascribed

to the out-of-plane deformation), along with high linearity ($R^2 = 0.98$) and negligible hysteresis (Figure 12b).^[205]

Although most strain sensors are optimized for sensing strain along one direction, the actions of humans and robots are associated with lateral strain in various directions. This necessitates multiaxial sensing,^[161] which can be achieved using two approaches. In the first approach, the sensing direction is estimated from the unidirectional responses of two perpendicularly stacked sensing layers.^[195,206–208] For example, Ko et al. perpendicularly stacked two strain-sensing layers with a wrinkled structure,^[206] which allowed the detection of various directions of strain (0° , 30° , 45° , and 90° with respect to x -axis), since layers wrinkled in the x - and y -directions responded most strongly to their specifically designed direction of sensitivity (Figure 12c). Similarly, Zhang et al. used two orthogonal CNT-PU sponge strips to detect various bending radius and bending directions.^[207] The second approach employs electrical impedance tomography (EIT) to image the strain direction by assessing the distribution of local conductivity inside a large-area sensor material after connecting several electrodes to its periphery, e.g., Park et al. detected the direction of local strain using a single strain sensor of a large area ($11 \times 11 \text{ cm}^2$).^[209]

Similar to pressure sensors, high-performance strain sensors can be used to detect vital signs. Dong et al. detected artery wrist pulse under various conditions (normal state, after exercise, during pregnancy) and jugular venous pressure using a crack-based strain sensor attached to the wrist and neck, respectively.^[198] Strain sensors are also suitable for monitoring body activities via detecting bending, e.g., Zhang et al. monitored the

real-time bending of fingers and knees after jogging, jumping, and squatting exercises.^[210] Additionally, strain sensors can be attached to the throat to detect minute strain changes to recognize phonation. When attached to robots and prosthesis to detect their proprioception, strain sensors can provide feedback when robots or people perform sophisticated actions.^[3,157]

3.2. Temperature Sensors

Our skin is not only able to detect mechanical stimuli such as pressure and strain, but also temperature through the use of thermoreceptors. Hence, temperature sensing is an essential aspect of tactile sensing that can be used in robotics or prosthetics. Temperature sensors can also be utilized to detect illnesses such as fever, heat stroke, and infection when used as skin-attachable devices.^[161] Commercial temperature sensors employ thermoresistive effect of pure metal or ceramic-based semiconductors; however, owing to their intrinsic rigidity, they are not compatible with e-skin devices.^[159] Therefore, structurally engineered metal and Si nanoribbons with enhanced stretchability (i.e., serpentine, buckling, net-shaped), CNT, graphene, nanoparticles (NPs), and nanocrystals (NCs) are considered to be promising materials for the fabrication of e-skin compatible thermoresistive sensors.^[211–219] The resistivity of thermoresistive materials changes with temperature due to the change in mobility and/or the charge carrier density. Metal-based thermoresistive sensors such serpentine-shaped metal,^[211] Cu NW mesh,^[212] and graphene nanowalls/PDMS^[213] have been demonstrated to exhibit an increase in resistivity (attributed to decrease in mobility) with increasing temperature. In particular, thermoresistive sensor based on Cu NW mesh showed a sensitivity of $0.7 \Omega ^\circ\text{C}^{-1}$ from room temperature to 48°C .^[212] Semiconducting or charge hopping dominant materials undergoes decrease in resistivity with increasing temperature due to the increased charge carrier density or increased thermally assisted charge carrier hopping, respectively. Some examples of these types of temperature sensors include polyaniline nanofibers,^[214] PEDOT:PSS-CNT film,^[215] CNT/self-healing polymer composite,^[216] reduced graphene oxide (rGO),^[183] and Ag nanocrystal/PDMS.^[220] Cho et al. demonstrated a rGO-based thermoresistive sensor, and obtained a high sensitivity of $0.83\% ^\circ\text{C}^{-1}$ from 22 – 70°C by optimizing the degree of reduction of rGO that affects the charge carrier hopping.^[183] Recently, Oh et al. fabricated temperature sensor with Ag NC film on PDMS substrate (**Figure 13a**).^[220] The charge transport properties of NC film was controlled by ligand treatment and nanocracks generated by thermal expansion of PDMS. Through this mechanism, the temperature sensor exhibited a very high sensitivity ($50\% ^\circ\text{C}^{-1}$) from 30 – 50°C .

In addition to thermoresistive effect, temperature sensors employ thermoelectric and pyroelectric effects, both of which relate to the generation of electricity (current and voltage) upon changes in temperature.^[159] Temperature sensors based on these two principles are advantageous as they do not need a power supply to operate.^[221,222] In the case of thermoelectric sensors, the temperature across the device generates electricity based on the Seebeck effect. Zhu et al. fabricated a temperature sensor based on porous PU and PEDOT:PSS (thermo-

electric material), showing high temperature detection resolution (<0.1 K) (**Figure 13b**).^[223] In addition, 12×12 sensor array attached to a prosthetics hand detected the temperature distribution of a human hand. In the case of a pyroelectric sensor, a change in temperature generates a transient voltage due to electric polarization. Ko et al. fabricated a temperature sensor based on reduced graphene oxide/poly(vinylidene fluoride) (rGO/PVDF) composites and showed high sensitivity of $2.93\% ^\circ\text{C}^{-1}$.^[222] It was used as a skin-attachable device detecting the temperature of human skin (0 – 100°C).

In addition to the high sensitivity and wide sensing range, high linearity and low hysteresis are also important in temperature sensors.^[159] Ha et al. fabricated a thermoresistive temperature sensor with polyaniline nanofiber-based film (**Figure 13c**).^[214] The homogeneous nanofiber was synthesized electrochemically, through which temperature sensor with a sensitivity of $1.0\% ^\circ\text{C}^{-1}$ with high linearity ($R^2 = 0.998$) and no hysteresis was demonstrated.

Unlike pressure and strain sensor, response and recovery time of temperature sensor are relatively long (approximately few seconds). The thermoelectric temperature sensor fabricated by Zhu et al. based on porous PU and PEDOT:PSS exhibited a response time of <2 s under a temperature change of 1°C . The authors found that response time was long due to the long thermal diffusion time of 1.7 s.^[223] Cho et al. reduced the thermal diffusion time in their device by reducing the thickness of the substrate in their rGO temperature sensor.^[183] A fast reaction time within 100 ms under a temperature change of 3°C was obtained by fast thermal conduction to the active material through a $3\ \mu\text{m}$ substrate.

For wearable applications, the temperature sensor should exhibit negligible sensitivity to mechanical strain. The common technique to achieve this is to use serpentine or island architecture (i.e., regions of high elastic modulus in or on a substrate with relatively low elastic modulus) to minimize the strain imposed on the material itself. For instance, Ha and co-workers placed temperature sensors on rigid islands to prevent electrical signal changes due to strain (0–30%).^[214] Interestingly, Oh and co-workers proposed another strategy to decouple the effect of temperature and strain by using two sensors composed of Ag NC (nanocrystal) with different coefficient of resistance (TCR: $(\Delta R/R_0)/\Delta T$) (**Figure 13d**). Algebraic calculation of the behavior of the two sensors allowed the differentiation of signal due to temperature and strain.^[217,218] Differentiating between temperature and strain as well as other tactile stimuli (pressure, slip, torsion, bending, and vibration) will be further discussed in subsection 3.4.

3.3. Slip and Force Vector Sensors

To grasp and manipulate objects, pressure, strain, and temperature sensing per se is insufficient; rather, detecting the slippage and direction of applied pressure (i.e., differentiation of normal and tangential forces) is critical. Since slippage requires dynamic input detection, piezoelectric^[222] and triboelectric devices are often used.^[224,225] Ko and co-workers fabricated parallel ridges on the surface of a PVDF-based piezoelectric pressure sensor to detect texture-induced vibrations, showing

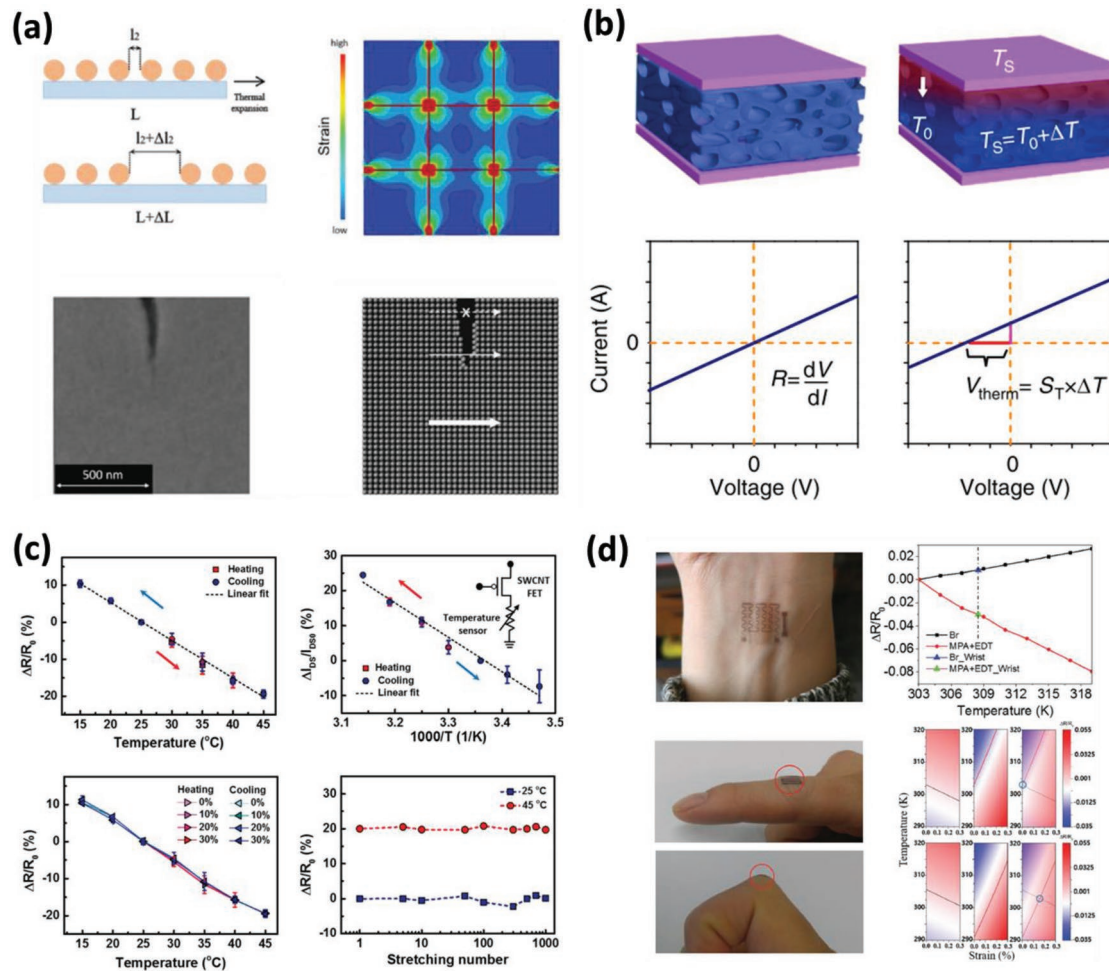


Figure 13. a) The charge transport properties of nanocrystal-based temperature sensor controlled by nanocracks, generated by thermal expansion. Reproduced with permission.^[220] Copyright 2019, Wiley-VCH. b) Thermoelectric temperature sensor based on porous PU and PEDOT:PSS. Reproduced with permission.^[223] Copyright 2015, Macmillan Publishing Ltd. c) Thermoresistive temperature sensor with polyaniline nanofiber, showing high linearity and low hysteresis. Reproduced with permission.^[214] Copyright 2015, Wiley-VCH. d) Temperature sensor comprising of two sensors with different coefficient of resistance, capable of differentiating strain and temperature. Reproduced with permission.^[217] Copyright 2017, Wiley-VCH.

that the surface roughness of various materials can be detected, i.e., exhibits texture perception capability (Figure 14a).^[222] Zhang and co-workers fabricated a fingerprint-inspired triboelectric nanogenerator for the detection of slippage and demonstrated that the responsiveness of each spiral CNT/PDMS electrode in the sensor to moving objects allows the detection of slip direction (Figure 14b).^[224]

To discriminate between normal and tangential forces, force direction can be obtained by simultaneously measuring multiple electrical signals (resistance or capacitance) on a single taxel. For example, Beccai and co-workers fabricated a force sensor comprising of one top electrode and four bottom electrodes separated by a dielectric material,^[226] showing that the measurement of four capacitances allows the differentiation of normal and tangential forces (Figure 14c). Bergbreiter and co-workers reported a force sensor by placing four blocks of conductive materials near each other, one block in the center surrounded by three blocks (Figure 14d).^[227] Upon the application of different force directions, the relative distances or contact area between the center and the surrounding blocks changed, through which

the force vector can be calculated. The output signal can be obtained both as capacitance or resistance. The authors also presented a human hand-attachable sensor array capable of detecting shear and normal loads. Moreover, Bao and co-workers made a capacitive sensor with pyramid structure as the top electrode and 25 bottom electrodes on a dome-like structure (Figure 14e).^[168] The application of different directions of force resulted in different capacitances between the top and bottom electrodes, through which force vector was deduced. The sensor was attached to an artificial hand and detected pressure and shear force in real time when the robot arm moved or held a light object.

3.4. Multifunctional Sensors and Decoupling Technology

The ability of the human skin to simultaneously detect and distinguish various external stimuli (e.g., pressure, strain, vibration, and temperature) can be attributed to the presence of various sensory receptors. These receptors include mechano-

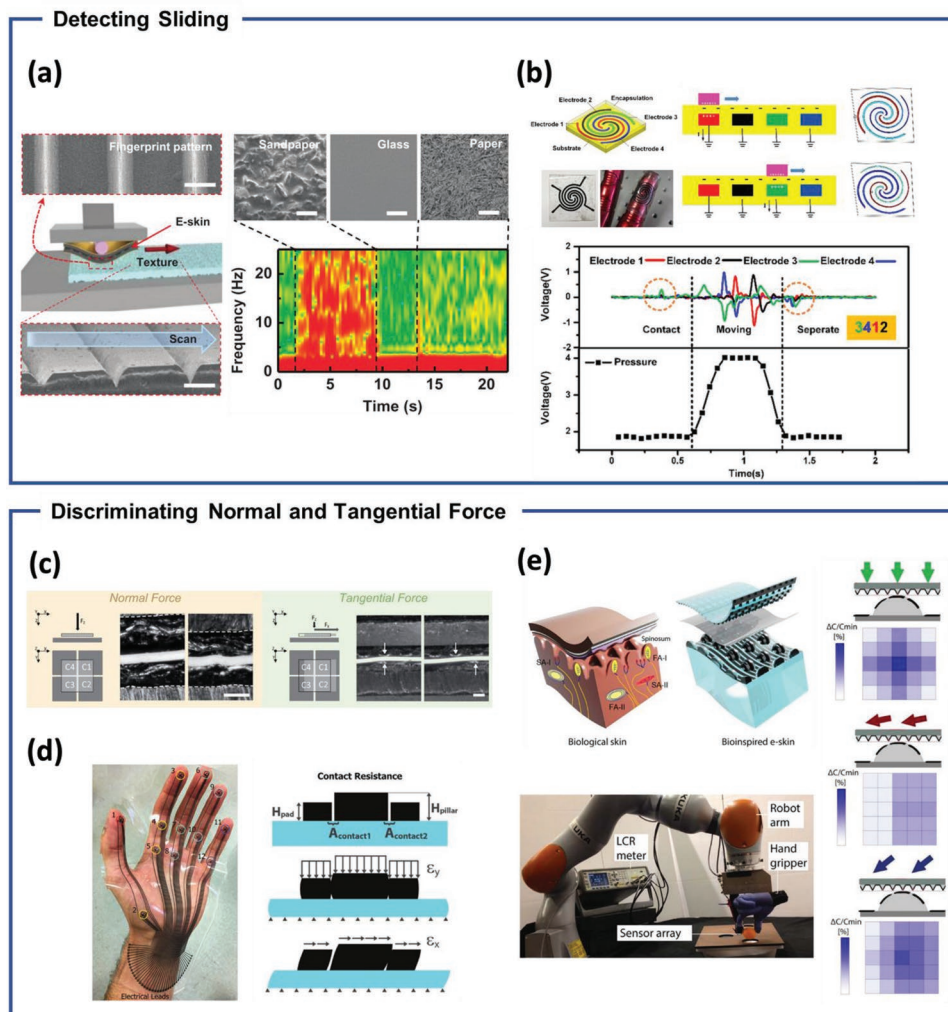


Figure 14. a) Texture-perceiving piezoelectric PVDF sensor detecting texture-induced vibration and featuring parallel ridges on the surface. Reproduced with permission.^[222] Copyright 2015, AAAS. b) Fingerprint-inspired triboelectric nanogenerator for sliding detection. Reproduced with permission.^[224] Copyright 2018, Elsevier. c) Capacitive sensors with one top and four bottom electrodes. Measurement of four different capacitance values across the top electrode and each of the bottom electrodes can distinguish between normal and tangential forces. Reproduced with permission.^[226] Copyright 2014, Wiley-VCH. d) Force vector sensor with three conductive blocks surrounding a center block. The relative change in contact resistance between the three blocks and the center block detected to measure tangential forces. Reproduced with permission.^[227] Copyright 2016, Wiley-VCH. e) Bioinspired e-skin based on pyramidal and dome structures detecting the direction of forces and the contact location. Reproduced with permission.^[168] Copyright 2018, AAAS.

thermo-, and nociceptors, and each receptor is specialized in detecting a specific stimulus and transmitting corresponding nerve impulses to the brain. In order for e-skin fully mimic the sensing properties of human skin, it should have the ability to detect and distinguish multiple stimuli.

Due to Poisson's effect or coupling of various mechanical stimuli, mechanical tactile inputs induce similar changes in the output signal of a typical capacitive or piezoresistive sensor. This complicates the discrimination between the tactile inputs. One strategy to overcome this limitation is to measure multiple output signals from a single device; the analyses of each signal and their combined signal patterns enable the distinguishing of tactile inputs. Bao and co-workers employed a porous PDMS-SWCNT film device to differentiate pressure, strain, and bending by measuring capacitance across porous PDMS

and the resistance of the SWCNT film (Figure 15b).^[228] An electronic fabric consisting of intertwined composite fibers with a piezoresistive rubber was reported to detect and differentiate pressure, strain, and bending^[229] by simultaneously measuring the resistance of each intertwined composite fiber and that of the piezoresistive rubber.

Another approach to distinguish mechanical stimuli is to fabricate a sensor sensitive to a single stimulus (Figure 15a). Someya and co-workers fabricated a bending-insensitive pressure sensor using composite nanofibers (Figure 15c).^[230] In this sensor, uniformly dispersed nanofibers change their alignment and accommodate to the bending deformation, thereby minimizing strain on an individual fiber under bending, which keep the resistance of the sensor constant under bending. On the other hand, when normal pressure

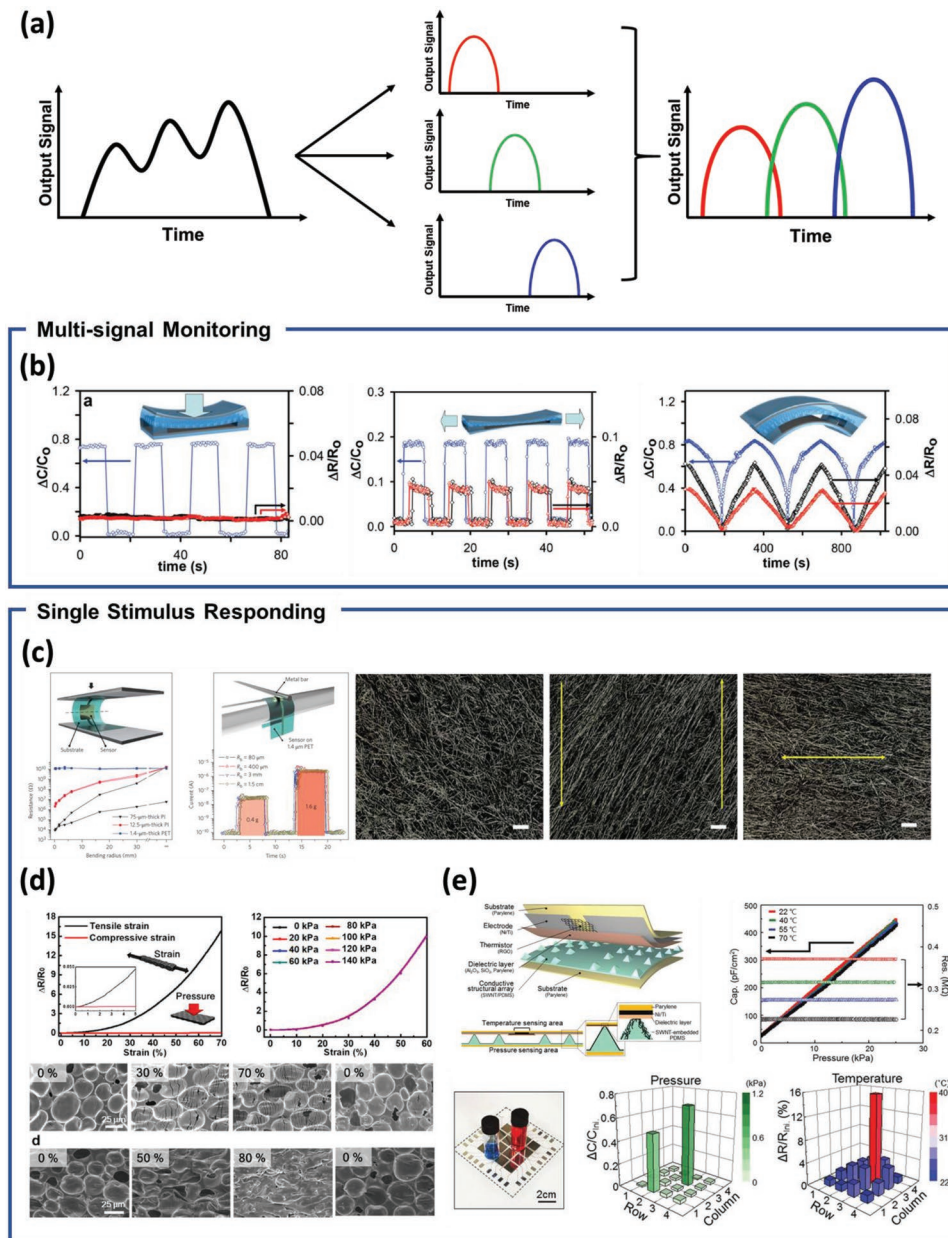


Figure 15. a) Decoupled output signals obtained from various simultaneously incoming input signals. b) Multifunctional tactile sensor comprising of porous dielectric layer and PDMS/SWCNT-based electrodes, capable of differentiating pressure, strain, and bending. Reproduced with permission.^[228] Copyright 2014, Wiley-VCH. c) Bending-insensitive pressure sensor containing composite nanofibers. Reproduced with permission.^[230] Copyright 2016, Macmillan Publishing Ltd. d) Pressure-insensitive strain sensor comprising porous CNT/PDMS composites. Reproduced with permission.^[209] Copyright 2018, American Chemical Society. e) Bimodal pressure and temperature sensor comprising of SWCNT-coated pyramidal PDMS and reduced graphene oxide. Reproduced with permission.^[183] Copyright 2018, Wiley-VCH.

is applied, CNTs efficiently form conductive paths with graphene fillers, which dramatically changes the resistance of the sensor even under very small pressure. Park and co-workers fabricated a pressure-insensitive strain sensor using porous CNT/PDMS composites,^[209] showing that the resistance of the microporous MWCNT/PDMS structure changed under lateral strain due to the formation of cracks in the CNT percolation network in the PDMS matrix (Figure 15d). On the other hand, the application of pressure closed the pores rather than

forming cracks. The deformation of pores under pressure was attributed to minimizing the change in the CNT percolation network, which consequently resulted in negligible resistance change. Lee and co-workers realized a strain-insensitive stretchable pressure sensor by controlling the local strain using a micropattern.^[231] Such single stimulus-sensitive sensors do not suffer from signal interference between different stimuli, which allows for facile signal processing when they are integrated into a sensor array.

Discrimination between mechanical and thermal stimuli is also important to properly mimic human skin. For example, Park and co-workers fabricated a pressure sensor that is negligibly sensitive to strain and temperature. The pressure sensors were fabricated on relatively rigid PDMS islands embedded in relatively soft elastomeric substrate. The use of capacitive sensor rendered the sensor insensitive to temperature.^[173] Cho and co-workers reported a bimodal sensor comprising of a capacitance pressure sensor and a reduced graphene oxide (rGO)-based thermoresistive sensor.^[183] The integrated sensor was designed so that the rGO did not experience pressure, and since capacitance sensor is by nature insensitive to temperature, pressure and temperature was differentiated (Figure 15e). Zhu and co-workers fabricated a pressure/temperature sensor based on PEDOT:PSS coated PU frames. Since thermoelectric and piezoresistive effects result in different IV characteristics, temperature and pressure were distinguished.^[223] Park and co-workers employed highly ordered microporous structures to fabricate capacitive and piezoresistive sensor and integrated two different sensors into a single taxel to distinguish pressure and temperature.^[167] Apart from these sensors, as mentioned above, temperature sensors that are insensitive to strain have been developed primarily by utilizing geometries such as serpentine, net-shaped, and island structures to minimize strain imposed on the material itself.^[211,212,214,219] Using such temperature sensors along with other sensors that are sensitive to a single stimulus, Wang and co-workers reported an integrated sensor array that can detect and distinguish pressure, strain, temperature, humidity, light, and magnetic force.^[232]

3.5. Challenges and Outlook

Despite the abundance of materials and structures that have been used to improve the performance of tactile sensors, there are still a variety of issues that need to be resolved for practical applications. First, manufacturing of sensors with high uniformity is of great importance. If for instance, sensors are used as an array, large sensor-to-sensor variability would require every sensor to be individually calibrated, rendering operation exceedingly difficult as complex circuitry would be needed. As the number of sensors in the array increases, tolerance toward sensor-to-sensor variability significantly decreases, making operation virtually impossible. For bulk composite-type piezoresistive sensors, the aggregation and nonuniform dispersion of conductive material in the elastomer matrix would intrinsically generate sensor-to-sensor variability. As the sensor size shrinks, such variability will increase. To solve these issues, uniform dispersion techniques will need to be developed that depends less on the random dispersion but rather on ordered and spatially controlled dispersion. In porous type capacitive and piezoresistive sensors, the pore size and shape variability has been shown to contribute to sensor-to-sensor variability.^[167,185] Hence, pore size uniformity is of great importance to ensure uniformity in sensors. In the future, the tactile sensor research community should specifically report uniformity of their sensors to further gauge the legitimacy of their technology toward practical applicability.

Currently in literature, focus is geared toward performance metrics such as sensitivity, gauge factor, dynamic range, and linearity. Although these are important parameters, hysteresis is also of great importance for practical applications, as explained above. Despite their importance, there is currently a lack of reports that specifically quantify the level of hysteresis in their sensors. Furthermore, as mentioned above, standardization of response and recovery time is of high importance. Response and recovery time can only be compared if the applied magnitude and the rate of pressure or strain are standardized. Similarly, reported sensitivity values are difficult to compare as sensitivity depends on the pressure range under which it is calculated. In addition, for piezoresistive sensors, researchers in some cases use output signal other than resistance (e.g., current, voltage, and conductance); hence, one must be cautious when comparing sensitivities between different sensors.

Also, despite the numerous research on differentiation of various stimuli, this is still a challenging issue. A sensor that is only responsive to a single stimuli is difficult to design and fabricate, especially when considering both mechanical stimuli and temperature change. For example, piezoresistive sensors would intrinsically be sensitive to temperature and rendering it temperature insensitive is a major challenge. In addition, although there is comparatively numerous report on pressure and strain sensors, slip and force vector sensors have been rarely reported. These sensors are essential for texture discrimination and object manipulation; hence, such sensors should be further developed in the future. Finally, although self-healing tactile sensors are desirable to fully mimic the properties of human skin, their sensing properties (especially with respect to hysteresis and response/recovery time) are currently sub-par. A highly elastic self-healing material would be ideal and should be researched upon in the future.

4. Progress and Future Prospects of Sensors for Health Monitoring

In addition to tactile sensing capabilities, detection of other physical and chemical information from the body will enable precise monitoring of basic health and early diagnosis of a variety of diseases. This section summarizes the recent advances in skin attachable chemical and electrophysiological sensors. The reader is also encouraged to refer to the following review articles regarding this topic.^[233–244]

4.1. Chemical Sensors

Biofluids typically contain electrolytes, metabolites, and hormones. Consequently, chemical sensors that detect and analyze such biomarkers will provide important physiological information at the molecular level,^[245,246] which will in turn enable early diagnosis and prevention of diseases, e.g., both the shortage and excess of heavy metals have detrimental effects on the human body.^[247] Therefore, constant monitoring of heavy metal concentration allows for appropriate actions to be taken. In this regard, skin-attachable chemical sensors for medical purposes are highly sought after. Over the past

few years, much research effort has been directed at chemical sensors, which have usually been fabricated on flexible substrates to ensure wearer comfort.

4.1.1. Working Principles of Chemical Sensors

Chemical sensors are primarily composed of electrochemical devices, chemiresistors, and transistors.^[1] Once exposed to target chemicals, these devices typically show changes in potential, current, or resistance. Exposure of electrochemical sensors (which contain reference, working, and auxiliary electrodes) to target analytes leads to a change of potential (for charged analytes) or current (for redox-active analytes). For instance, potentiometric sensors generally use ion-selective electrodes to selectively respond to target analytes, whereas in amperometric sensors, electrode-immobilized enzymes catalyze the redox reactions of target materials.^[242,248] Chemiresistors are composed of a sensing element in between two electrodes; the resistance of the sensing element changes upon the exposure to target analytes. Finally, transistor-based chemical sensors feature a semiconducting layer, a dielectric layer, and three (source, drain, and gate) electrodes. In other words, transistors can be viewed as chemiresistors modified with an added dielectric layer and a gate electrode to allow for signal amplification and high sensitivity.^[1,236,249]

The use of chemical sensors in practical applications requires many factors to be taken into account. For example, biofluids in human bodies contain chemicals at low concentrations; therefore, practically applicable chemical sensors should exhibit high selectivity, low limit of detection, high sensitivity (to precisely determine analyte concentrations), and a high level of repeatability.

4.1.2. Acquisition of Biofluids

Blood is the most widely used biofluid in medical clinics; however, invasive finger-pricking to extract blood limits their real-time and long-term usage. Thus, minimally invasive or noninvasive acquisition of biofluids is required for skin-attachable chemical sensors. Examples include tears, saliva, urine, sweat, and interstitial fluid (ISF).^[238,241,242,250] Among these biofluids, the analysis of tears, saliva, and urine samples is of inconvenience to the user. Thus, sweat and ISF sensors are preferable for long-term usage and comfort.^[238,250]

Sweat is acquired through vigorous exercise or exposure to heat. However, the chemical composition of sweat dynamically reflects physiological changes in the human body and therefore depends on the stimulation mechanism. In other words, the composition of sweat produced by exercise or heat may not be representative of the regular state of health. Therefore, health monitoring requires the use of local and on-demand sweat generation techniques such as iontophoresis, a process that stimulates local sweat secretion (Figure 16a)^[238,239] utilizing a sweat-inducing compound called pilocarpine. Specifically, a mild electric current causes pilocarpine to flow into the skin and stimulate sweat glands, which leads to the release of sweat. Secretions above $100 \text{ nL min}^{-1} \text{ cm}^{-2}$ can be acquired without

causing any discomfort to the subject,^[251] and this noninvasive and safe sweat generation technique has been approved by the FDA.^[252] Similarly, ISF can be acquired through reverse iontophoresis (Figure 16a).^[238,239] Unlike direct iontophoresis, reverse iontophoresis does not require the use of drugs and is based on the migration of certain chemicals (such as ions and glucose in the ISF) toward the skin surface once a mild current is applied to the epidermis. A single device can also be used to withdraw sweat and ISF at the same time by combining direct and reverse iontophoresis, enabling multiplexed chemical sensing.^[253]

4.1.3. Sweat Sensors

The past few years have witnessed significant advances in the field of wearable sweat sensors, as exemplified by the development of a wide range of sweat sensors for analyzing glucose,^[239,246,251,253–256] lactate,^[246,256–259] ethanol,^[253,260–263] pH,^[248,254–256,264,265] and electrolytes.^[246,251,252,256,259,266,267] These wearable sweat sensors are mostly composed of electrochemical electrodes. Specifically, amperometry is often used for the enzymatic detection of ethanol and metabolites, while charged species are mostly detected by potentiometry.^[268]

As mentioned above, amperometric sensors usually utilize redox reactions of biomolecules. In such devices, enzymes such as lactate oxidase, glucose oxidase, and alcohol oxidase are immobilized on the electrodes to allow for selective oxidation/reduction of target analytes.^[239,246,251,254,255,257–259,261–263] Since the measured current increases with analyte concentration, the latter parameter can be deduced from the former. For example, Mercier and co-workers developed a skin-worn wearable sensory system that detects both lactate and ECG signal^[258] (Figure 16c). Specifically, the lactate sensor utilized a working electrode functionalized with lactate oxidase, where the increase in current was correlated to lactate concentration in sweat.

Ion-selective electrodes are often used for potentiometric sensors, such as those previously developed for the detection of charged species (e.g., ammonium, potassium, and sodium ions as well as protons) in sweat.^[246,248,251,252,254,255,259,266,267] The electric potential of an ion-selective electrode strongly depends on the target analyte concentration, and analyte concentration can consequently be deduced from the potential difference between working and reference electrodes. Davis and co-workers fabricated a real-time wearable sensor system that extracts sweat and measures target analytes such as glucose, Na^+ , and Cl^- .^[251] Specifically, ion-selective electrodes were used, where the increase in ion concentrations led to a potential change. This potentiometric analysis inherently follows the Nernst equation, i.e., the sensitivity of electrolyte sensors is limited to 59 mV per one order of magnitude difference in concentration.^[265] Recently, Takei and co-workers used a charge-coupled device to develop a pH sensor that exceeded this sensitivity limit (Figure 16d),^[264,265] achieving a high sensitivity of 240 mV pH^{-1} by the accumulation of electron charge transfer cycles. More importantly, this strategy can potentially be applied to the detection of other electrolytes using ion-sensitive membranes. The pH sensory system attached to a human arm successfully monitored pH and temperature in real time.

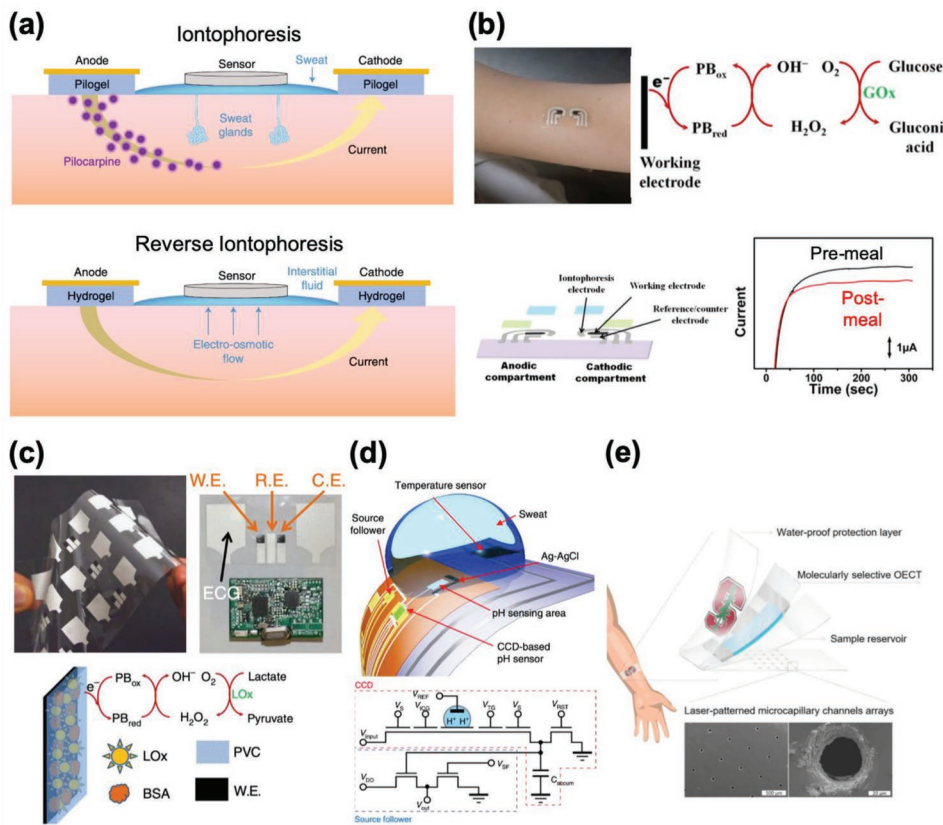


Figure 16. a) Schematic of iontophoresis and reverse iontophoresis. Sweat can be extracted electrochemically using a drug “pilocarpine.” Acquisition of interstitial fluid can be performed without a drug using reverse iontophoresis. Reproduced with permission.^[238] Copyright 2018, Macmillan Publishing Ltd. b) Glucose sensors using interstitial fluids. Redox reaction of glucose resulted in current change. Current change was significant after meal. Reproduced with permission.^[274] Copyright 2015, American Chemical Society. c) Sweat sensors for lactate and ECG. Simultaneous monitoring of lactate and ECG offered comprehensive information about health. Reproduced with permission.^[258] Copyright 2016, Macmillan Publishing Ltd. d) Sweat pH sensor with high sensitivity of 240 mV pH⁻¹. High sensitivity was achieved using a charge-coupled device format. Reproduced with permission.^[264] Copyright 2018, Macmillan Publishing Ltd. e) Sweat sensor capable of detecting cortisol. Molecularly selective OECTs exhibited change of current depending on cortisol concentration. Reproduced with permission.^[271] Copyright 2018, AAAS.

Hormones in biofluids can also be characterized by chemical sensors. However, the realization of reliable hormone sensors is hindered by their extremely low concentrations in biofluids. For example, despite the importance of cortisol (a stress-level-indicative hormone) as a biomarker, its detection in sweat has been described in only a few studies.^[269–271] Salleo and co-workers developed a cortisol sensor based on organic electrochemical transistors (OECTs) (Figure 16e)^[271] comprising a molecular imprinted layer that selectively binds to cortisol. In this sensor, bonding between cortisol molecules and the imprinted layer blocks the motion of ions and ultimately prohibits active layer doping, which allows cortisol concentration to be deduced from the change in current across OECTs. This OECT-based cortisol sensor was applied to a human forearm for real-time monitoring of cortisol in sweat. After physical exercise, significant current change was observed for the cortisol sensor, while the control device showed negligible response.

Finally, fully integrated chemical sensors for multiplexing are highly sought after. Although single-analyte biosensors can offer some information on health, the interpretation of such information may sometimes be misleading, as multiple

factors could result in the same outcome. Conversely, the actual causes of a physiological event can be clearly identified when multiple sensors are integrated into one platform. Javey and co-workers fabricated fully integrated wearable sensors for the *in situ* analysis of sweat (Figure 17a).^[246,250] This sensor platform simultaneously characterized glucose, lactate, sodium ion, and potassium ion concentrations, while employing temperature information for calibration purposes. More importantly, no external analysis was required, and all necessary information could be wirelessly transferred to portable devices and cloud servers. Kim and co-workers integrated a heater, along with temperature, humidity, glucose, and pH sensors into a single skin-attachable device (Figure 17b).^[254,255] Once a critical humidity value was reached by sweat secretion, the glucose sensors started functioning simultaneously with temperature and pH sensors, which corrected the glucose readings. This integrated device also contained microneedles capable of releasing drugs for diabetes treatment upon exposure to heat. High concentrations of glucose measured by glucose sensors activated heaters and hence triggered drug release.

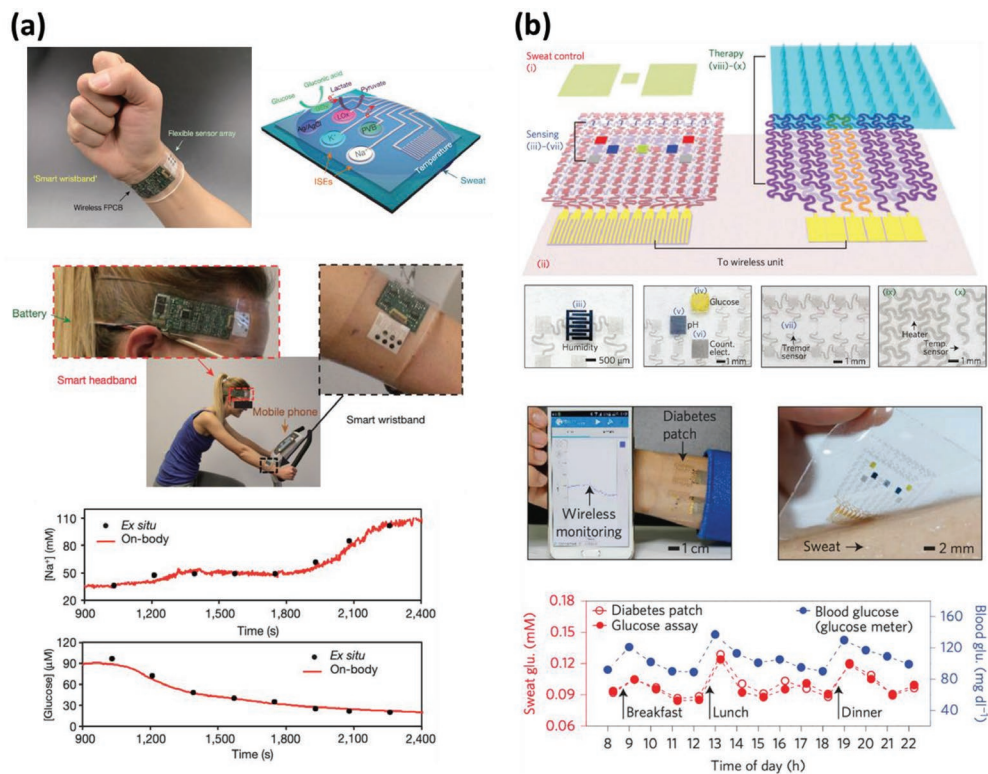


Figure 17. a) (top, left) A fully integrated wristband-type sweat sensor. (top, right) This sensor monitored temperature, metabolites, and electrolytes. (middle) The sweat sensor could have various shapes such as a headband, and a wristband. Monitored fitness information was directly transferred to a mobile phone. (bottom) Real-time concentrations of Na^+ and glucose measured using the multiplexed sensor. Ex situ and on-body concentrations had a good correlation. Reproduced with permission.^[246] Copyright 2016, Macmillan Publishing Ltd. b) (top) Schematic of a multiplexed sweat sensor with magnified optical images of sensors. (middle) Images of the sensors attached to human skin. The diabetes control system communicated with a mobile phone wirelessly. (bottom) Glucose concentration was measured using the integrated sensor. Glucose concentration increased after meals. Notably, sweat glucose and blood glucose levels showed a good correlation. Reproduced with permission.^[255] Copyright 2016, Macmillan Publishing Ltd.

4.1.4. ISF Sensors

In 2001, FDA approved the very first commercial noninvasive glucose sensors, namely GlucoWatch biophysiess.^[272,273] These wristband-type sensors used reverse iontophoresis to extract ISF and analyzed its glucose levels, which could be correlated to blood glucose levels. Importantly, GlucoWatch performed periodic glucose concentration measurements, which is desirable for patients with diabetes. However, many users of GlucoWatch reported discomfort and skin irritation,^[238,239,245,274] and the production of these sensors was subsequently decommissioned.^[237]

Recently, Wang et al. fabricated tattoo-like glucose sensors (Figure 16b)^[274] that demonstrated the significant increase of glucose level upon food ingestion. Skin-like noninvasive glucose sensors have also been developed,^[275] allowing accurate correlations between glucose concentrations in the ISF and blood. Finally, ISF sensors were integrated with sweat sensors for multiple analyte analysis, e.g., the levels of ethanol in sweat and glucose in ISF have been simultaneously measured.^[253] This skin-attachable sensor system for dual epidermal fluid analysis can be further developed to simultaneously monitor various biomarkers.

4.1.5. Challenges and Outlook

Several challenges remain before wearable chemical sensors can be commercialized. First, the correlation between analyte concentrations in blood and other biofluids should be extensively studied. Several studies have revealed that the concentration of some biomarkers in sweat or ISF is strongly correlated with that in blood.^[276,277] For practical applications of wearable chemical sensors, the correlation should be investigated for each target biomarker of interest, and a method to calibrate person-to-person variations should be developed.

Next, one should resolve several challenges related to sample acquisition. That is, although direct and reverse iontophoresis enable on-demand local secretion of biofluids, the extracted fluids may get altered before measurement. For example, the chemical composition of sweat may change as a result of evaporation on the skin surface, contamination with chemicals on the skin, and mixing with older sweat,^[238] which may negatively affect the accuracy of sensor readings.

The long-term stability and reliability of sensing materials could also present a problem, especially for enzyme-based bioelectronics. The detection of several biomolecules strongly relies on the use of enzymes, which may lose their activity

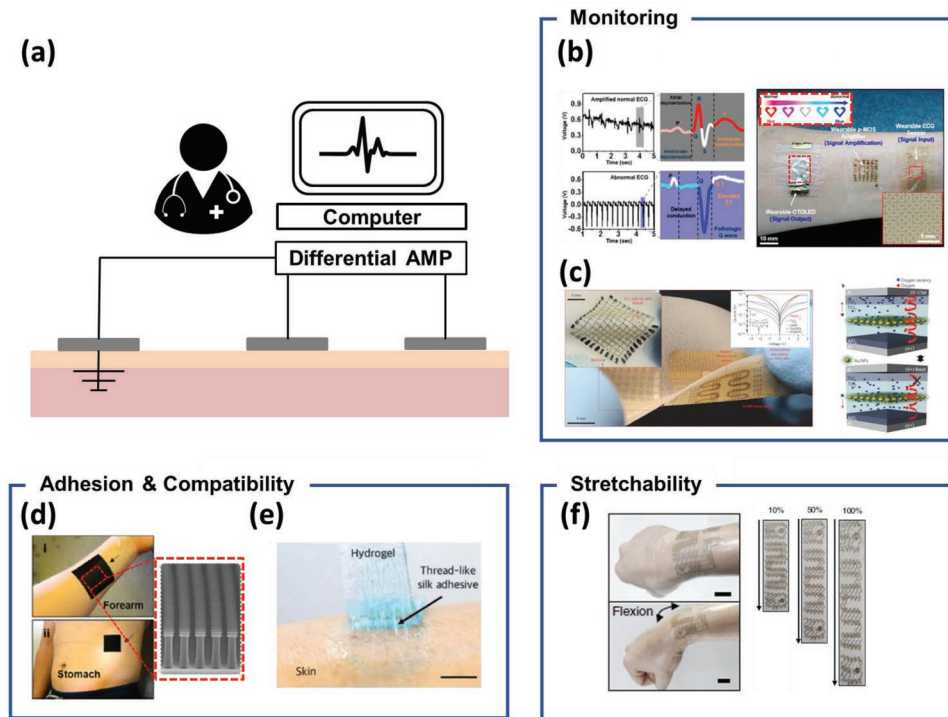


Figure 18. a) Illustration of electrophysiological sensing, which require the use of multiple (ground, reference, and sensing) electrodes and a computer. b) Organic materials employed for visualized ECG monitoring (e.g., consisting of CTOLEDs, CNT transistor amplifiers, etc.). Reproduced with permission.^[283] Copyright 2017, American Chemical Society. c) Wearable sensing devices with TiO₂-Au-based RRAM that can save the recorded EP signal at low power. Reproduced with permission.^[284] Copyright 2014, Macmillan Publishing Ltd. d) Strongly adhesive carbon nanocomposite-based electrode inspired by gecko feet structure. Reproduced with permission.^[285] Copyright 2016, American Chemical Society. e) Biocompatible and strongly adhesive electrodes based on Ca²⁺-modified silk. Reproduced with permission.^[286] Copyright 2018, Wiley-VCH. f) Highly stretchable, conductive, and biocompatible device based on Au sheath-coated Ag NWs. Reproduced with permission.^[49] Copyright 2018, Macmillan Publishing Ltd.

over time and hence complicate long-term usage. This activity change may occur through biofouling,^[242] i.e., the adsorption of biomolecules on sensors may disrupt the reactions of target analytes. Further, enzyme activity should be calibrated while considering environmental factors such as pH and temperature,^[241,242] that is, enzyme-based sensors should preferably be fully integrated systems containing temperature and pH sensors.^[242,246,254,255]

From a materials point of view, chemical sensors developed so far are mostly based on rigid or flexible materials, which presents a problem, since the repeated deformation of sensors may degrade their performance. Factoring in the importance of long-term sensor reliability, this problem should also be addressed, possibly via the use of stretchable materials and devices.^[240] For example, several wearable chemical sensors based on intrinsically stretchable materials and novel geometric designs have been reported,^[254–256,278,279] and the further development of stretchable chemical sensors is believed to facilitate the realization of mechanically robust health monitoring systems.

4.2. Electrophysiological Sensors for the Detection of Biopotential Signals

In view of the fact that organ, tissue, and neuronal activities are related to electrical potential, the monitoring of

electrophysiological (EP) signals can help detect abnormal vital signs. In particular, heart (electrocardiography: ECG), muscle tissue (electromyography: EMG),^[280] and brain (electroencephalography: EEG)^[281] related diseases such as arrhythmia, myocardial infarction, neuromuscular diseases, and epileptic seizures can be diagnosed using EP monitoring systems.^[233,244] Normally, an EP sensor is composed of three types of electrodes (recording, reference, and ground) conformally contacting the skin (Figure 18a). Ground electrodes are attached on a zero-potential area, as they define the base line of a sensory circuit, while recording and reference electrodes are placed on the targeted body part and extremities, respectively. For example, an ECG sensor needs 10 electrodes, six of which are attached to the thorax close to the heart (targeted body part), while the remaining four electrodes are placed on the extremities (arms and legs). These 10 electrodes read 12 distinctive electric signals recorded from different electrode combinations to allow physicians to diagnose abnormal heart activity at different anatomical areas.^[282]

A conventional EP sensing system features bulk electrodes affixed to the target regions of the body with tape, clamps, or sticky pads. In addition, the electrodes are kept in contact with the skin using a conductive medical gel. Although this platform results in accurate electrical reading, the use of such platform is inconvenient to the patient due to the movement restriction imposed by the large, rigid, and heavy electrodes.

To overcome these limitations, Rogers and co-workers introduced the new concept of a soft, ultrathin, and lightweight biocompatible epidermal electronics system (EES).^[10] This electronic device is fabricated by attaching filamentary serpentine-shaped metal interconnects to a soft elastomer to tune the mechanical properties of systems to match those of human skin. The above researchers employed this system to successfully record ECGs and EMGs, and demonstrated its integration with other electronic components such as strain sensors, wireless power supplies, and LEDs.

Conventionally, an EP signal is monitored by physicians in a hospital due to the complexity of signal analysis. To make EP signal monitoring suitable for homecare, Kim and co-workers fabricated an organic-based ECG monitoring system that changes color when an abnormal cardiac signal is detected (Figure 18b).^[283] In this system, red light is emitted under normal conditions, while blue light is emitted as an alarm for abnormal heart activity. In both cases, emission occurs through a CNT transistor amplifier and a CTOLEDs (color-tunable organic light-emitting diodes)-based display device.

The abovementioned EP monitoring systems can only be used connected to an external computer. Kim and co-workers developed a multifunctional device with a memory so that signal can be measured and stored without the need of an external computer (Figure 18c).^[284] The researchers recorded muscle activity in a memory cell, and monitored the tremor frequency to detect epilepsy or Parkinson's disease. The device exhibited low power operation due to the use of TiO₂–Au NP composite-based resistive RAM. This paper provided a proof-of-concept of portable EP monitoring system.

Strong adhesion of the electrode to the skin while ensuring firm electrical contact without the use of wet gel is also important for it to be a portable point-of-care diagnostics system. Jeon and co-workers developed a carbon nanocomposite-based electrodes with the surface structure of gecko's foot, which is known for its exceptional adhesion property (Figure 18d).^[285] This electrode was able to make strong electrical and physical contact with the skin, allowing ECGs to be measured without electrode detachment during activities. Strongly adhesive electrodes can also be fabricated by the exploitation of chemical properties of the electrode material, e.g., calcium-modified biocompatible silk fibroin has been used to prepare biocompatible electrodes that can be strongly attached to skin (Figure 18e).^[286] In this case, intercalated Ca²⁺ ions enhanced physical interlocking at the electrode–skin interface, allowing ECG measurement during active movement. Even if a sensing device can be securely attached to skin, it should not exert side effects such as skin irritation. In this regard, Someya and co-workers introduced an open Au nanomesh network that does not interfere with the air ventilation of the skin,^[154] and is therefore expected to be a suitable interfacing material for long-term EP signal recording.

Stretchability is also an important feature in electrodes as it enables conformable contact to irregularly shaped regions of the body and does not prevent breakage during daily activities where the skin is under repeated stretching. Ag NWs, which can serve as stretchable electrodes, offer numerous advantages such as excellent conductivity and ease of processability. However, the use of Ag is still challenged by the lack of biocompatibility and poor oxidation resistance. In this regard,

Kim and co-workers reported a Au sheath-coated Ag NW-based stretchable electronic device that combined the benefits of Au (biocompatibility and oxidation resistance) and Ag NWs (excellent conductivity and stretchability (maximum 840%)) (Figure 18f).^[49]

Despite the continuous development of EP signal-recording devices, they are still far from being of practical use in skin-attachable electronics due to their a) spatial restrictions owing to the fact that they need to be connected to an external computer with wiring, b) long-term chemical instability and biocompatibility, c) low robustness of the electrical and physical contact to skin under real-life daily activities. Thus, future work should be focused on the design of EP sensing systems with wireless communication capability, better chemical stability, epidermis compatibility, and strong adhesion to skin. For other reviews regarding this topic, refer to the following articles.^[233,244]

5. Fabrication and Integration

Fabrication and integration of sensors and their communication with our body or other external devices are exceedingly important for practical applications. In this section, we describe strategies to attain spatial resolution in tactile sensors, solution-based process for large-area device fabrication, and various types of communication strategies such as wireless signal processing, neuromorphic devices for bioinspired signal processing, and electrodes for neural interfaces. Wireless signal processing is particularly important for skin-attachable devices for healthcare monitoring, while in the case of prosthetics, the connection of electrodes to nerves is important.

5.1. Spatial Tactile Sensing

The accurate detection of human motion and tactile sensing requires high spatial resolution. The required spatial resolution differs depending on the body part the e-skin is mimicking. For instance, fingertip has the highest spatial resolution of about 1 mm while that of the palm is about 5 mm.^[287,288] Numerous researchers have worked on developing passive matrix arrays of pressure^[175,184,289] and strain^[196,202,290,291] sensors. For example, Bao and co-workers fabricated polypyrrole hydrogel-based 8 × 8 pressure sensor array (Figure 19a),^[292] while Hata and co-workers attached several strain sensors to each folded part of a glove finger^[196] to detect the bending motion of finger joints. However, since these sensors are large and limited in number, their spatial resolution is limited. The increase in sensor density in passive matrix, however, causes signal interference (crosstalk) due to the reduction of analog signal intensity of the smaller sensors, and the increase in the number of and the decrease in the spacing between interconnect lines.^[293]

To resolve the above issues, tactile sensors can be integrated with thin-film transistors (TFT) to form an active matrix, which can map 2D pressure distribution with low crosstalk while maintaining high spatial and temporal resolution. In contrast to passive matrix, active matrix allows random and individual access to each taxel with fast response time, attributed to shared electrode lines. Also, active matrix significantly reduces the

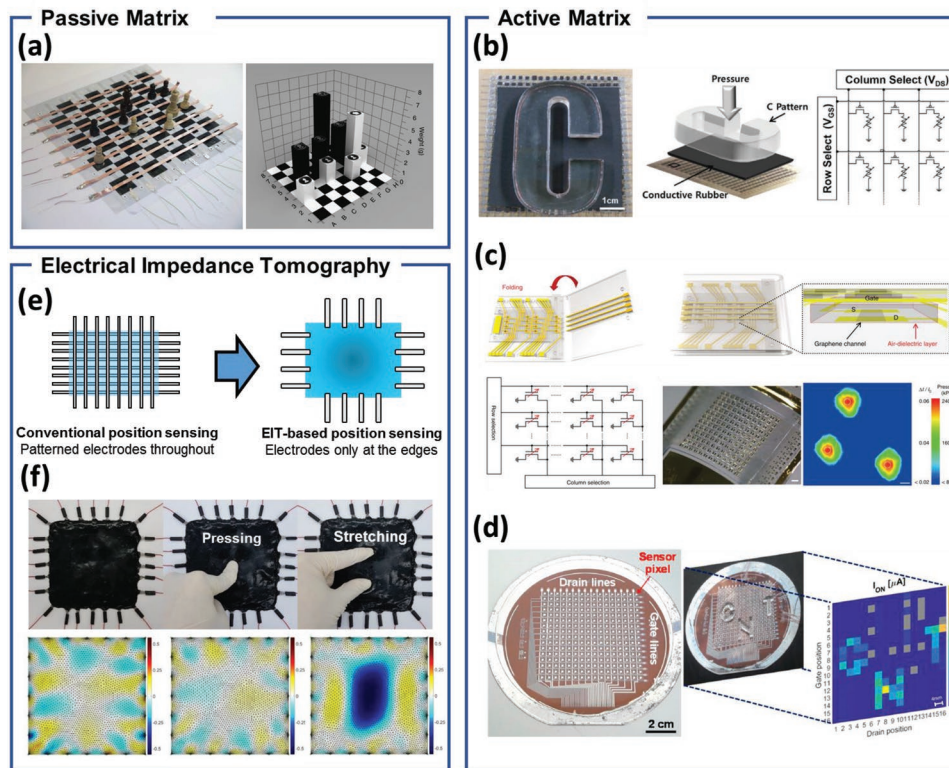


Figure 19. a) Polypyrrole hydrogel-based 8×8 pressure sensor array. Reproduced with permission.^[292] Copyright 2014, Macmillan Publishing Ltd. b) Large-area tactile sensing active matrix using carbon nanotube-based backplanes. Reproduced with permission.^[294] Copyright 2015, Wiley-VCH. c) Pressure-sensitive air-dielectric graphene FET-based active matrix. Reproduced with permission.^[295] Copyright 2017, Macmillan Publishing Ltd. d) 16×16 active matrix pressure sensing array with carbon nanotube thin-film transistors. Reproduced with permission.^[299] Copyright 2018, American Chemical Society. e) Schematic depiction of electrical impedance tomography (EIT). f) Large-area detection of local strain using EIT. Reproduced with permission.^[209] Copyright 2018, American Chemical Society.

number of addressing lines in a large $m \times n$ array from $m \times n$ to $m + n$ (i.e., a column or a row of the array shares a single word or bit line.) (Figure 19b).^[294] Additionally, active matrix addressing requires lower power consumption than passive matrix addressing.^[3]

To form a pressure sensing active matrix, capacitive pressure sensors are often used as transistor gate dielectrics,^[171,295,296] and resistive pressure sensors are often connected to the transistor drain.^[230,297,298] However, the fabrication of such devices requires complicated device layouts and expensive fabrication processes to bond pressure sensors to individual transistors.^[297] Recently, Park and co-workers demonstrated a simple active matrix fabrication technique by folding two opposing panels of an origami substrate to form an air-dielectric in every sensor over a 12×12 array (Figure 19c).^[295]

The performance of transistors such as mobility and current density dictates the speed and power consumption of the active matrix array. Han and co-workers have developed a 16×16 tactile sensing active matrix using CNT TFTs, exhibiting the fast response time of less than 30 ms, and high spatial resolution of 4 mm with a low operating voltage of 3 V (Figure 19d).^[299] Response time is also dependent on the overall RC delay of the circuit. High sensor density would naturally increase the resistance due to the thinner interconnect lines, and increase the capacitance due to an increase in the number

and distance between the interconnects. Therefore, the development of electrode materials with high conductivity and novel 3D architectures to reduce the parasitic capacitance between neighboring interconnects is of high importance.

Additionally, spatial detection of tactile input can be achieved using electrical impedance tomography (EIT) (Figure 19e). Here, the electrodes are connected at the periphery of a large area piezoresistive sensor, and the local resistance change is mapped by injecting current and measuring impedance at various electrode combinations.^[209,300] Contrary to active matrix array, EIT-based spatial detection does not require a complex fabrication process. Kim and co-workers developed an anisotropic EIT capable of detecting multipoint pressure and multidirectional tensile strain,^[300] while Park et al. showed that a large-area pressure-insensitive strain sensor employing EIT, which can selectively visualize the local strain (Figure 19f).^[209] For other reviews regarding this topic, refer to the following articles.^[1,3,293,301,302]

5.2. Solution-Based Large-Area Fabrication of Stretchable E-Skin

Of the five senses that humans possess, tactile sensing is unique in the sense that it requires large-area (i.e., for instance, the surface area of an average person is roughly 1.7×10^6 mm²). Hence, e-skin should have tactile sensors and signal

processing electronic components patterned over a large area, particularly for humanoid robot or prosthesis. Furthermore, e-skin should be stretchable and conformably attached to 3D irregularly shaped surfaces. Below we discuss strategies to fabricate stretchable e-skin and various solution-based patterning techniques.

There are various ways to fabricate e-skin devices (sensors, transistors etc.) such as template leaching (e.g., via solid templates such as nickel foam),^[154,182,187,198,303] vapor-phase deposition,^[190,232,295] photolithography,^[295,304] transfer processes,^[196,205,305] and solution-based processes.^[165,209,306–308] Of these fabrication techniques, solution-based printing processes such as ink-jet printing have advantages such as direct deposition of materials that minimizes materials waste, and simplicity in processability.^[307] Hong et al. reported hybrid stretchable electronics where stretchable electrodes and rigid islands were patterned on an elastomeric substrate using ink-jet printing; conventional rigid electronic chips (LED, logic gates) were placed on top of the rigid islands to minimize the strain imposed on the chips (**Figure 20a**).^[307,308] Also, via holes were generated on the substrate, which allowed the use of top and bottom surface of the substrate.^[308] One challenging issue with hybrid electronics is the mismatch of elastic modulus between the hard and soft components, which generates high stress at their interface. To solve this issue, gradient interface was engineered, where layers with an intermediate modulus was inserted between hard and soft regions.^[308] One limitation to hybrid electronics is that as the density of the rigid chips increase, so does the areal ratio of the rigid islands, which lowers the stretchability of the device.^[3] Another way to generate stretchable electronics is to make all electronic components intrinsically stretchable (e.g., stretchable transistors) (**Figure 20b**).^[99] For instance, Bao et al. spin-coated water-soluble sacrificial layer (dextran) on a silicon wafer. Thereafter, a stretchable dielectric layer was deposited on the sacrificial layer, followed by patterning of the dielectric layer via photolithography. Then, stretchable semiconducting layer, and stretchable conducting layer as source/drain electrodes and intercon-

nects were deposited. Then, a stretchable substrate was deposited on top, followed by soaking in water to release the device from the rigid substrate. Finally, the gate electrodes (and the second layer of interconnect) were deposited and patterned on the dielectric layer to complete the transistors. In the future, all printed electronics with intrinsically stretchable components can be envisioned. With this platform, there is no limitation to the density of electronic components. However, intrinsically stretchable electronic components such as transistors have lower performance (e.g., field-effect mobility) compared to that of conventional electronic chips, limiting their application space. Furthermore, although the properties of stretchable transistors should not change with strain, there is still a finite change that occurs.^[99]

The limitation of many currently existing processes is their restriction to planar surfaces. Our body, however, is 3D with irregularly shaped curves. One can envision three different patterning strategies to generate e-skin on 3D surfaces. First, planar e-skin can be generated using conventional printing or lithographic techniques and the e-skin can subsequently be attached to 3D surfaces (**Figure 21a**, left). Here, it is important to preconceive the surface to which the planar e-skin will be attached to and appropriately design the shape of the device. For example, Javey and co-workers fabricated an e-skin device with cut-out voided regions to conformally affix it onto a spherical surface (**Figure 21b**).^[309] In a similar strategy, Someya and co-workers measured ECG signal by attaching a large-area active organic field-effect transistor matrix with a grid pattern on the heart.^[310] Alternatively, Hong et al. developed skin attachable electronics by firstly adhering PDMS substrate on skin, followed by the attachment of rigid electronic components (sensor, IC chips, interconnect) that made conformal contact with the skin (**Figure 21c**). Bending at the joints were accurately measured, owing to the customization of layout based on the users' surface geometry.^[311]

Another technique to generate e-skin on 3D surfaces is to use 3D printing (**Figure 21a**, middle). Using 3D printing, stretchable electrodes with serpentine structure,^[312] tactile

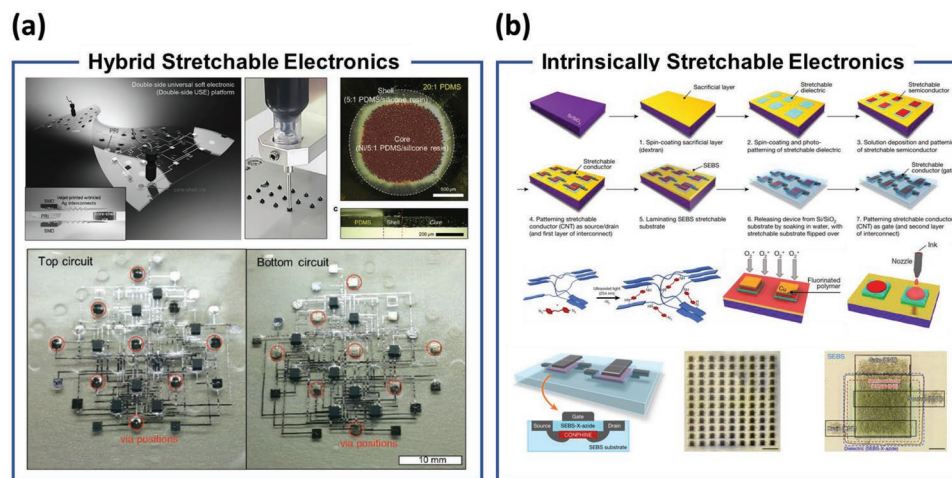


Figure 20. a) Hybrid stretchable electronics comprising of stretchable electrodes and conventional rigid electronic chips (LED, logic gates). Reproduced with permission.^[308] Copyright 2017, Wiley-VCH. b) Stretchable electronics comprising of intrinsically stretchable electronic components. Reproduced with permission.^[99] Copyright 2018, Macmillan Publishing Ltd.

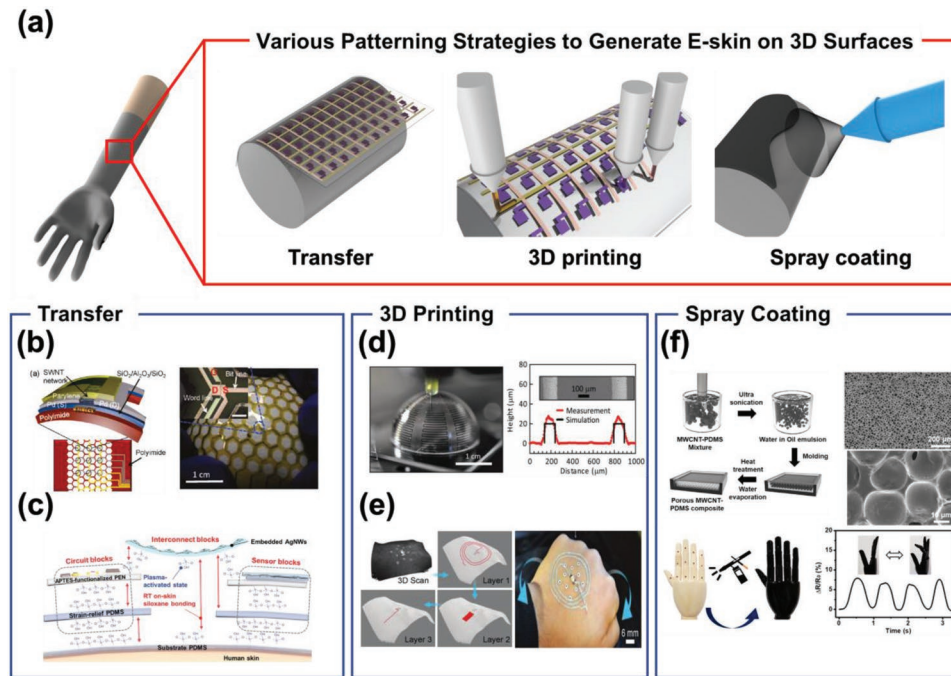


Figure 21. a) Schematic diagram of various patterning strategies on 3D surface. b) CNT-based electronics with honeycomb mesh structure showing conformal contact on a spherical object. Reproduced with permission.^[309] Copyright 2011, American Chemical Society. c) Oxygen plasma-induced bonding of electronic blocks (sensor, IC chips, interconnect) on a PDMS thin film. Reproduced with permission.^[311] Copyright 2018, Wiley-VCH. d) 3D printing of silver nanoparticle lines on a convex hemispherical surface. Reproduced with permission.^[315] Copyright 2011, Wiley-VCH. e) Adaptive 3D printing directly on a moving human hand. Reproduced with permission.^[306] Copyright 2018, Wiley-VCH. f) Spray coating on a hand figurine with emulsions containing multiwalled CNTs. Reproduced with permission.^[209] Copyright 2018, American Chemical Society.

sensor,^[313,314] and wireless antenna^[306,315] were generated. For example, Lewis and co-workers printed an antenna on a convex hemispherical surface by 3D printing silver nanoparticle-based electrodes (Figure 21d). The 3D structure improves device performance (optimized bandwidth) for wireless communication compared to that of conventional planar structures.^[315] As another example, McAlpine and co-workers developed adaptive 3D printing that allows Ag/thermoplastic polyurethane (TPU) ink to be printed directly on a moving human hand (Figure 21e).^[306] The 3D printer was integrated with a computer vision system that can track objects in real time; they fabricated wireless antenna on randomly moving hands and demonstrated wireless power transmission of light-emitting diode (LED). These demonstrations proved the feasibility of 3D printing for fabricating e-skin. However, the demonstrated devices are still relatively simple. The potential advantage of 3D printing is that multiple layers (i.e., with via holes) and multiple components can be patterned all in a single step. Also, the e-skin can be fabricated with an appropriate curvature, which can subsequently be attached to the corresponding 3D surface, or the e-skin can be directly printed onto a 3D surface. This is an exciting prospect of fabricating e-skin, especially for robotics and prosthetics.

The third technique to generate e-skin is to coat a sensing material on a 3D surface using conventional large-area coating techniques such as brush painting or spray coating (Figure 21a, right). This is the simplest way to make e-skin; however, since there is no patterning involved, only one type of sensor material can be operated at once. For example, Wu

and co-workers coated a bioinspired mineral-based self-healing hydrogel sensor that can detect pressure and strain.^[316] The hydrogel covered the surface of a finger (hand figurine) conformally and was firmly adhered to the surface even with continuous movement due to its optimized viscoelastic properties. Park and co-workers fabricated a large-area strain sensor on an irregularly-shaped 3D object (hand figurine) using spray coating, demonstrating that this sensor could detect finger bending (Figure 21f).^[209]

Despite the recent steady progress, there still exist many limitations in e-skin fabrication via solution-based processing. First, multifunctional integrated e-skin system consisting of various sensors and electronic components (e.g., transistors) is difficult to fabricate using solution-based processing due to resolution, layer-to-layer registration, and large area uniformity. This problem is even more difficult when considering fabrication on an irregularly-shaped surface. Also, inks with various functionalities that can be printed need to be developed. For instance, when 3D architectures are required (e.g., microstructuring for pressure sensors), the ink should possess appropriate viscosity and curing rate. Hybrid electronics is the most likely platform to be commercialized in the near future as it combines the use of high-performance conventional electronic chips with reliable stretchable interconnects.^[308,317] In the long run, fully printed e-skin can be envisioned with all of the components exhibiting intrinsic stretchability and high functionality. For other reviews regarding this topic, refer to the following articles.^[318–320]

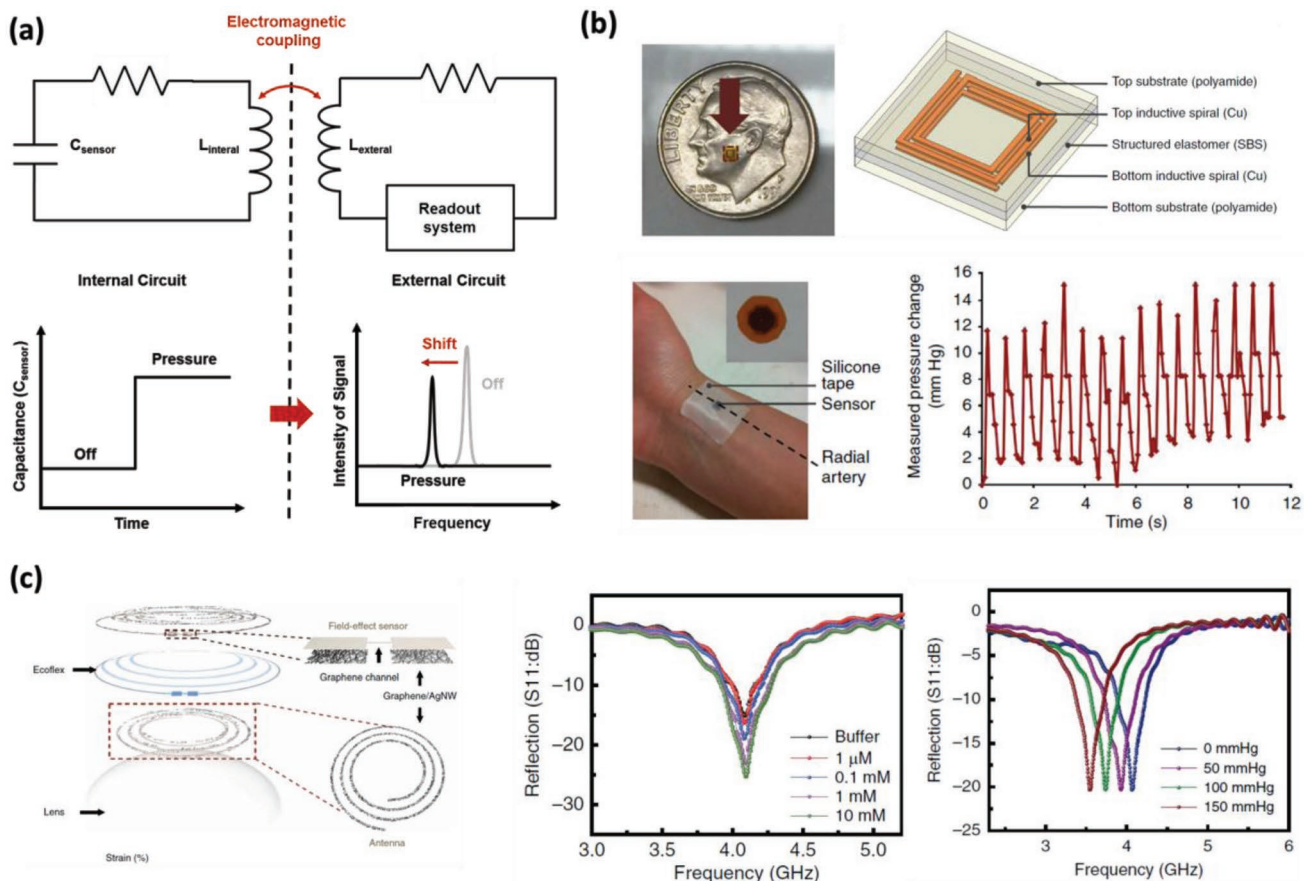


Figure 22. a) Wireless transmission of pressure data based on electromagnetic coupling. b) Resonant pressure sensing device containing ultrathin and small pressure sensors with wireless communication capability. Reproduced with permission.^[324] Copyright 2014, Macmillan Publishing Ltd. c) Intraocular sensor fabricated on a soft contact lens with antennas for wireless communication. Reproduced with permission.^[326] Copyright 2017, Macmillan Publishing Ltd.

5.3. Wireless Communication

Wireless systems, which can relieve spatial constraints and motion-related inconvenience due to wiring, are highly desirable in e-skin devices, especially in portable continuous health monitoring devices. In addition, if energy is transferred to the device using a wireless system, the device can be self-charged and the battery does not need to be replaced periodically.^[155,321] Currently, much effort is directed at designing wireless systems based on commercially available wireless devices such as Bluetooth and near-field communication (NFC) chips,^[155] which can be attached to human skin and connected to an external readout system. However, in view of rigidity and form factor considerations, the attachment of such devices can cause discomfort and limit the freedom of user motion. Hence, wireless devices should be fabricated with stretchability and flexibility similar to those of human skin, which can be achieved using electromagnetic coupling. In this section, we will highlight some of the recent work in wireless pressure and strain sensors. For a focused review on wireless communication, please refer to the following review articles.^[155,322]

Electromagnetic coupling is formed between an internal coil and an external reader coil, through which wireless

communication is established (Figure 22a). This technique can be used to transmit tactile signal wirelessly. For instance, in a work reported by Tai and co-workers, a device was fabricated as an RLC circuit (resonant circuit consisting of resistor, inductor, and capacitor), where the internal coil acted as inductor and the capacitance pressure sensor acted as the capacitor.^[323] The external coil was connected to an external circuit interfaced with a readout system. Applying pressure to the capacitance pressure sensor increases the capacitance, which reduces the resonance frequency, as given by the equation below^[324]

$$f = \frac{1}{2\pi\sqrt{LC}}$$

where f is sensor resonance frequency, L is the inductance of the internal coil, and C is sensor capacitance. Subsequently, the reduced resonance frequency was received by the external reader coil through electromagnetic coupling. The resonance frequency value is converted into a specific signal intensity such as power reflection distortion (PRD) or group delay distortion (GDD) intensities^[324] through the readout system of the circuit.

In designing the wireless system, one should carefully consider the resonance frequency of the sensor device compared to

the frequency detection range of the external reader (i.e., if the sensor's resonance frequency exceeds the maximum detection frequency of the external reader, signal cannot be detected).^[324] Generally, as sensor size decreases, the resonance frequency of the sensor device will increase and will eventually exceed the detection frequency range. This problem can be solved by increasing the sensor capacitance via thickness reduction and by increasing the inductance of the internal coil by increasing the number of turns and/or increase the size of the coil.

Bao and co-workers fabricated a wireless pressure sensor capable of detecting the change in pulse pressure. The pressure sensor was a sandwich structure with micropyramidal SBS (dielectric layer) between two inductive two-turn copper spiral electrodes with an area of $4 \times 4 \text{ mm}^2$ on a flexible polyimide substrate (Figure 22b).^[324] The recorded pressure signal was found to linearly increase in the range of 0–100 mm Hg. In this range, the applied pressure data transmitted by the wireless sensor was identical to that of the data transmitted by a reference wired sensor.

Jeong et al. fabricated a wireless resistive strain sensor featuring a circular antenna coil and circuit interconnections made from gallium-based liquid metal embedded in a PDMS elastomer, showing that this device exhibited high stretchability, durability against deformations, and skin attachability.^[325] Moreover, the above sensor could measure tensile and normal strains, through which human body motions such as wrist flexion, swallowing, and finger motion was detected. Furthermore, the device was self-charging and capable of active wireless communication to an external reader (i.e., power was transferred to the liquid metal antenna coil via electromagnetic coupling with an external NFC reader).

Park and co-workers fabricated transparent, stretchable, and multifunctional sensors on a soft contact lens to wirelessly detect intraocular pressure (for monitoring of glaucoma pathogenesis) and glucose concentration in tear (for monitoring of diabetes) (Figure 22c).^[326] The intraocular pressure sensor was a sandwiched structure, featuring a deformable dielectric layer (Ecoflex) stacked between two inductive spiral electrodes (graphene/Ag NW). The device formed two RLC circuits that produce electromagnetic coupling in the contact lens and with an external reader.

Wireless systems are especially attractive for implantable devices, as this negates the need for battery or wiring coming in and out of the body, which is often a source of infection. Bao and co-workers have implemented a flexible biodegradable device capable of measuring arterial-pulse in the body using a wireless system.^[327] Conventionally, medical practitioners observe the flow of blood through an implantable Doppler system. In this case, the electronic device in the body has to be connected to a medical monitoring system through a wire. In this paper, researchers instead implanted a wireless pressure sensor *in vivo*. In addition, since all the materials are biodegradable, a secondary surgical procedure to remove the implanted device is negated.

It is important to note that there is a trade-off between the size of the wireless sensor and the distance between the sensor and the readout system, i.e., the distance range becomes shorter with decreasing sensor size. For example, the signal generated by a $1 \times 1 \text{ mm}^2$ device can only be detected at a

maximal distance of 3 mm.^[324] In addition, metallic objects and electronics positioned in between the sensor and the external circuit may distort the electromagnetic field between the coils, interfering with the electromagnetic coupling.^[324] Electromagnetic field is also affected by the permittivity of the surrounding medium. Since the human body has different permittivity depending on the body region, the transmitted signal can change depending on the body part the sensor is attached to. Furthermore, the deformation of the skin during human motion can alter the structure of the device, unintentionally changing the transmitted signal. All of these factors need to be carefully considered when designing the wireless device.

5.4. Neuromorphic Devices for Biological Signal Processing

In order for electronic skin to be applied to prosthetics or robotics, signals coming from a large number of sensors over a large area need to be processed. However, this is not an easy task due to the complexity of wiring, high power consumption, and slow signal processing time, originating from a massive amount of data.^[158] Furthermore, the analog signal (such as current or voltage) coming out of sensors is affected by drift and noise when transmitted over long distances.^[328] To address these issues, biologically inspired signal processing techniques (i.e., spiking neural network or SNN) are currently being developed. These techniques mimic the brain's parallel signal processing capability of a large amount of data with low power consumption. Here, information is encoded in spike timing and frequency; theoretically, SNN are well suited for processing spatiotemporal information.^[329,330] Furthermore, efforts are currently being taken to convert analog signal coming out of the sensors into spike signals, which are less affected by noise during transmission and consume less power. Spike signals can also be used to communicate with neurons directly. In this section, the progress of the aforementioned research topics will be discussed. For a more focused review on neuromorphic hardware, please refer to the following review articles.^[331–336]

When mechanoreceptors receive tactile input, action potentials (spikes) are generated.^[3,337] These spikes, which contain encoded information of various factors (e.g., spatial, temporal, and magnitude), are transmitted via neurons to the brain, where they are processed (Figure 23a). In the human brain, the neurons are connected at the synapses to form a neural network. The human brain is composed of $\approx 10^{12}$ neurons and $\approx 10^{15}$ synapses.^[338] At the synapses, the connections (i.e., synaptic weights) between the neurons are constantly altered due to their spike time dependent plasticity (STDP) and spike rate dependent plasticity (STRP).^[338–340] When synaptic weight becomes stronger, it is referred to as potentiation; whereas, for weakening of synaptic weight, it is referred to as depreciation. Short-term potentiation (STP) refers to transient increase in synaptic weight while long-term potentiation (LTP) refers to persistent increase in synaptic weight. A neural network works simultaneously as a processor and memory, a direct contrast to von Neumann computer architecture where processor and memory are physically separated. Such a property along with parallel signal processability enables us to learn and process

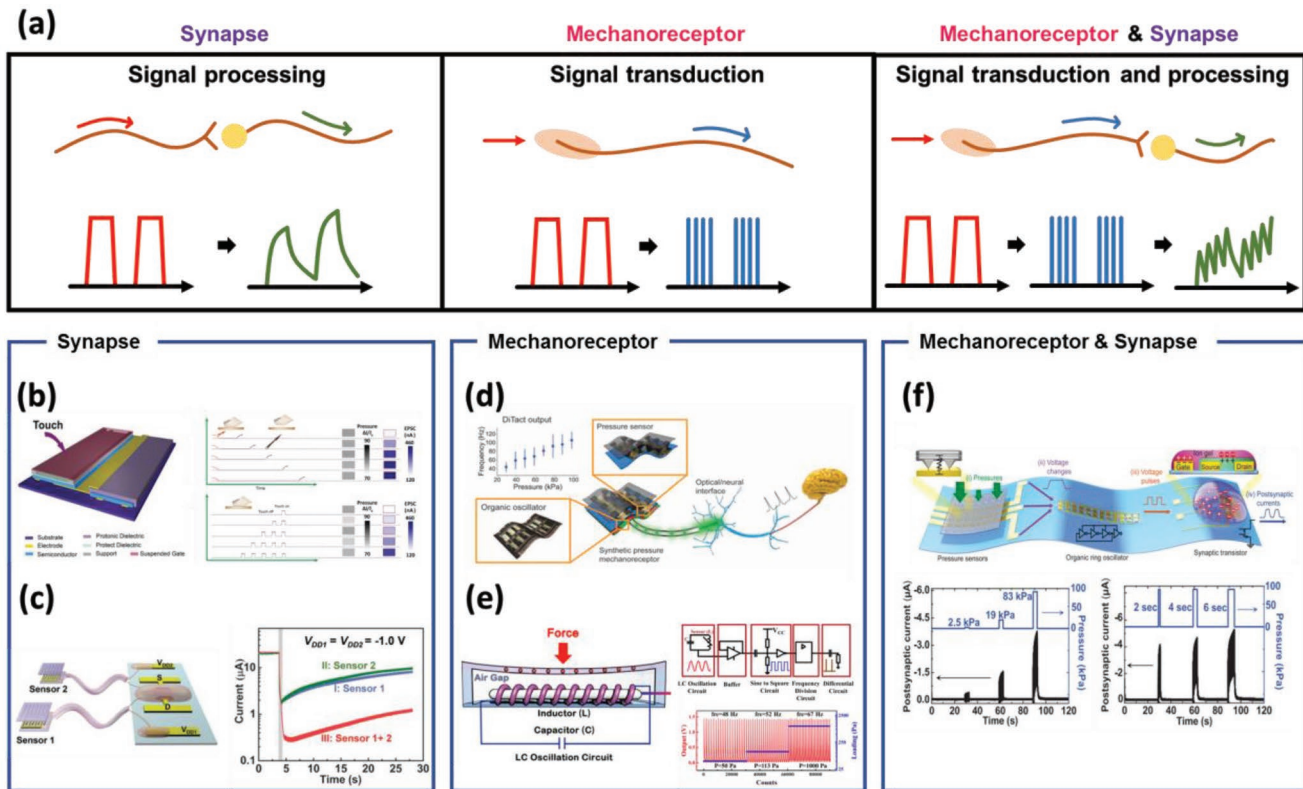


Figure 23. a) Schematic of tactile sensor signal processing using artificial biological structures such as a synapse, mechanoreceptor, or both. b) Dual organic transistor-based tactile perception system and its biological signal processing functionality. Reproduced with permission.^[359] Copyright 2017, Wiley-VCH. c) Artificial sensory system (comprising of piezoresistive pressure sensors and a synaptic transistor) capable of integrating and differentiating spatiotemporal features. Reproduced with permission.^[360] Copyright 2018, Wiley-VCH. d) Artificial mechanoreceptor comprising of a piezoresistive pressure sensor and a ring oscillator. Reproduced with permission.^[328] Copyright 2015, AAAS. e) Tactile sensor directly transducing force stimuli into digital frequency signals to mimic human stimuli responses. Reproduced with permission.^[362] Copyright 2018, AAAS. f) Flexible organic artificial afferent nerve. Reproduced with permission.^[188] Copyright 2018, AAAS.

information very efficiently, equivalent to that of dozens of supercomputers, but with exceedingly low power consumption (10 fJ per spike).^[338,339,341]

Neuromorphic hardware in combination with spike neural network (SNN) models can potentially mimic the computational power of the human brain with learning capability.^[329,330,336,342] Neuromorphic hardware are composed of artificial synaptic devices (i.e., memristors), which can alter their conductance with applied voltage spikes. This is analogous to the alteration of synaptic weight in biological systems. One performance metric of artificial synaptic devices is the number of conductance states. Furthermore, the conductance states should vary linearly and symmetrically, and its retention time should be controllable to mimic STP and LTP.^[333,339] Synaptic devices have been studied with various materials such as organic materials,^[343–346] inorganic materials,^[347–351] perovskites,^[352–354] and carbon-based materials.^[355–357] Among these, organic materials offer the advantages of low cost, large-area fabrication, and flexibility, rendering them particularly well suited for the integration with tactile sensors for soft electronic skin.

The operation of organic material-based synaptic devices, which typically comprise of ion-conducting materials such as electrolytes or ion gels, mainly relies on the behavior of ions. Upon the application of voltage, ions move to form an EDL

at the interface with the organic channel layer, or are injected into or extracted from the channel, which results in the modification of the channel layer conductance by electrochemical doping. Generally, short-term retention time is achieved due to the slow kinetics of the ions. For long retention times, electrical neutrality should be maintained at the semiconducting channel and at the electrolyte or ion gel.^[332] The above devices closely mimic the biological behavior of synapses, since they use ion kinetics and consume low power.^[332,358] For a more focused review on organic neuromorphic devices, please refer to the following articles.^[332,358]

Various studies have been conducted to emulate the biological processing of tactile signals by connecting tactile sensors with synaptic devices.^[359–361] Zhu et al. fabricated a sensor with synapse-like signal processing by connecting a synaptic transistor (prepared from a chitosan proton dielectric layer and an organic semiconductor (PDPP3T)) to a pressure-sensing transistor (Figure 23b).^[359] This system realized STP through the periodic application of pressure stimuli, and the excitatory postsynaptic current (EPSC) gradually increased when the stimulus became stronger, longer, and more frequent. Chen and co-workers realized a system for parallel recognition of tactile sensing by connecting two piezoresistive pressure sensors to one synaptic transistor with an ionic cable consisting of PVA

and PDMS (Figure 23c).^[360] The conductance of this synaptic transistor depended on the operating state of the two sensors, i.e., on whether sensors were pressed one by one or simultaneously. If the relationship between sensors was excitatory, the change of conductance synergistically increased, while the reverse was true for an inhibitory relationship.

The research mentioned above confirmed that tactile sensors can be integrated with synaptic devices, and that sensor signals can potentially be processed in a parallel manner. However, unlike a biological neural network, the above sensor-synaptic devices do not operate with spike signals. Therefore, these studies do not perfectly simulate a biological system. As mentioned above, biological spike signals allow electronic skin to interact directly with human nerves, can be transmitted over long distances without loss of information,^[328] and consume less power. In an attempt to mimic the spike signal generation of mechanoreceptors, Han and co-workers implemented an artificial sensory nerve by connecting a piezoresistive pressure sensor that outputs a spike signal with a nafion-based memristor.^[361] Here, the spike was generated by a source meter. Bao et al. used an organic ring oscillator to convert the analog signals of piezoresistive sensors into spikes (Figure 23d),^[328] showing that the frequency of spikes similar to that of the human body (<200 Hz) increased as pressure increased. The above system was then connected to an LED to optically stimulate a brain slice, and the cell potential measured in the brain slice was shown to behave very similarly to the sensor-generated spike signal. This finding reveals that an artificially generated spike signal can potentially be connected to a real human nervous system. Lee and co-workers proposed a system that mimics afferent nerves based on a concept that integrates artificial mechanoreceptors and synapses (Figure 23f).^[188] The above authors used ring oscillators to transduce an analog signal to spikes (<100 Hz) and connected it to a synaptic transistor, realizing synaptic plasticity, parallel signal processing between two artificial mechanoreceptors and one synaptic transistor, and error tolerance. Li and co-workers demonstrated a tactile sensor in which the sensor signal is directly transduced to digital-frequency signals using an inductance-capacitance (LC) oscillation circuit (Figure 23e).^[362] The above sensor was composed of magnetic particles embedded in a PDMS membrane and amorphous cobalt wire wound by a copper coil, located under the membrane with an air gap in between. Upon the application of pressure, magnetic particles got closer to the cobalt wire, which increased the magnetic flux passing through the coil and reduced the impedance. As a result, the frequency of the LC oscillation circuit is modulated. Additionally, the design of an additional circuit connected to the LC oscillation circuit allowed the generation of biological spikes whose frequency is proportional to the intensity of the pressure. Recently, Thakor and co-workers quantified the difference between touch and pain by analyzing the resistance change of multilayered e-dermis consisting of two tactile sensors in the dermal layer and one tactile sensor in the epidermal layer.^[156] They converted the analog signals from the sensors into biological spike patterns. Through this, the amputee was able to perceive both innocuous stimuli and pain, when spikes were transmitted to an upper limb via a stimulator.

We note that in the above mentioned reports, the transduction of analog signal into spikes requires additional circuits. Therefore, this can complicate the integration of a large number sensors and such a system can even consume more power. Hence, it is imperative to come up with new ideas to convert analog tactile input into spike signal in a low power and simple manner, without additional circuitry. Furthermore, although multiple sensors and synapses were connected as a proof-of-concept demonstration of parallel processing, it is still unclear as to how the magnitude and spatiotemporal information of tactile input can be processed in parallel in a large neural network. This is partly due to the fact that there is currently no well-established algorithm for SNN suitable for sensory stimulus.^[333] This is hence an important research topic moving forward. A short-term goal should be to implement neuromorphic hardware to emulate artificial neural networks, since these have well-established learning algorithms. Here, the purpose of neuromorphic hardware is to conduct vector-matrix multiplications in parallel to accelerate computation speed, and the conductance values represent the synaptic weights in artificial neural network. Also, in fabricating the neuromorphic hardware, device-to-device uniformity and reproducibility are likely to be major issues. Long-term conductance cyclability is also important to ensure durability and reliability. It is expected that when the aforementioned hardware issues (artificial mechanoreceptor and synaptic network) are resolved and the software is fully developed, the signal coming from a large array of tactile sensors can not only be processed in a low power and parallel manner, but learning based tasks can also be implemented, such as noise elimination and classification of unforeseen signal pattern. This is an exciting vision for both e-skin and neuromorphic research community.

5.5. Electrodes for Neural Interfaces

The construction of bioelectronic systems such as prosthetics requires the establishment of connection between biological tissues and electronic devices, through the use of electrodes. In regard to electrodes for neural interfaces, electrical properties, mechanical properties, and biocompatibility of the electrode material should be carefully considered. This section briefly discusses the challenges and future prospects of neural electrodes. For more information, we recommend the following review papers, which carefully treat the current topics in neural interfaces.^[363,364]

5.5.1. Early Development and Challenges

Early neural electrodes were single or multmicrowires fabricated with metals such as tungsten, stainless steel, gold, and platinum, due to their high conductivity and chemical stability in physiological environments.^[365] These electrodes have impedance between 100 kΩ and 1 MΩ at 1 kHz, which enables the measurement of endogenous neural activities,^[366,367] and the charge injection capacity from 0.1 to 1 mC cm⁻² for brain stimulation.^[368,369] Later, with advances in microfabrication technology, researchers started to use heavily doped semiconductors as electrodes (Figure 24a).^[370–373] For example, to record neuronal signal

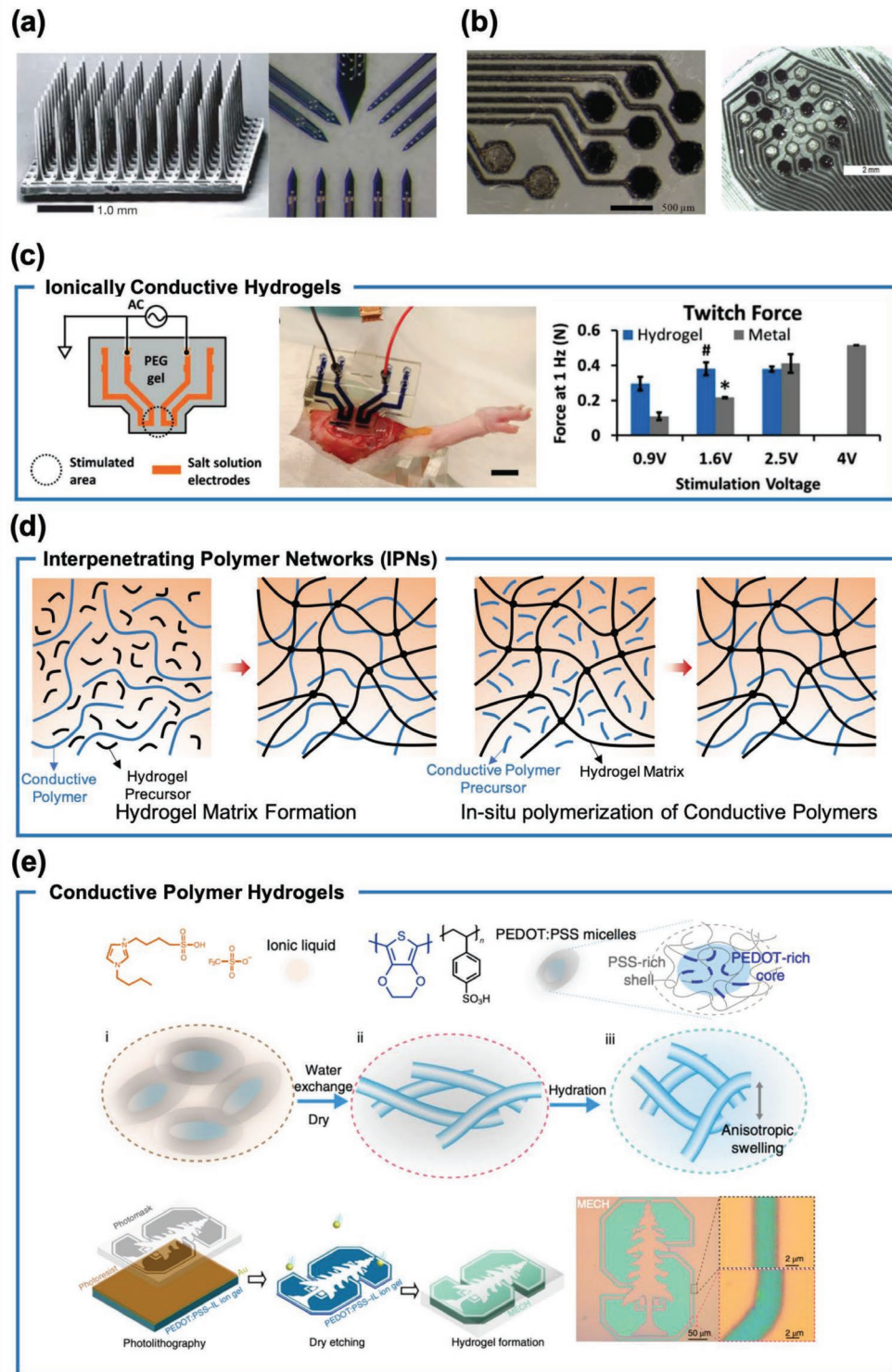


Figure 24. a) (left) A magnified image of Utah electrode array. Reproduced with permission.^[371] Copyright 2006, Macmillan Publishing Ltd. (right) A magnified image of Michigan electrodes. Reproduced with permission.^[373] Copyright 2008, Society for Neuroscience. b) PEDOT-coated platinum electrode arrays. Reproduced with permission.^[410] Copyright 2013, IOP Publishing. c) (left) Schematic of an ionic circuit using an ionically conductive hydrogel. (middle) A photograph of the circuit for muscle stimulation. (right) Muscle was stimulated with various pulsed signals. Reproduced with permission.^[437] Copyright 2018, Wiley-VCH. d) Synthesis scheme of conductive interpenetrating polymer networks (IPNs). e) (top) Synthesis of highly conductive and soft PEDOT:PSS hydrogels. (bottom) Such hydrogels can be patterned via photolithography. Reproduced with permission.^[459] Copyright 2019, Macmillan Publishing Ltd.

from a large surface and from multiple layers of the cortex, devices with silicon-based needle-like electrode arrays such as Utah array was developed.^[370,371] Similarly, long silicon-based electrodes like the Michigan probe was also introduced to attain recording from the deep regions of the brain.^[372,373]

Though the abovementioned electrodes provided the proper acquisition and stimulation of neural signals with high spatial resolution, large injection current, and signal-to-noise ratio (SNR) along with the ease of manufacturability, the large bending stiffness of these electrodes compared to that of neural tissues generates a series of immune response, rendering it problematic for long-term usage.^[374,375] During physiological displacement, glial scarring and the breach of blood-brain barrier^[376–379] occur near the electrode surface (i.e., there is always a relative displacement between the neural tissues and the devices attached to the skull, either due to the micromotion originating from respiration and heartbeat, and/or due to the macromotion originating from body movement). Subsequently, the death of neurons and the activation of glia such as astrocyte and microglia occur, which generate an insulation layer or sheath near the electrodes. The sheath becomes increasingly denser in 6 weeks following implantation^[380] and inhibits the regrowth of axons near the electrodes.^[381,382] As a consequence, the impedance level between the electrodes and the neural tissues increases, which significantly lowers the SNR during recording and prevents effective neural stimulation.^[383,384]

5.5.2. Potential Solutions

There are several strategies to reduce the immune response due to the neural electrodes. One way is controlling hydrophobicity of the probes by coating hydrogels composed of hyaluronic acid or polyethylene glycol (PEG).^[385–387] Although these materials have been shown to prevent gliosis near the electrodes, they failed over time due to their eventual oxidization.^[388,389] Another technique is to bind bioactive molecules^[390,391] or drugs such as dexamethasone^[392–394] on the surface of electrodes. These materials were shown to prevent the death of neuronal cell,^[395] or promote the attachment of neurons near the electrodes.^[396,397] Recently, coating of biomolecule L1^[398–400] or growing stem cells on the surface of the electrodes^[401,402] were shown to simultaneously prevent gliosis and encourage neurite growth.

Although the abovementioned strategies work reasonably well, they do not solve the inherent problem of bending stiffness mismatch between the neural tissues and the electrodes. Bending stiffness is determined by 1) the moment of inertia of the electrode structure, and 2) the elastic modulus of the constituent materials. Therefore, to lower the bending stiffness, the electrodes can be geometrically engineered (i.e., reducing the size of the electrodes), and/or materials with low elastic modulus can be used.

In regard to geometrical engineering of electrodes to reduce the bending stiffness, various shapes such as mesh and fractal-based structures were utilized. These shapes provided high flexibility while allowing the use of high modulus materials, which has advantages such as better signal recording and the usability of microfabrication process.^[8,10,403–407] For peripheral nervous system (PNS) interfaces, the shape of the devices is

particularly important to alleviate demyelination and nerve loss for long-term neural stimulation and recording. For instance, cuff electrodes were deposited on an ultrathin substrate layer; the device was then rolled onto a cylindrical-shaped nerve. Such an interface minimally damaged the peripheral nerve while attaining high quality signal.^[408]

Despite their moderate success, the geometrical engineering of electrodes alone cannot completely resolve the rigidness of neural electrodes. Therefore, the development of novel soft materials with low elastic modulus is highly desirable.

5.5.3. Conductive Polymers and Carbon-Based Materials for Neural Electrodes

Conductive polymers have shown great potential as neural electrodes.^[391,409–411] The electrochemical polymerization of conductive polymers enables the deposition of conducting materials onto various surfaces with tunable thickness and conductivity.^[412] Among conductive polymers, polypyrrole (PPy) and PEDOT have been most widely studied for neural interface applications (Figure 24b).^[391,409–411,413–416] The use of such polymers as a coating material on conventional metal electrodes has also been shown to reduce impedance and increase SNR.^[413–416]

Carbon-based materials such as CNT and graphene have also been used for the neural electrodes. For instance, devices with tiny carbon nanotube-based electrodes with a diameter of 5 to 10 μm were developed,^[382,417] and have been demonstrated of lowering glial scarring and subsequent immune response. Carbon fiber-based electrodes with even smaller dimensions (3–5 μm in diameter) were also demonstrated.^[409,418,419] Other researchers deposited graphene and graphene oxide as a transparent electrode on planar devices, which could be coupled with optical imaging.^[420–422]

Composites containing mixtures of polymers, carbon, metal, or conjugated organic nanoparticles have been implemented to reduce the stiffness of the electrodes while maintaining high conductivity.^[423–425] One common composite is the mixture of CNTs with polymers. CNTs have also been wrapped with graphene sheets and were deposited on a substrate to form large area soft electrodes with high conductivity.^[426–428] These carbon-based composites can be made to have high-resolution as conventional microfabrication techniques can be used.

Conductive polymers and carbon-based materials currently have lower electrical performance compared to that of conventional rigid metal or silicon-based electrodes. Therefore, although feasibility toward neural activity recording has been demonstrated, their use as whole electrodes for neural stimulation is currently limited. Presently, conductive polymers and carbon-based materials are being mainly utilized as a coating material on conventional rigid electrodes to enhance electrical performance.^[429–431] Conductive polymers and carbon-based materials are also relatively stiff compared to neural tissues (elastic modulus of ≈1 GPa). To address these challenges, composites containing conductive polymers and soft components such as hydrogels are being developed, as described in the following section.

5.5.4. Conductive Hydrogels

Hydrogels are crosslinked polymer networks with high water content. The biggest advantage of using hydrogels is the similarity between their mechanical properties and those of biological tissues. Rigid implantable electrodes coated with soft hydrogels have been shown to significantly improve the biocompatibility (induced by the reduction of mechanical mismatch), while the change in electrical properties was negligible.^[432–436] Similar to conductive polymers, hydrogel coatings can also contain bioactive materials.^[432–436]

Conductive hydrogels have drawn significant attention over the past few years. Typically, hydrogels are electronic insulators that can, however, become ionically or electronically conductive through the incorporation of salts or electronically conductive components, respectively. Ionically conductive hydrogels are generally unsuitable for implantable devices because of either low conductivity or low stability induced by ion diffusion.^[437] To resolve these issues, Kaplan and co-workers developed ionically conductive hydrogels containing phase-separated poly(ethylene glycol) and salt (Figure 24c).^[437] In these hydrogels, phase separation prevented ion diffusion while allowing for increased softness and higher ionic conductivity. These ionic conductors consequently showed a high level of biocompatibility *in vivo*.

Electrically conductive hydrogels can be realized by the addition of conductive fillers such as metal NWs, CNTs, and graphene.^[438–442] Similar to stretchable conductors described in Subsection 2.1.3, conductive fillers should be percolated to enable electronic conductivity; thus, high-aspect-ratio fillers are preferred to minimize their total content. Conductive hydrogel nanocomposites may exhibit both high conductivity and mechanical compliance, making them highly promising for neural electrodes.

Instead of using conductive fillers, one can synthesize conductive hydrogels with conducting polymers. One type of hydrogel is a mixture of cross-linked conductive polymer and supporting hydrogel polymer network; they are called interpenetrating network hydrogels (IPNs). Several IPNs containing PEDOT:PSS, PPy, or polyaniline (PANI) as the conductive polymer have been reported.^[443–451] IPNs are generally prepared by either *in situ* polymerization of conductive components inside a supporting hydrogel network or by mixing of conductive polymers into hydrogel precursors (Figure 24d).^[365] Although the resulting hydrogels are mechanically compliant, their use in bioelectronics is hindered by their overly low conductivities.^[452] A potential solution for this challenge was suggested by Bao et al.^[452] who demonstrated that in IPNs containing PEDOT:PSS and poly(acrylic acid) (PAA), gelation of PEDOT:PSS allowed for the establishment of well-connected conductive pathways and hence resulted in high conductivities of up to 23 S m^{-1} . More importantly, the mechanical properties of these IPNs could be tuned without any significant compromise in conductivity by varying the molecular compositions of PEDOT:PSS and PAA.

The second type of hydrogel is intrinsically conductive hydrogels composed of conductive polymers without supporting polymer networks,^[453–458] and consequently exhibit higher conductivities than IPNs. For example, Shi and co-workers reported PEDOT:PSS hydrogels with conductivities (as high as 880 S m^{-1}) significantly greater than the typical values of IPNs.^[454] Recently, Bao et al. prepared interconnected

PEDOT:PSS hydrogels with conductivities of 47.4 S cm^{-1} (Figure 24e).^[459] Here, PEDOT:PSS became interconnected with an ionic liquid additive that was removed via water exchange after gelation. The resulting PEDOT:PSS hydrogel exhibited low modulus, aqueous stability, and biocompatibility. More importantly, lithography allowed the hydrogels to be patterned into complex microstructures and micropillar electrode arrays. The photolithographically patterned micropillar electrode arrays showed higher SNR and signal amplitude than those fabricated with iridium oxide *in vivo*.^[460]

Conductive hydrogels are regarded as the most promising alternative to conventional rigid electrodes for neural interfaces, since their modulus is similar to that of neural tissues. So far, research has mostly been limited to the improvement of mechanical and electrical properties, while the performance of conductive hydrogels in living organisms has been underexplored. Thus, integrated device-level *in vivo* demonstrations are necessary to confirm their practical feasibility. According to recent reports, conductive polymers can have poor biocompatibility *in vivo*, despite featuring satisfactory *in vitro* performances.^[412] Likewise, the practical application of conductive hydrogels in neural interfacing may face unexpected challenges. One positive attribute of using conductive polymers and hydrogels is that their properties are tunable; hence, functionalities such as biodegradability and self-healability can be added. Specifically, the use of biodegradable conductors may obviate the need for the undesirable process of removing implanted devices, while mechanical robustness and long-term reliability may be achieved by using self-healing materials and devices. Most importantly, in the short term, research should be focused on lowering the impedance of these materials as it is currently insufficient for use in neural recording.

6. Summary and Future Prospects

In this review, we discussed the recent progress in e-skin research, focusing on the technologies needed for three specific applications: skin attachable devices, robotics, and prosthetics. If developed fully, e-skin devices can enable continuous health monitoring and point-of-care diagnostics to improve people's health. This is particularly important in this day and age as the life expectancy and various health risks are simultaneously on the rise. Also, e-skin will endow robotics and prosthetics with a "sense of touch," enabling a wide variety of tasks currently not possible, such as manipulation of various objects and interaction with people. One can envision exciting possibilities such as robots that can conduct every day house chores and exchanging emotion with humans through tactile communication. Furthermore, amputees would regain full functionalities of human tactile capacity or even exceed it if the sensors can be engineered to detect external stimuli that are not possible with human skin. The research community has been working intensely toward this vision, and significant progress has been made over the past decade. Materials with intrinsic stretchability and self-healing ability have been developed through a variety of methods. Sensors of various kinds (tactile, chemical, and electrophysiological sensors) have been developed. Additionally, large-area fabrication and integration techniques, along with wireless communication,

low-power-consumption signal processing technologies, and neural interfacing electrodes are being developed. However, despite these efforts, many challenges still remain. Below, we succinctly highlight some of these challenges.

- 1) Intrinsic stretchable and self-healing materials: Devices fabricated using stretchable conductors, insulators, and semiconductors suffer from problems such as interfacial issues (contact resistance, delamination, and defects) under strain and the relatively low performance of n-type transistors compared to that of p-type transistors. Moreover, the application of self-healing materials to devices is still at a proof-of-concept stage.
- 2) Tactile, chemical, and electrophysiological sensors: Until now, most studies have concentrated on improving the sensitivity and sensing range of the tactile sensor. In contrast, literature specifically addressing hysteresis and sensor-to-sensor uniformity has been rarely reported. The fundamental origin and mitigation of hysteresis should be explored. The measurement of hysteresis and response/recovery time should be standardized. Slip and force vectors sensors, which have not yet been explored extensively, should be further developed as such sensors are important for texture discrimination and object manipulation. Discrimination of various tactile inputs is also important and needs to be further explored. For chemical and electrophysiological sensors, their feasibility in real life settings (in the presence of external noise of various kinds) should be fully tested.
- 3) Large-area fabrication and integration techniques: Ensuring high spatial resolution over a large area is difficult due to the increasing density and thinning of the interconnect lines, which increases the parasitic capacitance and resistance, and hence the overall impedance and noise level. Therefore, electrode materials with high conductivity and novel device architectures are required. Since stretchable materials and self-healing materials are generally not suitable for conventional lithography, development of a novel fabrication process is required. Multifunctional integrated e-skin system consisting of various sensors and electronic components (e.g., transistors) is difficult to fabricate due to the limitation in resolution, layer-to-layer registration, and large area uniformity. This problem is even more difficult when considering fabrication on an irregularly-shaped surface.
- 4) Wireless communication and signal processing technologies: In contrast to rigid wireless devices, flexible wireless devices can only deliver signal over short distances and are prone to external noise (depending on the presence of conductor nearby or where the device is attached, the acquired signal can change). Neuromorphic devices that process signal from sensor arrays are still at the proof-of-concept stage of development. Algorithm for SNN needs to be developed and the synaptic devices need to be furthermore optimized.
- 5) Electrodes for neural interfaces: Neural tissue is affected by micro- and macromotion of rigid electrodes, through which an immune response and formation of an insulating glia layer is initiated. Hence, electrodes should be engineered to have low stiffness. In this context, developing new materials possessing similar elastic modulus with that of neural tissue, along with high conductivity and ease of manufacturability is needed. The electrodes should also have long-term robustness *in vivo*.

Apart from these challenges, some other problems should be resolved for practical use of e-skin. For example, devices intended for robotics and prosthetics applications should have reasonable performance while being aesthetically suitable. Moreover, the employed materials should not cause any discomfort and negatively affect human skin when attached, be easy to remove, and provide reliable data during extreme activities such as swimming and playing sports. Devices intended for use in prosthetics should be user customizable, since the perception of the same stimulus varies between people. Devices for robotic applications should be fabricated in a variety of shapes reflecting the diversity of robots. Up to now, various flexible printed circuit board (PCB)-based robotic skin systems (e.g., fingertip, patches) were integrated with rigid robots, such as iCub robot.^[461–464] These systems successfully demonstrated reliable tactile sensing with millimeter-scale spatial resolution and moderate sensitivity.^[158] However, their lack of stretchability would hinder their practical applications due to the limited degree of freedom and inadequate mechanical robustness. Finally, to successfully apply e-skin in a variety of fields, one should overcome the associated portable power and long-term durability issues.

Acknowledgements

This article is part of the Advanced Materials Hall of Fame article series, which recognizes the excellent contributions of leading researchers to the field of materials science. J.C.Y. and J.M. contributed equally to this work. The author wishes to thank Gun-Hee Lee, Su Yeong Kim, and Da Won Kim for helpful discussion on Section 4.2. (Electrophysiological sensors), 5.3. (Wireless communication), and 5.4. (Neuromorphic devices), respectively. J.M. acknowledges Samsung Scholarship and Samsung Electronics for financial support. Z.B. acknowledges support by the Air Force Office of Scientific Research under award number FA9550-18-1-0143. Work in KAIST was supported by the KUSTAR-KAIST Institute, KAIST, Korea and a research which has been conducted as part of the KAIST-funded Global Singularity Research Program for 2019.

Note: A second affiliation for Prof. Seongjun Park was added on December 3, 2019, after initial publication online. The first names of Prof. Seongjun Park and Prof. Steve Park were also added to clarify the affiliation attributions.

Conflict of Interest

The authors declare no conflict of interest.

Keywords

electronic skins, prosthetics, robotics, stretchable devices, wearable devices

Received: July 24, 2019

Revised: August 26, 2019

Published online: September 19, 2019

[1] M. L. Hammock, A. Chortos, B. C. K. Tee, J. B. H. Tok, Z. Bao, *Adv. Mater.* **2013**, *25*, 5997.

[2] A. Chortos, Z. Bao, *Mater. Today* **2014**, *17*, 321.

[3] A. Chortos, J. Liu, Z. Bao, *Nat. Mater.* **2016**, *15*, 937.

- [4] M. Gonzalez, F. Axisa, M. Vanden Bulcke, D. Brosteaux, B. Vandevelde, J. Vanfleteren, *Microelectron. Reliab.* **2008**, *48*, 825.
- [5] J. Vanfleteren, M. Gonzalez, F. Bossuyt, Y. Y. Hsu, T. Vervust, I. De Wolf, M. Jablonski, *MRS Bull.* **2012**, *37*, 254.
- [6] S. Xu, Y. Zhang, J. Cho, J. Lee, X. Huang, L. Jia, J. A. Fan, Y. Su, J. Su, H. Zhang, H. Cheng, B. Lu, C. Yu, C. Chuang, T. Il Kim, T. Song, K. Shigeta, S. Kang, C. Dagdeviren, I. Petrov, P. V. Braun, Y. Huang, U. Paik, J. A. Rogers, *Nat. Commun.* **2013**, *4*, 1543.
- [7] I. M. Graz, D. P. J. Cotton, A. Robinson, S. P. Lacour, *Appl. Phys. Lett.* **2011**, *98*, 124101.
- [8] R. H. Kim, D. H. Kim, J. Xiao, B. H. Kim, S. Il Park, B. Panilaitis, R. Ghaffari, J. Yao, M. Li, Z. Liu, V. Malyarchuk, D. G. Kim, A. P. Le, R. G. Nuzzo, D. L. Kaplan, F. G. Omenetto, Y. Huang, Z. Kang, J. A. Rogers, *Nat. Mater.* **2010**, *9*, 929.
- [9] S. Xu, Y. Zhang, L. Jia, K. E. Mathewson, K. Jang, J. Kim, H. Fu, X. Huang, P. Chava, R. Wang, S. Bhole, L. Wang, Y. J. Na, Y. Guan, M. Flavin, Z. Han, Y. Huang, J. A. Rogers, *Science* **2014**, *344*, 70.
- [10] D. H. Kim, N. Lu, R. Ma, Y. S. Kim, R. H. Kim, S. Wang, J. Wu, S. M. Won, H. Tao, A. Islam, K. J. Yu, T. I. Kim, R. Chowdhury, M. Ying, L. Xu, M. Li, H. J. Chung, H. Keum, M. McCormick, P. Liu, Y. W. Zhang, F. G. Omenetto, Y. Huang, T. Coleman, J. A. Rogers, *Science* **2011**, *333*, 838.
- [11] D.-H. Kim, J.-H. Ahn, W. M. Choi, H.-S. Kim, T.-H. Kim, J. Song, Y. Y. Huang, Z. Liu, C. Lu, J. A. Rogers, *Nature* **2008**, *320*, 507.
- [12] D.-H. Kim, R. Ghaffari, N. Lu, J. A. Rogers, *Annu. Rev. Biomed. Eng.* **2012**, *14*, 113.
- [13] D.-H. Kim, J. Xiao, J. Song, Y. Huang, J. A. Rogers, *Adv. Mater.* **2010**, *22*, 2108.
- [14] J. A. Rogers, T. Someya, Y. Huang, *Science* **2010**, *327*, 1603.
- [15] D.-H. Kim, N. Lu, Y. Huang, J. A. Rogers, *MRS Bull.* **2012**, *37*, 226.
- [16] R. Shankar, T. K. Ghosh, R. J. Spontak, *Soft Matter* **2007**, *3*, 1116.
- [17] A. Chortos, J. Lim, J. W. F. To, M. Vosgueritchian, T. J. Dusseault, T.-H. H. Kim, S. Hwang, Z. Bao, *Adv. Mater.* **2014**, *26*, 4253.
- [18] J. Y. Oh, S. Rondeau-Gagné, Y.-C. Chiu, A. Chortos, F. Lissel, G.-J. N. Wang, B. C. Schroeder, T. Kurosawa, J. Lopez, T. Katsumata, J. Xu, C. Zhu, X. Gu, W.-G. Bae, Y. Kim, L. Jin, J. W. Chung, J. B.-H. Tok, Z. Bao, *Nature* **2016**, *539*, 411.
- [19] J. Mun, G.-J. N. Wang, J. Y. Oh, T. Katsumata, F. L. Lee, J. Kang, H.-C. Wu, F. Lissel, S. Rondeau-Gagné, J. B.-H. Tok, Z. Bao, *Adv. Funct. Mater.* **2018**, *28*, 1804222.
- [20] J. Xu, S. Wang, G.-J. N. Wang, C. Zhu, S. Luo, L. Jin, X. Gu, S. Chen, V. R. Feig, J. W. F. To, S. Rondeau-Gagné, J. Park, B. C. Schroeder, C. Lu, J. Y. Oh, Y. Wang, Y.-H. Kim, H. Yan, R. Sinclair, D. Zhou, G. Xue, B. Murmann, C. Linder, W. Cai, J. B.-H. Tok, J. W. Chung, Z. Bao, *Science* **2017**, *355*, 59.
- [21] B. Chu, X. Zhou, K. Ren, B. Neese, M. Lin, Q. Wang, F. Bauer, Q. M. Zhang, *Science* **2006**, *313*, 334.
- [22] R. P. Ortiz, A. Facchetti, T. J. Marks, *Chem. Rev.* **2010**, *110*, 205.
- [23] N. Guo, S. A. DiBenedetto, D.-K. Kwon, L. Wang, M. T. Russell, M. T. Lanagan, A. Facchetti, T. J. Marks, *J. Am. Chem. Soc.* **2007**, *129*, 766.
- [24] A. Maliakal, H. Katz, P. M. Cotts, S. Subramoney, P. Mirau, *J. Am. Chem. Soc.* **2005**, *127*, 14655.
- [25] F.-C. Chen, C.-W. Chu, J. He, Y. Yang, J.-L. Lin, *Appl. Phys. Lett.* **2004**, *85*, 3295.
- [26] M. D. Bartlett, A. Fassler, N. Kazem, E. J. Markvicka, P. Mandal, C. Majidi, *Adv. Mater.* **2016**, *28*, 3726.
- [27] K. Oh, J. Y. Lee, S. S. Lee, M. Park, D. Kim, H. Kim, *Compos. Sci. Technol.* **2013**, *83*, 40.
- [28] F. Galantini, S. Bianchi, V. Castelvetro, G. Gallone, *Smart Mater. Struct.* **2013**, *22*, 055025.
- [29] H. Stoyanov, M. Kollosche, D. N. McCarthy, G. Kofod, *J. Mater. Chem.* **2010**, *20*, 7558.
- [30] G. Kofod, S. Risse, H. Stoyanov, D. N. McCarthy, S. Sokolov, R. Krahnert, *ACS Nano* **2011**, *5*, 1623.
- [31] J. Liang, L. Li, D. Chen, T. Hajagos, Z. Ren, S.-Y. Chou, W. Hu, Q. Pei, *Nat. Commun.* **2015**, *6*, 7647.
- [32] J. H. Cho, J. Lee, Y. He, B. Kim, T. P. Lodge, C. D. Frisbie, *Adv. Mater.* **2008**, *20*, 686.
- [33] J. H. Cho, J. Lee, Y. Xia, B. Kim, Y. He, M. J. Renn, T. P. Lodge, C. Daniel Frisbie, *Nat. Mater.* **2008**, *7*, 900.
- [34] M. Shin, J. H. Song, G. H. Lim, B. Lim, J. J. Park, U. Jeong, *Adv. Mater.* **2014**, *26*, 3706.
- [35] F. Xu, M.-Y. Wu, N. S. Safron, S. S. Roy, R. M. Jacobberger, D. J. Bindl, J.-H. Seo, T.-H. Chang, Z. Ma, M. S. Arnold, *Nano Lett.* **2014**, *14*, 682.
- [36] H.-J. Kim, K. Sim, A. Thukral, C. Yu, *Sci. Adv.* **2017**, *3*, e1701114.
- [37] C. Wang, W. Y. Lee, D. Kong, R. Pfattner, G. Schweicher, R. Nakajima, C. Lu, J. Mei, T. H. Lee, H. C. Wu, J. Lopez, Y. Diao, X. Gu, S. Himmelberger, W. Niu, J. R. Matthews, M. He, A. Salleo, Y. Nishi, Z. Bao, *Sci. Rep.* **2015**, *5*, 17849.
- [38] D. Kong, R. Pfattner, A. Chortos, C. Lu, A. C. Hinckley, C. Wang, W.-Y. Lee, J. W. Chung, Z. Bao, *Adv. Funct. Mater.* **2016**, *26*, 4680.
- [39] K. H. Lee, M. S. Kang, S. Zhang, Y. Gu, T. P. Lodge, C. D. Frisbie, *Adv. Mater.* **2012**, *24*, 4457.
- [40] J. Lee, L. G. Kaake, J. H. Cho, X.-Y. Zhu, T. P. Lodge, C. D. Frisbie, *J. Phys. Chem. C* **2009**, *113*, 8972.
- [41] T. L. Atallah, M. V. Gustafsson, E. Schmidt, C. D. Frisbie, X. Y. Zhu, *J. Phys. Chem. Lett.* **2015**, *6*, 4840.
- [42] S. P. Lacour, D. Chan, S. Wagner, T. Li, Z. Suo, *Appl. Phys. Lett.* **2006**, *88*, 204103.
- [43] N. Lu, X. Wang, Z. Suo, J. Vlassak, *Appl. Phys. Lett.* **2007**, *91*, 221909.
- [44] I. M. Graz, D. P. J. Cotton, S. P. Lacour, *Appl. Phys. Lett.* **2009**, *94*, 071902.
- [45] K. Y. Chun, Y. Oh, J. Rho, J. H. Ahn, Y. J. Kim, H. R. Choi, S. Baik, *Nat. Nanotechnol.* **2010**, *5*, 853.
- [46] P. Lee, J. Lee, H. Lee, J. Yeo, S. Hong, K. H. Nam, D. Lee, S. S. Lee, S. H. Ko, *Adv. Mater.* **2012**, *24*, 3326.
- [47] M. Amjadi, A. Pichitpajongkit, S. Lee, S. Ryu, I. Park, *ACS Nano* **2014**, *8*, 5154.
- [48] S. Hong, H. Lee, J. Lee, J. Kwon, S. Han, Y. D. Suh, H. Cho, J. Shin, J. Yeo, S. H. Ko, *Adv. Mater.* **2015**, *27*, 4744.
- [49] S. Choi, S. I. Han, D. Jung, H. J. Hwang, C. Lim, S. Bae, O. K. Park, C. M. Tschaubrunn, M. Lee, S. Y. Bae, J. W. Yu, J. H. Ryu, S.-W. Lee, K. Park, P. M. Kang, W. B. Lee, R. Nezafat, T. Hyeon, D.-H. Kim, *Nat. Nanotechnol.* **2018**, *13*, 1048.
- [50] T. Sekitani, Y. Noguchi, K. Hata, T. Fukushima, T. Aida, T. Someya, *Science* **2008**, *321*, 1468.
- [51] Y. Zhang, C. J. Sheehan, J. Zhai, G. Zou, H. Luo, J. Xiong, Y. T. Zhu, Q. X. Jia, *Adv. Mater.* **2010**, *22*, 3027.
- [52] D. J. Lipomi, M. Vosgueritchian, B. C. K. Tee, S. L. Hellstrom, J. A. Lee, C. H. Fox, Z. Bao, *Nat. Nanotechnol.* **2011**, *6*, 788.
- [53] L. Cai, J. Li, P. Luan, H. Dong, D. Zhao, Q. Zhang, X. Zhang, M. Tu, Q. Zeng, W. Zhou, S. Xie, *Adv. Funct. Mater.* **2012**, *22*, 5238.
- [54] Y. Wang, C. Zhu, R. Pfattner, H. Yan, L. Jin, S. Chen, F. Molina-Lopez, F. Lissel, J. Liu, N. I. Rabiah, Z. Chen, J. W. Chung, C. Linder, M. F. Toney, B. Murmann, Z. Bao, *Sci. Adv.* **2017**, *3*, e1602076.
- [55] Y. Y. Lee, H. Y. Kang, S. H. Gwon, G. M. Choi, S. M. Lim, J. Y. Sun, Y. C. Joo, *Adv. Mater.* **2016**, *28*, 1636.
- [56] M. Z. Seyedin, J. M. Razal, P. C. Innis, G. G. Wallace, *Adv. Funct. Mater.* **2014**, *24*, 2957.
- [57] J.-S. Noh, *RSC Adv.* **2014**, *4*, 1857.
- [58] M. Park, J. Im, M. Shin, Y. Min, J. Park, H. Cho, S. Park, M.-B. Shim, S. Jeon, D.-Y. Chung, J. Bae, J. Park, U. Jeong, K. Kim, *Nat. Nanotechnol.* **2012**, *7*, 803.
- [59] Y. Kim, J. Zhu, B. Yeom, M. Di Prima, X. Su, J. G. Kim, S. J. Yoo, C. Uher, N. A. Kotov, *Nature* **2013**, *500*, 59.
- [60] T. Q. Trung, N.-E. E. Lee, *Adv. Mater.* **2017**, *29*, 1603167.

- [61] B. W. An, B. G. Hyun, S. Y. Kim, M. Kim, M. S. Lee, K. Lee, J. B. Koo, H. Y. Chu, B. S. Bae, J. U. Park, *Nano Lett.* **2014**, *14*, 6322.
- [62] P. Lee, J. Ham, J. Lee, S. Hong, S. Han, Y. D. Suh, S. E. Lee, J. Yeo, S. S. Lee, D. Lee, S. H. Ko, *Adv. Funct. Mater.* **2014**, *24*, 5671.
- [63] S. Lee, S. Shin, S. Lee, J. Seo, J. Lee, S. Son, H. J. Cho, H. Algadi, S. Al-Sayari, D. E. Kim, T. Lee, *Adv. Funct. Mater.* **2015**, *25*, 3114.
- [64] N. Liu, A. Chortos, T. Lei, L. Jin, T. R. Kim, W. G. Bae, C. Zhu, S. Wang, R. Pfattner, X. Chen, R. Sinclair, Z. Bao, *Sci. Adv.* **2017**, *3*, e1700159.
- [65] J. Y. Oh, S. Kim, H.-K. Baik, U. Jeong, *Adv. Mater.* **2016**, *28*, 4564.
- [66] M. Y. Teo, N. Kim, S. Kee, B. S. Kim, G. Kim, S. Hong, S. Jung, K. Lee, *ACS Appl. Mater. Interfaces* **2017**, *9*, 819.
- [67] A. Hirsch, H. O. Michaud, A. P. Gerratt, S. de Mulaatier, S. P. Lacour, *Adv. Mater.* **2016**, *28*, 4507.
- [68] R. K. Kramer, C. Majidi, R. J. Wood, *Adv. Funct. Mater.* **2013**, *23*, 5292.
- [69] A. Fassler, C. Majidi, *Adv. Mater.* **2015**, *27*, 1928.
- [70] I. D. Joshipura, H. R. Ayers, C. Majidi, M. D. Dickey, *J. Mater. Chem. C* **2015**, *3*, 3834.
- [71] J. Yoon, S. Y. Hong, Y. Lim, S.-J. Lee, G. Zi, J. S. Ha, *Adv. Mater.* **2014**, *26*, 6580.
- [72] S. Cheng, Z. Wu, *Lab Chip* **2010**, *10*, 3227.
- [73] M. S. Lee, K. Lee, S. Y. Kim, H. Lee, J. Park, K. H. Choi, H. K. Kim, D. G. Kim, D. Y. Lee, S. Nam, J. U. Park, *Nano Lett.* **2013**, *13*, 2814.
- [74] M. Vosgueritchian, D. J. Lipomi, Z. Bao, *Adv. Funct. Mater.* **2012**, *22*, 421.
- [75] N. Matsuhisa, M. Kaltenbrunner, T. Yokota, H. Jinno, K. Kuribara, T. Sekitani, T. Someya, *Nat. Commun.* **2015**, *6*, 7461.
- [76] N. Matsuhisa, D. Inoue, P. Zalar, H. Jin, Y. Matsuba, A. Itoh, T. Yokota, D. Hashizume, T. Someya, *Nat. Mater.* **2017**, *16*, 834.
- [77] S. H. Kim, S. Jung, I. S. Yoon, C. Lee, Y. Oh, J. M. Hong, *Adv. Mater.* **2018**, *30*, e1800109.
- [78] H. Jin, N. Matsuhisa, S. Lee, M. Abbas, T. Yokota, T. Someya, *Adv. Mater.* **2017**, *29*, 1605848.
- [79] B. O'Connor, E. P. Chan, C. Chan, B. R. Conrad, L. J. Richter, R. J. Kline, M. Heeney, I. McCulloch, C. L. Soles, D. M. DeLongchamp, *ACS Nano* **2010**, *4*, 7538.
- [80] B. O'Connor, R. J. Kline, B. R. Conrad, L. J. Richter, D. Gundlach, M. F. Toney, D. M. DeLongchamp, *Adv. Funct. Mater.* **2011**, *21*, 3697.
- [81] D. Gargi, R. J. Kline, D. M. DeLongchamp, D. A. Fischer, M. F. Toney, B. T. O'Connor, *J. Phys. Chem. C* **2013**, *117*, 17421.
- [82] J. S. Kim, J. H. Kim, W. Lee, H. Yu, H. J. Kim, I. Song, M. Shin, J. H. Oh, U. Jeong, T. S. Kim, B. J. Kim, *Macromolecules* **2015**, *48*, 4339.
- [83] C. Müller, S. Goffri, D. W. Breiby, J. W. Andreasen, H. D. Chanzy, R. A. J. Janssen, M. M. Nielsen, C. P. Radano, H. Sirringhaus, P. Smith, N. Stingelin-Stutzmann, *Adv. Funct. Mater.* **2007**, *17*, 2674.
- [84] R. Peng, B. Pang, D. Hu, M. Chen, G. Zhang, X. Wang, H. Lu, K. Cho, L. Qiu, *J. Mater. Chem. C* **2015**, *3*, 3599.
- [85] M. Shin, J. Y. Oh, K.-E. Byun, Y.-J. Lee, B. Kim, H.-K. Baik, J.-J. Park, U. Jeong, *Adv. Mater.* **2015**, *27*, 1255.
- [86] E. Song, B. Kang, H. H. Choi, D. H. Sin, H. Lee, W. H. Lee, K. Cho, *Adv. Electron. Mater.* **2016**, *2*, 1500250.
- [87] H.-R. Tseng, L. Ying, B. B. Y. Hsu, L. A. Perez, C. J. Takacs, G. C. Bazan, A. J. Heeger, *Nano Lett.* **2012**, *12*, 6353.
- [88] G. Kim, S. J. Kang, G. K. Dutta, Y. K. Han, T. J. Shin, Y. Y. Noh, C. Yang, *J. Am. Chem. Soc.* **2014**, *136*, 9477.
- [89] B. Nkietia-Yawson, H. S. Lee, D. Seo, Y. Yoon, W. T. Park, K. Kwak, H. J. Son, B. Kim, Y. Y. Noh, *Adv. Mater.* **2015**, *27*, 3045.
- [90] W. Zhang, J. Smith, S. E. Watkins, R. Gysel, M. McGehee, A. Salleo, J. Kirkpatrick, S. Ashraf, T. Anthopoulos, M. Heeney, I. McCulloch, *J. Am. Chem. Soc.* **2010**, *132*, 11437.
- [91] D. Venkateshvaran, M. Nikolla, A. Sadhanala, V. Lemaur, M. Zelazny, M. Kepa, M. Hurhangee, A. J. Kronemeijer, V. Pecunia, I. Nasrallah, I. Romanov, K. Broch, I. McCulloch, D. Emin, Y. Olivier, J. Cornil, D. Beljonne, H. Sirringhaus, *Nature* **2014**, *515*, 384.
- [92] Y. Li, W. K. Tatum, J. W. Onorato, Y. Zhang, C. K. Luscombe, *Macromolecules* **2018**, *51*, 6352.
- [93] C. Lu, W. Y. Lee, X. Gu, J. Xu, H. H. Chou, H. Yan, Y. C. Chiu, M. He, J. R. Matthews, W. Niu, J. B. H. Tok, M. F. Toney, W. C. Chen, Z. Bao, *Adv. Electron. Mater.* **2017**, *3*, 1600311.
- [94] G.-J. N. Wang, L. Shaw, J. Xu, T. Kurosawa, B. C. Schroeder, J. Y. Oh, S. J. Benight, Z. Bao, *Adv. Funct. Mater.* **2016**, *26*, 7254.
- [95] Y. Zhao, A. Gumyusenge, J. He, G. Qu, W. W. McNutt, Y. Long, H. Zhang, L. Huang, Y. Diao, J. Mei, *Adv. Funct. Mater.* **2018**, *28*, 1705584.
- [96] S. Savagatrup, X. Zhao, E. Chan, J. Mei, D. J. Lipomi, *Macromol. Rapid Commun.* **2016**, *37*, 1623.
- [97] J. Xu, H.-C. Wu, C. Zhu, A. Ehrlich, L. Shaw, M. Nikolla, S. Wang, F. Molina-Lopez, X. Gu, S. Luo, D. Zhou, Y.-H. Kim, G.-J. N. Wang, K. Gu, V. R. Feig, S. Chen, Y. Kim, T. Katsumata, Y.-Q. Zheng, H. Yan, J. W. Chung, J. Lopez, B. Murmann, Z. Bao, *Nat. Mater.* **2019**, *18*, 594.
- [98] A. Chortos, G. I. Koleilat, R. Pfattner, D. Kong, P. Lin, R. Nur, T. Lei, H. Wang, N. Liu, Y. C. Lai, M. G. Kim, J. W. Chung, S. Lee, Z. Bao, *Adv. Mater.* **2016**, *28*, 4441.
- [99] S. Wang, J. Xu, W. Wang, G.-J. N. Wang, R. Rastak, F. Molina-Lopez, J. W. Chung, S. Niu, V. R. Feig, J. Lopez, T. Lei, S.-K. Kwon, Y. Kim, A. M. Foudeh, A. Ehrlich, A. Gasperini, Y. Yun, B. Murmann, J. B.-H. Tok, Z. Bao, *Nature* **2018**, *555*, 83.
- [100] T. P. Huynh, P. Sonar, H. Haick, *Adv. Mater.* **2017**, *29*, 1604973.
- [101] S. Burattini, H. M. Colquhoun, J. D. Fox, D. Friedmann, B. W. Greenland, P. J. F. Harris, W. Hayes, M. E. MacKay, S. J. Rowan, *Chem. Commun.* **2009**, 6717.
- [102] S. Burattini, B. W. Greenland, W. Hayes, M. E. MacKay, S. J. Rowan, H. M. Colquhoun, *Chem. Mater.* **2011**, *23*, 6.
- [103] F. Herbst, D. Döhler, P. Michael, W. H. Binder, *Macromol. Rapid Commun.* **2013**, *34*, 203.
- [104] Y. J. Tan, J. Wu, H. Li, B. C. K. Tee, *ACS Appl. Mater. Interfaces* **2018**, *10*, 15331.
- [105] S. J. Benight, C. Wang, J. B. H. Tok, Z. Bao, *Prog. Polym. Sci.* **2013**, *38*, 1961.
- [106] J. Kang, J. B. H. Tok, Z. Bao, *Nat. Electron.* **2019**, *2*, 144.
- [107] Q. Zhang, L. Liu, C. Pan, D. Li, *J. Mater. Sci.* **2018**, *53*, 27.
- [108] S. R. White, N. R. Sottos, P. H. Geubelle, J. S. Moore, M. R. Kessler, S. R. Sriram, E. N. Brown, S. Viswanathan, *Nature* **2001**, *409*, 794.
- [109] Y. Li, S. Chen, M. Wu, J. Sun, *Adv. Mater.* **2012**, *24*, 4578.
- [110] P. Cordier, F. Tournilhac, C. Soulié-Ziakovic, L. Leibler, *Nature* **2008**, *451*, 977.
- [111] B. C. K. Tee, C. Wang, R. Allen, Z. Bao, *Nat. Nanotechnol.* **2012**, *7*, 825.
- [112] H. Sun, X. You, Y. Jiang, G. Guan, X. Fang, J. Deng, P. Chen, Y. Luo, H. Peng, *Angew. Chem., Int. Ed.* **2014**, *53*, 9526.
- [113] J. A. Neal, D. Mozhdehi, Z. Guan, *J. Am. Chem. Soc.* **2015**, *137*, 4846.
- [114] W. Huang, K. Besar, Y. Zhang, S. Yang, G. Wiedman, Y. Liu, W. Guo, J. Song, K. Hemker, K. Hristova, I. J. Kymmissis, H. E. Katz, *Adv. Funct. Mater.* **2015**, *25*, 3745.
- [115] D. Son, J. Kang, O. Vardoulis, Y. Kim, N. Matsuhisa, J. Y. Oh, J. W. To, J. Mun, T. Katsumata, Y. Liu, A. F. McGuire, M. Krason, F. Molina-Lopez, J. Ham, U. Kraft, Y. Lee, Y. Yun, J. B.-H. Tok, Z. Bao, *Nat. Nanotechnol.* **2018**, *13*, 1057.
- [116] J. Kang, D. Son, G.-J. N. Wang, Y. Liu, J. Lopez, Y. Kim, J. Y. Oh, T. Katsumata, J. Mun, Y. Lee, L. Jin, J. B.-H. Tok, Z. Bao, *Adv. Mater.* **2018**, *30*, 1706846.

- [117] Q. Zhang, S. Niu, L. Wang, J. Lopez, S. Chen, Y. Cai, R. Du, Y. Liu, J.-C. Lai, L. Liu, C.-H. Li, X. Yan, C. Liu, J. B. H. Tok, X. Jia, Z. Bao, *Adv. Mater.* **2018**, *30*, 1801435.
- [118] X. Yan, Z. Liu, Q. Zhang, J. Lopez, H. Wang, H.-C. Wu, S. Niu, H. Yan, S. Wang, T. Lei, J. Li, D. Qi, P. Huang, J. Huang, Y. Zhang, Y. Wang, G. Li, J. B. H. Tok, X. Chen, Z. Bao, *J. Am. Chem. Soc.* **2018**, *140*, 5280.
- [119] L. Xing, Q. Li, G. Zhang, X. Zhang, F. Liu, L. Liu, Y. Huang, Q. Wang, *Adv. Funct. Mater.* **2016**, *26*, 3524.
- [120] Y.-L. Rao, A. Chortos, R. Pfattner, F. Lissel, Y.-C. Chiu, V. Feig, J. Xu, T. Kurosawa, X. Gu, C. Wang, M. He, J. W. Chung, Z. Bao, *J. Am. Chem. Soc.* **2016**, *138*, 6020.
- [121] C.-H. Li, C. Wang, C. Keplinger, J.-L. Zuo, L. Jin, Y. Sun, P. Zheng, Y. Cao, F. Lissel, C. Linder, X.-Z. You, Z. Bao, *Nat. Chem.* **2016**, *8*, 618.
- [122] R. J. Varley, S. van der Zwaag, *Acta Mater.* **2008**, *56*, 5737.
- [123] R. John Varley, S. van der Zwaag, *Polym. Test.* **2008**, *27*, 11.
- [124] S.-M. Kim, H. Jeon, S.-H. Shin, S.-A. Park, J. Jegal, S. Y. Hwang, D. X. Oh, J. Park, *Adv. Mater.* **2018**, *30*, 1705145.
- [125] K. A. Williams, A. J. Boydston, C. W. Bielawski, J. R. Soc., *Interface* **2007**, *4*, 359.
- [126] G. Cai, J. Wang, K. Qian, J. Chen, S. Li, P. S. Lee, *Adv. Sci.* **2017**, *4*, 1600190.
- [127] K. Guo, D.-L. Zhang, X.-M. Zhang, J. Zhang, L.-S. Ding, B.-J. Li, S. Zhang, *Angew. Chem., Int. Ed.* **2015**, *54*, 12127.
- [128] C. Gong, J. Liang, W. Hu, X. Niu, S. Ma, H. T. Hahn, Q. Pei, *Adv. Mater.* **2013**, *25*, 4186.
- [129] J. Li, J. Liang, L. Li, F. Ren, W. Hu, J. Li, S. Qi, Q. Pei, *ACS Nano* **2014**, *8*, 12874.
- [130] E. Palleau, S. Reece, S. C. Desai, M. E. Smith, M. D. Dickey, *Adv. Mater.* **2013**, *25*, 1589.
- [131] E. J. Markvicka, M. D. Bartlett, X. Huang, C. Majidi, *Nat. Mater.* **2018**, *17*, 618.
- [132] Y. Zhao, X. Zhao, M. Roders, A. Gumussege, A. L. Ayzner, J. Mei, *Adv. Mater.* **2017**, *29*, 1605056.
- [133] B. J. Blaiszik, S. L. B. Kramer, M. E. Grady, D. A. McIlroy, J. S. Moore, N. R. Sottos, S. R. White, *Adv. Mater.* **2012**, *24*, 398.
- [134] E. D'Elia, S. Barg, N. Ni, V. G. Rocha, E. Saiz, *Adv. Mater.* **2015**, *27*, 4788.
- [135] J. Kang, D. Son, O. Vardoulis, J. Mun, N. Matsuhisa, Y. Kim, J. Kim, J. B.-H. Tok, Z. Bao, *Adv. Mater. Technol.* **2019**, *4*, 1800417.
- [136] S. W. Hwang, C. H. Lee, H. Cheng, J. W. Jeong, S. K. Kang, J. H. Kim, J. Shin, J. Yang, Z. Liu, G. A. Ameer, Y. Huang, J. A. Rogers, *Nano Lett.* **2015**, *15*, 2801.
- [137] K. K. Fu, Z. Wang, J. Dai, M. Carter, L. Hu, *Chem. Mater.* **2016**, *28*, 3527.
- [138] V. R. Feig, H. Tran, Z. Bao, *ACS Cent. Sci.* **2018**, *4*, 337.
- [139] J. M. Anderson, J. J. Langone, *J. Controlled Release* **1999**, *57*, 107.
- [140] M. Irimia-Vladu, *Chem. Soc. Rev.* **2014**, *43*, 588.
- [141] U. Zschieschang, T. Yamamoto, K. Takimiya, H. Kuwabara, M. Ikeda, T. Sekitani, T. Someya, H. Klauk, *Adv. Mater.* **2011**, *23*, 654.
- [142] J. W. Chang, C. G. Wang, C. Y. Huang, T. Da Tsai, T. F. Guo, T. C. Wen, *Adv. Mater.* **2011**, *23*, 4077.
- [143] A. Dezieck, O. Acton, K. Leong, E. E. Oren, H. Ma, C. Tamerler, M. Sarikaya, A. K. Y. Jen, *Appl. Phys. Lett.* **2010**, *97*, 013307.
- [144] M. Irimia-Vladu, P. A. Troshin, M. Reisinger, L. Shmygleva, Y. Kanbur, G. Schwabegger, M. Bodea, R. Schwödauer, A. Mumyatov, J. W. Fergus, V. F. Razumov, H. Sitter, N. S. Sariciftci, S. Bauer, *Adv. Funct. Mater.* **2010**, *20*, 4069.
- [145] M.-C. Bélanger, Y. Marois, *J. Biomed. Mater. Res.* **2001**, *58*, 467.
- [146] Y. Onuki, U. Bhardwaj, F. Papadimitrakopoulos, D. J. Burgess, *J. Diabetes Sci. Technol.* **2008**, *2*, 1003.
- [147] D. Ghezzi, M. R. Antognazza, R. MacCarone, S. Bellani, E. Lanzarini, N. Martino, M. Mete, G. Pertile, S. Bisti, G. Lanzani, F. Benfenati, *Nat. Photonics* **2013**, *7*, 400.
- [148] D. Ghezzi, M. R. Antognazza, M. Dal Maschio, E. Lanzarini, F. Benfenati, G. Lanzani, *Nat. Commun.* **2011**, *2*, 164.
- [149] V. Gautam, D. Rand, Y. Hanein, K. S. Narayan, *Adv. Mater.* **2014**, *26*, 1751.
- [150] D. T. Simon, S. Kurup, K. C. Larsson, R. Hori, K. Tybrandt, M. Goiny, E. W. H. Jager, M. Berggren, B. Canlon, A. Richter-Dahlfors, *Nat. Mater.* **2009**, *8*, 742.
- [151] D. Khodagholy, J. N. Gelinas, T. Thesen, W. Doyle, O. Devinsky, G. G. Malliaras, G. Buzsáki, *Nat. Neurosci.* **2015**, *18*, 310.
- [152] K. Feron, R. Lim, C. Sherwood, A. Keynes, A. Brichta, P. Dastoor, *Int. J. Mol. Sci.* **2018**, *19*, 2382.
- [153] S. K. Smart, A. I. Cassady, G. Q. Lu, D. J. Martin, *Carbon* **2006**, *44*, 1034.
- [154] A. Miyamoto, S. S. Lee, N. F. Cooray, S. S. Lee, M. Mori, N. Matsuhisa, H. Jin, L. Yoda, T. Yokota, A. Itoh, M. Sekino, H. Kawasaki, T. Ebihara, M. Amagai, T. Someya, *Nat. Nanotechnol.* **2017**, *12*, 907.
- [155] M. Ha, S. Lim, H. Ko, *J. Mater. Chem. B* **2018**, *6*, 4043.
- [156] L. E. Osborn, A. Dragomir, J. L. Betthauser, C. L. Hunt, H. H. Nguyen, R. R. Kaliki, N. V. Thakor, *Sci. Rob.* **2018**, *3*, eaat3818.
- [157] H. Wang, M. Totaro, L. Beccai, *Adv. Sci.* **2018**, *5*, 1800541.
- [158] C. Bartolozzi, L. Natale, F. Nori, G. Metta, *Nat. Mater.* **2016**, *15*, 921.
- [159] T. Yang, D. Xie, Z. Li, H. Zhu, *Mater. Sci. Eng., R* **2017**, *115*, 1.
- [160] M. Amjadi, K. U. Kyung, I. Park, M. Sitti, *Adv. Funct. Mater.* **2016**, *26*, 1678.
- [161] S. Yao, P. Swetha, Y. Zhu, *Adv. Healthcare Mater.* **2018**, *7*, 1700889.
- [162] A. Qiu, P. Li, Z. Yang, Y. Yao, I. Lee, J. Ma, *Adv. Funct. Mater.* **2019**, *29*, 1806306.
- [163] B. C. K. Tee, A. Chortos, R. R. Dunn, G. Schwartz, E. Eason, Z. Bao, *Adv. Funct. Mater.* **2014**, *24*, 5427.
- [164] H.-H. Chou, A. Nguyen, A. Chortos, J. W. F. To, C. Lu, J. Mei, T. Kurosawa, W.-G. Bae, J. B.-H. Tok, Z. Bao, *Nat. Commun.* **2015**, *6*, 8011.
- [165] S. Jung, J. H. J. H. Kim, J. H. J. H. Kim, S. Choi, J. Lee, I. Park, T. Hyeon, D. H. Kim, *Adv. Mater.* **2014**, *26*, 4825.
- [166] D. Kwon, T. I. Lee, J. Shim, S. Ryu, M. S. Kim, S. Kim, T. S. Kim, I. Park, *ACS Appl. Mater. Interfaces* **2016**, *8*, 16922.
- [167] J. O. Kim, S. Y. Kwon, Y. Kim, H. B. Choi, J. C. Yang, J. Oh, H. S. Lee, J. Y. Sim, S. Ryu, S. Park, *ACS Appl. Mater. Interfaces* **2019**, *11*, 1503.
- [168] C. M. Bouthry, M. Negre, M. Jorda, O. Vardoulis, A. Chortos, O. Khatib, Z. N. Bao, *Sci. Rob.* **2018**, *3*, eaau6914.
- [169] M. Ha, S. Lim, J. Park, D.-S. S. Um, Y. Lee, H. Ko, *Adv. Funct. Mater.* **2015**, *25*, 2841.
- [170] Z. Wang, L. Zhang, J. Liu, H. Jiang, C. Li, *Nanoscale* **2018**, *10*, 10691.
- [171] S. C. B. Mannsfeld, B. C.-K. Tee, R. M. Stoltenberg, C. V. H.-H. Chen, S. Barman, B. V. O. Muir, A. N. Sokolov, C. Reese, Z. Bao, *Nat. Mater.* **2010**, *9*, 859.
- [172] S. R. A. Ruth, L. Beker, H. Tran, V. R. Feig, N. Matsuhisa, Z. Bao, *Adv. Funct. Mater.* **2019**, <https://doi.org/10.1002/adfm.201903100>.
- [173] J. C. Yang, J.-O. Kim, J. Oh, S. Y. Kwon, J. Y. Sim, D. W. Kim, H. B. Choi, S. Park, *ACS Appl. Mater. Interfaces* **2019**, *11*, 19472.
- [174] C. Luo, N. Liu, H. Zhang, W. Liu, Y. Yue, S. Wang, J. Rao, C. Yang, J. Su, X. Jiang, Y. Gao, *Nano Energy* **2017**, *41*, 527.
- [175] M. Liu, X. Pu, C. Jiang, T. Liu, X. Huang, L. Chen, C. Du, J. Sun, W. Hu, Z. L. Wang, *Adv. Mater.* **2017**, *29*, 1703700.
- [176] N. Luo, W. Dai, C. Li, Z. Zhou, L. Lu, C. C. Y. Poon, S.-C. Chen, Y. Zhang, N. Zhao, *Adv. Funct. Mater.* **2016**, *26*, 1178.
- [177] Y. Pang, K. Zhang, Z. Yang, S. Jiang, Z. Ju, Y. Li, X. Wang, D. Wang, M. Jian, Y. Zhang, R. Liang, H. Tian, Y. Yang, T. L. Ren, *ACS Nano* **2018**, *12*, 2346.
- [178] C. Yang, L. Li, J. Zhao, J. Wang, J. Xie, Y. Cao, M. Xue, C. Lu, *ACS Appl. Mater. Interfaces* **2018**, *10*, 25811.

- [179] B. Nie, S. Xing, J. D. Brandt, T. Pan, *Lab Chip* **2012**, *12*, 1110.
- [180] Z. Qiu, Y. Wan, W. Zhou, J. Yang, J. Yang, J. Huang, J. Zhang, Q. Liu, S. Huang, N. Bai, Z. Wu, W. Hong, H. Wang, C. F. Guo, *Adv. Funct. Mater.* **2018**, *28*, 1802343.
- [181] S. M. S. H. Cho, S. W. Lee, S. Yu, H. Kim, S. Chang, D. Kang, I. Hwang, H. S. Kang, B. Jeong, E. H. Kim, S. M. S. H. Cho, K. L. Kim, H. Lee, W. Shim, C. Park, *ACS Appl. Mater. Interfaces* **2017**, *9*, 10128.
- [182] G. Y. Bae, S. W. Pak, D. Kim, G. Lee, H. Kim do, Y. Chung, K. Cho, *Adv. Mater.* **2016**, *28*, 5300.
- [183] G. Y. Bae, J. T. Han, G. Lee, S. Lee, S. W. Kim, S. Park, J. Kwon, S. Jung, K. Cho, *Adv. Mater.* **2018**, *30*, 1803388.
- [184] Y. Lee, J. Park, S. Cho, Y. E. Shin, H. Lee, J. Kim, J. Myoung, S. Cho, S. Kang, C. Baig, H. Ko, *ACS Nano* **2018**, *12*, 4045.
- [185] J. Oh, J. Kim, Y. Kim, H. B. Choi, J. C. Yang, S. Lee, M. Pyatykh, J. Kim, J. Y. Sim, S. Park, *Small* **2019**, *15*, 1901744.
- [186] Z. Zhu, R. Li, T. Pan, *Adv. Mater.* **2018**, *30*, 1705122.
- [187] N. Luo, Y. Huang, J. Liu, S. C. Chen, C. P. Wong, N. Zhao, *Adv. Mater.* **2017**, *29*, 1702675.
- [188] Y. Kim, A. Chortos, W. Xu, Y. Liu, J. Y. Oh, D. Son, J. Kang, A. M. Foudeh, C. Zhu, Y. Lee, S. Niu, J. Liu, R. Pfattner, Z. Bao, T.-W. Lee, *Science* **2018**, *360*, 998.
- [189] F. Pan, S.-M. Chen, Y. Li, Z. Tao, J. Ye, K. Ni, H. Yu, B. Xiang, Y. Ren, F. Qin, S.-H. Yu, Y. Zhu, *Adv. Funct. Mater.* **2018**, *28*, 1803221.
- [190] X. Li, R. Zhang, W. Yu, K. Wang, J. Wei, D. Wu, A. Cao, Z. Li, Y. Cheng, Q. Zheng, R. S. Ruoff, H. Zhu, *Sci. Rep.* **2012**, *2*, 870.
- [191] S. Lee, J. Oh, J. C. Yang, J. Y. Sim, J. Ryu, J.-O. Kim, S. Park, *Adv. Mater. Technol.* **2018**, *3*, 1800307.
- [192] S. Zhao, L. Guo, J. J. Li, N. Li, G. Zhang, Y. Gao, J. J. Li, D. Cao, W. Wang, Y. Jin, R. Sun, C. P. Wong, *Small* **2017**, *13*, 1700944.
- [193] C.-J. Lee, K. H. Park, C. J. Han, M. S. Oh, B. You, Y.-S. Kim, J.-W. Kim, *Sci. Rep.* **2017**, *7*, 7959.
- [194] C. Sui, Y. Yang, R. J. Headrick, Z. Pan, J. Wu, J. Zhang, S. Jia, X. Li, W. Gao, O. S. Dewey, C. Wang, X. He, J. Kono, M. Pasquali, J. Lou, *Nanoscale* **2018**, *10*, 14938.
- [195] S. Ryu, P. Lee, J. B. Chou, R. Z. Xu, R. Zhao, A. J. Hart, S. G. Kim, *ACS Nano* **2015**, *9*, 5929.
- [196] T. Yamada, Y. Hayamizu, Y. Yamamoto, Y. Yomogida, A. Izadi-Najafabadi, D. N. Futaba, K. Hata, *Nat. Nanotechnol.* **2011**, *6*, 296.
- [197] Q. Liu, J. Chen, Y. Li, G. Shi, *ACS Nano* **2016**, *10*, 7901.
- [198] Y. Cai, J. Shen, Z. Dai, X. Zang, Q. Dong, G. Guan, L. J. Li, W. Huang, X. Dong, *Adv. Mater.* **2017**, *29*, 1606411.
- [199] Y. Sun, L. Yang, K. Xia, H. Liu, D. Han, Y. Zhang, J. Zhang, *Adv. Mater.* **2018**, *30*, 1803189.
- [200] J. Ryu, J. Kim, J. Oh, S. Lim, J. Y. Sim, J. S. Jeon, K. No, S. Park, S. Hong, *Nano Energy* **2019**, *55*, 348.
- [201] S. Wu, J. Zhang, R. B. Ladani, A. R. Ravindran, A. P. Mouritz, A. J. Kinloch, C. H. Wang, *ACS Appl. Mater. Interfaces* **2017**, *9*, 14207.
- [202] H. J. Kim, A. Thukral, C. Yu, *ACS Appl. Mater. Interfaces* **2018**, *10*, 5000.
- [203] J. T. Muth, D. M. Vogt, R. L. Truby, Y. Mengüç, D. B. Kolesky, R. J. Wood, J. A. Lewis, Y. Mengüç, D. B. Kolesky, R. J. Wood, J. A. Lewis, *Adv. Mater.* **2014**, *26*, 6307.
- [204] M. Amjadi, Y. J. Yoon, I. Park, *Nanotechnology* **2015**, *26*, 375501.
- [205] R. Nur, N. Matsuhisa, Z. Jiang, M. O. G. Nayeem, T. Yokota, T. Someya, *Nano Lett.* **2018**, *18*, 5610.
- [206] K. K. Kim, S. Hong, H. M. Cho, J. Lee, Y. D. Suh, J. Ham, S. H. Ko, *Nano Lett.* **2015**, *15*, 5240.
- [207] H. Chen, Z. Su, Y. Song, X. Cheng, X. Chen, B. Meng, Z. Song, D. Chen, H. Zhang, *Adv. Funct. Mater.* **2017**, *27*, 1604434.
- [208] K. H. Kim, N. S. Jang, S. H. Ha, J. H. Cho, J. M. Kim, *Small* **2018**, *14*, 1704232.
- [209] J. Oh, J. C. Yang, J. O. Kim, H. Park, S. Y. Kwon, S. Lee, J. Y. Sim, H. W. Oh, J. Kim, S. Park, *ACS Nano* **2018**, *12*, 7546.
- [210] C. Wang, X. Li, E. Gao, M. Jian, K. Xia, Q. Wang, Z. Xu, T. Ren, Y. Zhang, *Adv. Mater.* **2016**, *28*, 6640.
- [211] R. C. Webb, A. P. Bonifas, A. Behnaz, Y. Zhang, K. J. Yu, H. Cheng, M. Shi, Z. Bian, Z. Liu, Y. Kim, W. Yeo, J. S. Park, J. Song, Y. Li, Y. Huang, A. M. Gorbach, J. A. Rogers, *Nat. Mater.* **2013**, *12*, 938.
- [212] S. Han, M. K. Kim, B. Wang, D. S. Wie, S. Wang, C. H. Lee, *Adv. Mater.* **2016**, *28*, 10257.
- [213] J. Yang, D. Wei, L. Tang, X. Song, W. Luo, J. Chu, T. Gao, H. Shi, C. Du, *RSC Adv.* **2015**, *5*, 25609.
- [214] S. Y. Hong, Y. H. Lee, H. Park, S. W. Jin, Y. R. Jeong, J. Yun, I. You, G. Zi, J. S. Ha, *Adv. Mater.* **2016**, *28*, 930.
- [215] S. Harada, W. Honda, T. Arie, S. Akita, K. Takei, *ACS Nano* **2014**, *8*, 3921.
- [216] H. Yang, D. Qi, Z. Liu, B. K. Chandran, T. Wang, J. Yu, X. Chen, *Adv. Mater.* **2016**, *28*, 9175.
- [217] H. Joh, S.-W. Lee, M. Seong, W. S. Lee, S. J. Oh, *Small* **2017**, *13*, 1700247.
- [218] H. Joh, W. S. Lee, M. S. Kang, M. Seong, H. Kim, J. Bang, S. W. Lee, M. A. Hossain, S. J. Oh, *Chem. Mater.* **2019**, *31*, 436.
- [219] C. Yan, J. Wang, P. S. Lee, *ACS Nano* **2015**, *9*, 2130.
- [220] J. Bang, W. S. Lee, B. Park, H. Joh, H. K. Woo, S. Jeon, J. Ahn, C. Jeong, T. Kim, S. J. Oh, *Adv. Funct. Mater.* **2019**, *29*, 1903047.
- [221] C. Hou, H. Wang, Q. Zhang, Y. Li, M. Zhu, *Adv. Mater.* **2014**, *26*, 5018.
- [222] J. Park, M. Kim, Y. Lee, H. S. Lee, H. Ko, *Sci. Adv.* **2015**, *1*, e1500661.
- [223] F. Zhang, Y. Zang, D. Huang, C. A. Di, D. Zhu, *Nat. Commun.* **2015**, *6*, 8356.
- [224] H. Chen, Y. Song, H. Guo, L. Miao, X. Chen, Z. Su, H. Zhang, *Nano Energy* **2018**, *51*, 496.
- [225] H. Chen, L. Miao, Z. Su, Y. Song, M. Han, X. Chen, X. Cheng, D. Chen, H. Zhang, *Nano Energy* **2017**, *40*, 65.
- [226] L. Viry, A. Levi, M. Totaro, A. Mondini, V. Mattoli, B. Mazzolai, L. Beccai, *Adv. Mater.* **2014**, *26*, 2659.
- [227] A. Charalambides, S. Bergbreiter, *Adv. Mater. Technol.* **2017**, *2*, 1600188.
- [228] S. Park, H. H. Kim, M. Vosgueritchian, S. Cheon, H. H. Kim, J. H. Koo, T. R. Kim, S. Lee, G. Schwartz, H. Chang, Z. Bao, *Adv. Mater.* **2014**, *26*, 7324.
- [229] J. Ge, L. Sun, F. R. Zhang, Y. Zhang, L. A. Shi, H. Y. Zhao, H. W. Zhu, H. L. Jiang, S. H. Yu, *Adv. Mater.* **2016**, *28*, 722.
- [230] S. Lee, A. Reuveny, J. Reeder, S. Lee, H. Jin, Q. Liu, T. Yokota, T. Sekitani, T. Isayama, Y. Abe, Z. Suo, T. Someya, *Nat. Nanotechnol.* **2016**, *11*, 472.
- [231] E. Roh, H. B. Lee, D. Il Kim, N. E. Lee, *Adv. Mater.* **2017**, *29*, 1703004.
- [232] Q. Hua, J. Sun, H. Liu, R. Bao, R. Yu, J. Zhai, C. Pan, Z. L. Wang, *Nat. Commun.* **2018**, *9*, 244.
- [233] T. Q. Trung, N. E. Lee, *Adv. Mater.* **2016**, *28*, 4338.
- [234] K. Takei, W. Honda, S. Harada, T. Arie, S. Akita, *Adv. Healthcare Mater.* **2015**, *4*, 487.
- [235] G. Matzeu, L. Florea, D. Diamond, *Sens. Actuators, B* **2015**, *211*, 403.
- [236] H. Li, W. Shi, J. Song, H.-J. Jang, J. Dailey, J. Yu, H. E. Katz, *Chem. Rev.* **2019**, *119*, 3.
- [237] M. D. Steinberg, P. Kassal, I. M. Steinberg, *Electroanalysis* **2016**, *28*, 1149.
- [238] M. Bariya, H. Y. Y. Nyein, A. Javey, *Nat. Electron.* **2018**, *1*, 160.
- [239] J. Kim, A. S. Campbell, J. Wang, *Talanta* **2018**, *177*, 163.
- [240] A. J. Bandodkar, I. Jeerapani, J. Wang, *ACS Sens.* **2016**, *1*, 464.
- [241] Y. Yang, W. Gao, *Chem. Soc. Rev.* **2019**, *48*, 1465.
- [242] J. Kim, I. Jeerapani, J. R. Sempionatto, A. Barfidokht, R. K. Mishra, A. S. Campbell, L. J. Hubble, J. Wang, *Acc. Chem. Res.* **2018**, *51*, 2820.

- [243] J. Kim, A. S. Campbell, B. E. F. de Ávila, J. Wang, *Nat. Biotechnol.* **2019**, *37*, 389.
- [244] S. Choi, H. Lee, R. Ghaffari, T. Hyeon, D. H. Kim, *Adv. Mater.* **2016**, *28*, 4203.
- [245] J. Heikenfeld, A. Jajack, J. Rogers, P. Gutruf, L. Tian, T. Pan, R. Li, M. Khine, J. Kim, J. Wang, J. Kim, *Lab Chip* **2018**, *18*, 217.
- [246] W. Gao, S. Emaminejad, H. Y. Y. Nyein, S. Challa, K. Chen, A. Peck, H. M. Fahad, H. Ota, H. Shiraki, D. Kiriya, D. H. Lien, G. A. Brooks, R. W. Davis, A. Javey, *Nature* **2016**, *529*, 509.
- [247] W. Gao, H. Y. Y. Nyein, Z. Shahpar, H. M. Fahad, K. Chen, S. Emaminejad, Y. Gao, L. C. Tai, H. Ota, E. Wu, J. Bullock, Y. Zeng, D. H. Lien, A. Javey, *ACS Sens.* **2016**, *1*, 866.
- [248] A. J. Bandodkar, V. W. S. Hung, W. Jia, G. Valdés-Ramírez, J. R. Windmiller, A. G. Martinez, J. Ramírez, G. Chan, K. Kerman, J. Wang, *Analyst* **2013**, *138*, 123.
- [249] M. Y. Lee, H. R. Lee, C. H. Park, S. G. Han, J. H. Oh, *Acc. Chem. Res.* **2018**, *51*, 2829.
- [250] J. Heikenfeld, *Nature* **2016**, *529*, 475.
- [251] S. Emaminejad, W. Gao, E. Wu, Z. A. Davies, H. Y. Y. Nyein, S. Challa, S. P. Ryan, H. M. Fahad, K. Chen, Z. Shahpar, S. Talebi, C. Milla, A. Javey, R. W. Davis, *Proc. Natl. Acad. Sci. USA* **2017**, *114*, 4625.
- [252] D. P. Rose, M. E. Ratterman, D. K. Griffin, L. Hou, N. Kelley-Loughnane, R. R. Naik, J. A. Hagen, I. Papautsky, J. C. Heikenfeld, *IEEE Trans. Biomed. Eng.* **2015**, *62*, 1457.
- [253] J. Kim, J. R. Sempionatto, S. Imani, M. C. Hartel, A. Barfidokht, G. Tang, A. S. Campbell, P. P. Mercier, J. Wang, *Adv. Sci.* **2018**, *5*, 1800880.
- [254] H. Lee, C. Song, Y. S. Hong, M. S. Kim, H. R. Cho, T. Kang, K. Shin, S. H. Choi, T. Hyeon, D.-H. Kim, *Sci. Adv.* **2017**, *3*, e1601314.
- [255] H. Lee, T. K. Choi, Y. B. Lee, H. R. Cho, R. Ghaffari, L. Wang, H. J. Choi, T. D. Chung, N. Lu, T. Hyeon, S. H. Choi, D. H. Kim, *Nat. Nanotechnol.* **2016**, *11*, 566.
- [256] S. Sugama, K. Sekiyama, T. Kodama, Y. Takamatsu, M. Hashimoto, C. Bruno, Y. Kakinuma, M. Systems, C. Biology, L. Jolla, *Sci. Transl. Med. Sci.* **2017**, *8*, 39.
- [257] W. Jia, A. J. Bandodkar, G. Valdés-Ramírez, J. R. Windmiller, Z. Yang, J. Ramírez, G. Chan, J. Wang, *Anal. Chem.* **2013**, *85*, 6553.
- [258] S. Imani, A. J. Bandodkar, A. M. V. Mohan, R. Kumar, S. Yu, J. Wang, P. P. Mercier, *Nat. Commun.* **2016**, *7*, 11650.
- [259] J. R. Sempionatto, T. Nakagawa, A. Pavinatto, S. T. Mensah, S. Imani, P. Mercier, J. Wang, *Lab Chip* **2017**, *17*, 1834.
- [260] A. Panneer Selvam, S. Muthukumar, V. Kamakoti, S. Prasad, *Sci. Rep.* **2016**, *6*, 23111.
- [261] M. Gamella, S. Campuzano, J. Manso, G. G. de Rivera, F. López-Colino, A. J. Reviejo, J. M. Pingarrón, *Anal. Chim. Acta* **2014**, *806*, 1.
- [262] A. S. Campbell, J. Kim, J. Wang, *Curr. Opin. Electrochem.* **2018**, *10*, 126.
- [263] J. Kim, I. Jeerapan, S. Imani, T. N. Cho, A. Bandodkar, S. Cinti, P. P. Mercier, J. Wang, *ACS Sens.* **2016**, *1*, 1011.
- [264] S. Nakata, M. Shiomi, Y. Fujita, T. Arie, S. Akita, K. Takei, *Nat. Electron.* **2018**, *1*, 596.
- [265] Y. Yang, W. Gao, *Nat. Electron.* **2018**, *1*, 580.
- [266] T. Guinovart, A. J. Bandodkar, J. R. Windmiller, F. J. Andrade, J. Wang, *Analyst* **2013**, *138*, 7031.
- [267] A. J. Bandodkar, D. Molinuss, O. Mirza, T. Guinovart, J. R. Windmiller, G. Valdés-Ramírez, F. J. Andrade, M. J. Schöning, J. Wang, *Biosens. Bioelectron.* **2014**, *54*, 603.
- [268] A. J. Bandodkar, W. Jia, J. Wang, *Electroanalysis* **2015**, *27*, 562.
- [269] D. Kinnamon, R. Ghanta, K. C. Lin, S. Muthukumar, S. Prasad, *Sci. Rep.* **2017**, *7*, 13312.
- [270] R. D. Munje, S. Muthukumar, A. Panneer Selvam, S. Prasad, *Sci. Rep.* **2015**, *5*, 14586.
- [271] O. Parlak, S. T. Keene, A. Marais, V. F. Curto, A. Salleo, *Sci. Adv.* **2018**, *4*, eaar2904.
- [272] M. J. Tierney, J. A. Tamada, R. O. Potts, L. Jovanovic, S. Garg, *Biosens. Bioelectron.* **2001**, *16*, 621.
- [273] M. J. Tierney, Y. Jayalakshmi, N. A. Parris, M. P. Reidy, C. Uhegbu, P. Vijayakumar, *Clin. Chem.* **1999**, *45*, 1681.
- [274] A. J. Bandodkar, W. Jia, C. Yardimci, X. Wang, J. Ramirez, J. Wang, *Anal. Chem.* **2015**, *87*, 394.
- [275] Y. Chen, S. Lu, S. Zhang, Y. Li, Z. Qu, Y. Chen, B. Lu, X. Wang, X. Feng, *Sci. Adv.* **2017**, *3*, e1701629.
- [276] J. P. Bantle, W. Thomas, *J. Lab. Clin. Med.* **1997**, *130*, 436.
- [277] M. J. Buono, *Exp. Phys.* **1999**, *84*, 401.
- [278] A. J. Bandodkar, I. Jeerapan, J. M. You, R. Nuñez-Flores, J. Wang, *Nano Lett.* **2016**, *16*, 721.
- [279] A. J. Bandodkar, R. Nuñez-Flores, W. Jia, J. Wang, *Adv. Mater.* **2015**, *27*, 3060.
- [280] C. J. De Luca, *J. Appl. Biomech.* **1997**, *13*, 135.
- [281] R. B. Reilly, T. C. Lee, *Technol. Health Care* **2010**, *18*, 443.
- [282] L. Edenbrandt, O. Pahlm, *J. Electrocardiol.* **1988**, *21*, 361.
- [283] J. H. Koo, S. Jeong, H. J. Shim, D. Son, J. Kim, D. C. Kim, S. Choi, J. I. Hong, D. H. Kim, *ACS Nano* **2017**, *11*, 10032.
- [284] D. Son, J. Lee, S. Qiao, R. Ghaffari, J. Kim, J. E. Lee, C. Song, S. J. Kim, D. J. Lee, S. W. Jun, S. Yang, M. Park, J. Shin, K. Do, M. Lee, K. Kang, C. S. Hwang, N. Lu, T. Hyeon, D. H. Kim, *Nat. Nanotechnol.* **2014**, *9*, 397.
- [285] T. Kim, J. Park, J. Sohn, D. Cho, S. Jeon, *ACS Nano* **2016**, *10*, 4770.
- [286] J.-W. Seo, H. Kim, K. Kim, S. Q. Choi, H. J. Lee, *Adv. Funct. Mater.* **2018**, *28*, 1800802.
- [287] R. S. Dahiya, G. Metta, M. Valle, G. Sandini, *IEEE Trans. Rob.* **2009**, *26*, 1.
- [288] R. S. Johansson, A. B. Vallbo, *J. Physiol.* **1979**, *286*, 283.
- [289] Y. Wan, Z. Qiu, J. Huang, J. Yang, Q. Wang, P. Lu, J. Yang, J. Zhang, S. Huang, Z. Wu, C. F. Guo, *Small* **2018**, *14*, 1801657.
- [290] J. Shintake, E. Piskarev, S. H. Jeong, D. Floreano, *Adv. Mater. Technol.* **2018**, *3*, 1700284.
- [291] J. Lee, S. Shin, S. Lee, J. Song, S. Kang, H. Han, S. Kim, S. Kim, J. Seo, D. Kim, T. Lee, *ACS Nano* **2018**, *12*, 4259.
- [292] L. Pan, A. Chortos, G. Yu, Y. Wang, S. Isaacson, R. Allen, Y. Shi, R. Dauskardt, Z. Bao, *Nat. Commun.* **2014**, *5*, 3002.
- [293] S. Chen, K. Jiang, Z. Lou, D. Chen, G. Shen, *Adv. Mater. Technol.* **2018**, *3*, 1700248.
- [294] C. Yeom, K. Chen, D. Kiriya, Z. Yu, G. Cho, A. Javey, *Adv. Mater.* **2015**, *27*, 1561.
- [295] S. H. Shin, S. Ji, S. Choi, K. H. Pyo, B. W. An, J. Park, J. Kim, J. Y. Kim, K. S. Lee, S. Y. Kwon, J. Heo, B. G. Park, J. U. Park, *Nat. Commun.* **2017**, *8*, 14950.
- [296] G. Schwartz, B. C.-K. Tee, J. Mei, A. L. Appleton, D. H. Kim, H. Wang, Z. Bao, *Nat. Commun.* **2013**, *4*, 1859.
- [297] K. Takei, T. Takahashi, J. C. Ho, H. Ko, A. G. Gillies, P. W. Leu, R. S. Fearing, A. Javey, *Nat. Mater.* **2010**, *9*, 821.
- [298] M. Kaltenbrunner, T. Sekitani, J. Reeder, T. Yokota, K. Kuribara, T. Tokuhara, M. Drack, R. Schwodauer, I. Graz, S. Bauer-Gogonea, S. Bauer, T. Someya, *Nature* **2013**, *499*, 458.
- [299] L. Nela, J. Tang, Q. Cao, G. Tulevski, S. J. Han, *Nano Lett.* **2018**, *18*, 2054.
- [300] H. Lee, D. Kwon, H. Cho, I. Park, J. Kim, *Sci. Rep.* **2017**, *7*, 39837.
- [301] T. Sekitani, T. Someya, *Adv. Mater.* **2010**, *22*, 2228.
- [302] X. Wang, Z. Liu, T. Zhang, *Small* **2017**, *13*, 1602790.
- [303] D. Y. Choi, M. H. Kim, Y. S. Oh, S. H. Jung, J. H. Jung, H. J. Sung, H. W. Lee, H. M. Lee, *ACS Appl. Mater. Interfaces* **2017**, *9*, 1770.
- [304] Y. Gao, H. Ota, E. W. Schaler, K. Chen, A. Zhao, W. Gao, H. M. Fahad, Y. Leng, A. Zheng, F. Xiong, C. Zhang, L. C. Tai, P. Zhao, R. S. Fearing, A. Javey, *Adv. Mater.* **2017**, *29*, 1701985.
- [305] L. M. Ferrari, S. Sudha, S. Tarantino, R. Esposti, F. Bolzoni, P. Cavallari, C. Cipriani, V. Mattoli, F. Greco, *Adv. Sci.* **2018**, *5*, 1700771.

- [306] Z. Zhu, S. Z. Guo, T. Hirdler, C. Eide, X. Fan, J. Tolar, M. C. McAlpine, *Adv. Mater.* **2018**, *30*, 1707495.
- [307] J. Byun, B. Lee, E. Oh, H. Kim, S. Kim, S. Lee, Y. Hong, *Sci. Rep.* **2017**, *7*, 45328.
- [308] J. Byun, E. Oh, B. Lee, S. Kim, S. Lee, Y. Hong, *Adv. Funct. Mater.* **2017**, *27*, 1701912.
- [309] T. Takahashi, K. Takei, A. G. Gillies, R. S. Fearing, A. Javey, *Nano Lett.* **2011**, *11*, 5408.
- [310] W. Lee, S. Kobayashi, M. Nagase, Y. Jimbo, I. Saito, Y. Inoue, T. Yambe, M. Sekino, G. G. Malliaras, T. Yokota, M. Tanaka, T. Someya, *Sci. Adv.* **2018**, *4*, eaau2426.
- [311] J. Yoon, Y. Joo, E. Oh, B. Lee, D. Kim, S. Lee, T. Kim, J. Byun, Y. Hong, *Adv. Sci.* **2019**, *6*, 1801682.
- [312] H. Wei, K. Li, W. G. Liu, H. Meng, P. X. Zhang, C. Y. Yan, *Adv. Eng. Mater.* **2017**, *19*, 1700341.
- [313] A. D. Valentine, T. A. Busbee, J. W. Boley, J. R. Raney, A. Chortos, A. Kotikian, J. D. Berrigan, M. F. Durstock, J. A. Lewis, *Adv. Mater.* **2017**, *29*, 1703817.
- [314] S. Z. Guo, K. Qiu, F. Meng, S. H. Park, M. C. McAlpine, *Adv. Mater.* **2017**, *29*, 1701218.
- [315] J. J. Adams, E. B. Duoss, T. F. Malkowski, M. J. Motala, B. Y. Ahn, R. G. Nuzzo, J. T. Bernhard, J. A. Lewis, *Adv. Mater.* **2011**, *23*, 1335.
- [316] Z. Lei, Q. Wang, S. Sun, W. Zhu, P. Wu, *Adv. Mater.* **2017**, *29*, 1700321.
- [317] J. Byun, Y. Lee, J. Yoon, B. Lee, E. Oh, S. Chung, T. Lee, K. J. Cho, J. Kim, Y. Hong, *Sci. Rob.* **2018**, *3*, eaas9020.
- [318] Y. Huang, H. Wu, L. Xiao, Y. Duan, H. Zhu, J. Bian, D. Ye, Z. Yin, *Mater. Horiz.* **2019**, *6*, 642.
- [319] Z. Ma, S. Li, H. Wang, W. Cheng, Y. Li, L. Pan, Y. Shi, *J. Mater. Chem. B* **2019**, *7*, 173.
- [320] Y. Huang, X. Fan, S. C. Chen, N. Zhao, *Adv. Funct. Mater.* **2019**, *29*, 1808509.
- [321] Y. Yue, Z. Yang, N. Liu, W. Liu, H. Zhang, Y. Ma, C. Yang, J. Su, L. Li, F. Long, Z. Zou, Y. Gao, *ACS Nano* **2016**, *10*, 11249.
- [322] Y. H. Lee, O. Y. Kweon, H. Kim, J. H. Yoo, S. G. Han, J. H. Oh, *J. Mater. Chem. C* **2018**, *6*, 8569.
- [323] P. J. Chen, D. C. Rodger, S. Saati, M. S. Humayun, Y. C. Tai, *J. Microelectromech. Syst.* **2008**, *17*, 1342.
- [324] L. Y. Chen, B. C. Tee, A. L. Chortos, G. Schwartz, V. Tse, D. J. Lipomi, H. S. Wong, M. V. McConnell, Z. Bao, *Nat. Commun.* **2014**, *5*, 5028.
- [325] Y. R. Jeong, J. Kim, Z. Xie, Y. Xue, S. M. Won, G. Lee, S. W. Jin, S. Y. Hong, X. Feng, Y. Huang, J. A. Rogers, J. S. Ha, *NPG Asia Mater.* **2017**, *9*, e443.
- [326] J. Kim, M. Kim, M. S. Lee, K. Kim, S. Ji, Y. T. Kim, J. Park, K. Na, K. H. Bae, H. K. Kim, F. Bien, C. Y. Lee, J. U. Park, *Nat. Commun.* **2017**, *8*, 14997.
- [327] C. M. Boutry, L. Beker, Y. Kaizawa, C. Vassos, H. Tran, A. C. Hinckley, R. Pfattner, S. Niu, J. Li, J. Claverie, Z. Wang, J. Chang, P. M. Fox, Z. Bao, *Nat. Biomed. Eng.* **2019**, *3*, 47.
- [328] B. C. K. Tee, A. Chortos, A. Berndt, A. K. Nguyen, A. Tom, A. McGuire, Z. L. C. Lin, K. Tien, W. G. Bae, H. L. Wang, P. Mei, H. H. Chou, B. X. Cui, K. Deisseroth, T. N. Ng, Z. Bao, *Science* **2015**, *350*, 313.
- [329] W. Maass, *Neural Networks* **1997**, *10*, 1659.
- [330] D. V. Buonomano, W. Maass, *Nat. Rev. Neurosci.* **2009**, *10*, 113.
- [331] M. A. Zidan, J. P. Strachan, W. D. Lu, *Nat. Electron.* **2018**, *1*, 22.
- [332] Y. van de Burgt, A. Melianas, S. T. Keene, G. Malliaras, A. Salleo, *Nat. Electron.* **2018**, *1*, 386.
- [333] D. S. Jeong, C. S. Hwang, *Adv. Mater.* **2018**, *30*, 1704729.
- [334] C.-H. Kim, S. Lim, S. Y. Woo, W.-M. Kang, Y.-T. Seo, S.-T. Lee, S. Lee, D. Kwon, S. Oh, Y. Noh, H. Kim, J. Kim, J.-H. Bae, J.-H. Lee, *Nanotechnology* **2019**, *30*, 032001.
- [335] D. Kuzum, S. Yu, H. S. Philip Wong, *Nanotechnology* **2013**, *24*, 382001.
- [336] F. Walter, F. Röhrbein, A. Knoll, *Neural Networks* **2015**, *72*, 152.
- [337] V. E. Abraira, D. D. Ginty, *Neuron* **2013**, *79*, 618.
- [338] V. M. Ho, J.-A. Lee, K. C. Martin, *Science* **2011**, *334*, 623.
- [339] W. G. Regehr, L. F. Abbott, *Nature* **2004**, *431*, 796.
- [340] R. S. Zucker, W. G. Regehr, *Annu. Rev. Physiol.* **2002**, *64*, 355.
- [341] C. Mead, *Proc. IEEE* **1990**, *78*, 1629.
- [342] L. F. Abbott, B. DePasquale, R. M. Memmesheimer, *Nat. Neurosci.* **2016**, *19*, 350.
- [343] P. Gkoupidenis, D. A. Koutsouras, G. G. Malliaras, *Nat. Commun.* **2017**, *8*, 15448.
- [344] P. Gkoupidenis, N. Schaefer, B. Garlan, G. G. Malliaras, *Adv. Mater.* **2015**, *27*, 7176.
- [345] Y. van de Burgt, E. Lubberman, E. J. Fuller, S. T. Keene, G. C. Faria, S. Agarwal, M. J. Marinella, A. Alec Talin, A. Salleo, A. A. Talin, A. Salleo, *Nat. Mater.* **2017**, *16*, 414.
- [346] W. Xu, S.-Y. Min, H. Hwang, T.-W. Lee, *Sci. Adv.* **2016**, *2*, e1501326.
- [347] S. Choi, S. H. Tan, Z. Li, Y. Kim, C. Choi, P. Y. Chen, H. Yeon, S. Yu, J. Kim, *Nat. Mater.* **2018**, *17*, 335.
- [348] X. Zhu, D. Li, X. Liang, W. D. Lu, *Nat. Mater.* **2019**, *18*, 141.
- [349] T. Turma, A. Pantazi, M. Le Gallo, A. Sebastian, E. Eleftheriou, *Nat. Nanotechnol.* **2016**, *11*, 693.
- [350] Z. H. Tan, R. Yang, K. Terabe, X. B. Yin, X. D. Zhang, X. Guo, *Adv. Mater.* **2016**, *28*, 377.
- [351] L. Q. Zhu, C. J. Wan, L. Q. Guo, Y. Shi, Q. Wan, *Nat. Commun.* **2014**, *5*, 3158.
- [352] S. Wang, C. Chen, Z. Yu, Y. He, X. Chen, Q. Wan, Y. Shi, D. W. Zhang, H. Zhou, X. Wang, P. Zhou, *Adv. Mater.* **2019**, *31*, e1806227.
- [353] R. A. John, N. Yantara, Y. F. Ng, G. Narasimman, E. Mosconi, D. Meggiolaro, M. R. Kulkarni, P. K. Gopalakrishnan, C. A. Nguyen, F. De Angelis, S. G. Mhaisalkar, A. Basu, N. Mathews, *Adv. Mater.* **2018**, *30*, e1805454.
- [354] W. Xu, H. Cho, Y.-H. Kim, Y.-T. Kim, C. Wolf, C.-G. Park, T.-W. Lee, *Adv. Mater.* **2016**, *28*, 5916.
- [355] M. T. Sharbati, Y. Du, J. Torres, N. D. Ardolino, M. Yun, F. Xiong, *Adv. Mater.* **2018**, *30*, e1802353.
- [356] A. M. Shen, C.-L. Chen, K. Kim, B. Cho, A. Tudor, Y. Chen, *ACS Nano* **2013**, *7*, 6117.
- [357] K. Kim, C. L. Chen, Q. Truong, A. M. Shen, Y. Chen, *Adv. Mater.* **2013**, *25*, 1693.
- [358] J. Sun, Y. Fu, Q. Wan, *J. Phys. D: Appl. Phys.* **2018**, *51*, 314004.
- [359] Y. Zang, H. Shen, D. Huang, C. Di, D. Zhu, *Adv. Mater.* **2017**, *29*, 1606088.
- [360] C. Wan, G. Chen, Y. Fu, M. Wang, N. Matsuhisa, S. Pan, L. Pan, H. Yang, Q. Wan, L. Zhu, X. Chen, *Adv. Mater.* **2018**, *30*, 1801291.
- [361] C. Zhang, W. Bin Ye, K. Zhou, H.-Y. Chen, J.-Q. Yang, G. Ding, X. Chen, Y. Zhou, L. Zhou, F. Li, S.-T. Han, *Adv. Funct. Mater.* **2019**, *29*, 1808783.
- [362] Y. Wu, Y. Liu, Y. Zhou, Q. Man, C. Hu, W. Asghar, F. Li, Z. Yu, J. Shang, G. Liu, M. Liao, R.-W. Li, *Sci. Rob.* **2018**, *3*, eaat0429.
- [363] S. Park, G. Loke, Y. Fink, P. Anikeeva, *Chem. Soc. Rev.* **2019**, *48*, 1826.
- [364] A. Canales, S. Park, A. Kilias, P. Anikeeva, *Acc. Chem. Res.* **2018**, *51*, 829.
- [365] H. Yuk, B. Lu, X. Zhao, *Chem. Soc. Rev.* **2019**, *48*, 1642.
- [366] M. S. Fee, A. Leonardo, *J. Neurosci. Methods* **2001**, *112*, 83.
- [367] C. Herry, S. Ciocchi, V. Senn, L. Demmou, C. Müller, A. Lüthi, *Nature* **2008**, *454*, 600.
- [368] T. L. Rose, L. S. Robblee, *IEEE Trans. Biomed. Eng.* **1990**, *37*, 1118.
- [369] S. F. Cogan, P. R. Troyk, J. Ehrlich, T. D. Plante, D. E. Detlefsen, *IEEE Trans. Biomed. Eng.* **2006**, *53*, 327.
- [370] G. Buzsáki, K. Wise, J. Hetke, Z. Horvath, R. Urioste, *Science* **1992**, *256*, 1025.

- [371] L. R. Hochberg, M. D. Serruya, G. M. Friehs, J. A. Mukand, M. Saleh, A. H. Caplan, A. Branner, D. Chen, R. D. Penn, J. P. Donoghue, *Nature* **2006**, 442, 164.
- [372] K. D. Wise, *IEEE Eng. Med. Biol. Mag.* **2005**, 24, 22.
- [373] D. R. Kipke, W. Shain, G. Buzsaki, E. Fetz, J. M. Henderson, J. F. Hetke, G. Schalk, *J. Neurosci.* **2008**, 28, 11830.
- [374] S. P. Lacour, G. Courtine, J. Guck, *Nat. Rev. Mater.* **2016**, 1, 16063.
- [375] J. W. Jeong, G. Shin, S. Il Park, K. J. Yu, L. Xu, J. A. Rogers, *Neuron* **2015**, 86, 175.
- [376] M. P. Ward, P. Rajdev, C. Ellison, P. P. Irazoqui, *Brain Res.* **2009**, 1282, 183.
- [377] J. C. Barrese, N. Rao, K. Paroo, C. Triebwasser, C. Vargas-Irwin, L. Franquemont, J. P. Donoghue, *J. Neural Eng.* **2013**, 10, 066014.
- [378] V. S. Polikov, P. A. Tresco, W. M. Reichert, *J. Neurosci. Methods* **2005**, 148, 1.
- [379] H. Lee, R. V. Bellamkonda, W. Sun, M. E. Levenston, *J. Neural Eng.* **2005**, 2, 81.
- [380] S. Yao, Y. Zhu, *Adv. Mater.* **2015**, 27, 1480.
- [381] S. Kirkpatrick, *Rev. Mod. Phys.* **1973**, 45, 574.
- [382] G. Guitchounts, J. E. Markowitz, W. A. Liberti, T. J. Gardner, *J. Neural Eng.* **2013**, 10, 046016.
- [383] L. Hu, H. S. Kim, J.-Y. Lee, P. Peumans, Y. Cui, *ACS Nano* **2010**, 4, 2955.
- [384] W. M. Grill, S. E. Norman, R. V. Bellamkonda, *Annu. Rev. Biomed. Eng.* **2009**, 11, 1.
- [385] E. Azemi, W. R. Stauffer, M. S. Gostock, C. F. Lagenaour, X. T. Cui, *Acta Biomater.* **2008**, 4, 1208.
- [386] T. D. Y. Kozai, A. L. Vazquez, *J. Mater. Chem. B* **2015**, 3, 4965.
- [387] T. D. Y. Kozai, A. L. Vazquez, C. L. Weaver, S. G. Kim, X. T. Cui, *J. Neural Eng.* **2012**, 9, 066001.
- [388] A. W. Bridges, A. J. García, *J. Diabetes Sci. Technol.* **2008**, 2, 984.
- [389] H. Zhang, M. Chiao, *J. Med. Biol. Eng.* **2015**, 35, 143.
- [390] D. E. Labaye, C. Jérôme, V. M. Geskin, P. Louette, R. Lazzaroni, L. Martinot, R. Jérôme, *Langmuir* **2002**, 18, 5222.
- [391] R. A. Green, R. T. Hassarati, L. Bouchinet, C. S. Lee, G. L. M. Cheong, J. F. Yu, C. W. Dodds, G. J. Suaning, L. A. Poole-Warren, N. H. Lovell, *Biomaterials* **2012**, 33, 5875.
- [392] T. D. Y. Kozai, A. S. Jaquins-Gerstl, A. L. Vazquez, A. C. Michael, X. T. Cui, *Biomaterials* **2016**, 87, 157.
- [393] A. Mercanzini, S. T. Reddy, D. Velluto, P. Colin, A. Maillard, J. C. Bensadoun, J. A. Hubbell, P. Renaud, *J. Controlled Release* **2010**, 145, 196.
- [394] W. Shain, L. Spataro, J. Dilgen, K. Haverstick, S. Retterer, M. Isaacson, M. Saltzman, J. N. Turner, *IEEE Trans. Neural Syst. Rehabil. Eng.* **2003**, 11, 186.
- [395] W. R. Stauffer, X. T. Cui, *Biomaterials* **2006**, 27, 2405.
- [396] J. C. Sanchez, N. Alba, T. Nishida, C. Batich, P. R. Carney, *IEEE Trans. Neural Syst. Rehabil. Eng.* **2006**, 14, 217.
- [397] E. Patrick, M. E. Orazem, J. C. Sanchez, T. Nishida, *J. Neurosci. Methods* **2011**, 198, 158.
- [398] J. R. Eles, A. L. Vazquez, N. R. Snyder, C. Lagenaour, M. C. Murphy, T. D. Y. Kozai, X. T. Cui, *Biomaterials* **2017**, 113, 279.
- [399] E. Azemi, C. F. Lagenaour, X. T. Cui, *Biomaterials* **2011**, 32, 681.
- [400] C. L. Kolarcik, D. Bourbeau, E. Azemi, E. Rost, L. Zhang, C. F. Lagenaour, D. J. Weber, X. T. Cui, *Acta Biomater.* **2012**, 8, 3561.
- [401] P. Kennedy, D. Andreasen, J. Bartels, P. Ehirim, H. Mao, M. Velliste, T. Wichmann, J. Wright, *Prog. Brain Res.* **2011**, 194, 1.
- [402] E. Azemi, G. T. Gobbel, X. T. Cui, *J. Neurosurg.* **2010**, 113, 673.
- [403] S. Park, Y. Guo, X. Jia, H. K. Choe, B. Grenja, J. Kang, J. Park, C. Lu, A. Canales, R. Chen, Y. S. Yim, G. B. Choi, Y. Fink, P. Anikeeva, *Nat. Neurosci.* **2017**, 20, 612.
- [404] T. J. Richner, C. Lu, I. Brown, S. Park, P. Anikeeva, C. Hou, A. Derry, C. T. Mortiz, J. Kang, S. Rao, Y. Fink, *Sci. Adv.* **2017**, 3, e1600955.
- [405] J. A. Fan, W.-H. Yeo, Y. Su, Y. Hattori, W. Lee, S.-Y. Jung, Y. Zhang, Z. Liu, H. Cheng, L. Falgout, M. Bajema, T. Coleman, D. Gregoire, R. J. Larsen, Y. Huang, J. A. Rogers, *Nat. Commun.* **2014**, 5, 3266.
- [406] B. Tian, X. Liu, B. Tu, C. Yu, J. Fan, L. Wang, S. Xie, G. D. Stucky, D. Zhao, *Nat. Mater.* **2003**, 2, 159.
- [407] C. Xie, J. Liu, T. M. Fu, X. Dai, W. Zhou, C. M. Lieber, *Nat. Mater.* **2015**, 14, 1286.
- [408] E. Valderrama, T. Stieglitz, X. Navarro, *J. Neurosci. Methods* **2000**, 98, 105.
- [409] T. D. Yoshida Kozai, N. B. Langhals, P. R. Patel, X. Deng, H. Zhang, K. L. Smith, J. Lahann, N. A. Kotov, D. R. Kipke, *Nat. Mater.* **2012**, 11, 1065.
- [410] R. A. Green, P. B. Matteucci, R. T. Hassarati, B. Giraud, C. W. D. Dodds, S. Chen, P. J. Byrnes-Preston, G. J. Suaning, L. A. Poole-Warren, N. H. Lovell, *J. Neural Eng.* **2013**, 10, 016009.
- [411] S. Venkatraman, J. Hendricks, Z. A. King, A. J. Sereno, S. Richardson-Burns, D. Martin, J. M. Carmena, *IEEE Trans. Neural Syst. Rehabil. Eng.* **2011**, 19, 307.
- [412] R. Green, M. R. Abidian, *Adv. Mater.* **2015**, 27, 7620.
- [413] N. Gomez, J. Y. Lee, J. D. Nickels, C. E. Schmidt, *Adv. Funct. Mater.* **2007**, 17, 1645.
- [414] X. Cui, J. Wiler, M. Dzaman, R. A. Altschuler, D. C. Martin, *Biomaterials* **2003**, 24, 777.
- [415] P. M. George, A. W. Lyckman, D. A. Lavan, A. Hegde, Y. Leung, R. Avasare, C. Testa, P. M. Alexander, R. Langer, M. Sur, *Biomaterials* **2005**, 26, 3511.
- [416] X. Cui, J. F. Hetke, J. A. Wiler, D. J. Anderson, D. C. Martin, *Sens. Actuators, A* **2001**, 93, 8.
- [417] F. Vitale, S. R. Summerson, B. Aazhang, C. Kemere, M. Pasquali, *ACS Nano* **2015**, 9, 4465.
- [418] P. R. Patel, H. Zhang, M. T. Robbins, J. B. Nofar, S. P. Marshall, M. J. Kobylarek, T. D. Y. Kozai, N. A. Kotov, C. A. Chestek, *J. Neural Eng.* **2016**, 13, 066002.
- [419] M. Armstrong-James, J. Millar, *J. Neurosci. Methods* **1979**, 1, 279.
- [420] X. Luo, C. L. Weaver, S. Tan, X. T. Cui, *J. Mater. Chem. B* **2013**, 1, 1340.
- [421] D. W. Park, A. A. Schendel, S. Mikael, S. K. Brodnick, T. J. Richner, J. P. Ness, M. R. Hayat, F. Atry, S. T. Frye, R. Pashaie, S. Thongpong, Z. Ma, J. C. Williams, *Nat. Commun.* **2014**, 5, 5258.
- [422] D. Kuzum, H. Takano, E. Shim, J. C. Reed, H. Juul, A. G. Richardson, J. De Vries, H. Bink, M. A. Dichter, T. H. Lucas, D. A. Coulter, E. Cubukcu, B. Litt, *Nat. Commun.* **2014**, 5, 5259.
- [423] B. Li, X. Cao, H. G. Ong, J. W. Cheah, X. Zhou, Z. Yin, H. Li, J. Wang, F. Boey, W. Huang, H. Zhang, *Adv. Mater.* **2010**, 22, 3058.
- [424] N. Rakhilin, B. Barth, J. Choi, N. L. Muñoz, S. Kulkarni, J. S. Jones, D. M. Small, Y. T. Cheng, Y. Cao, C. Lavinka, E. Kan, X. Dong, M. Spencer, P. Pasricha, N. Nishimura, X. Shen, *Nat. Commun.* **2016**, 7, 11800.
- [425] H. C. Tian, J. Q. Liu, D. X. Wei, X. Y. Kang, C. Zhang, J. C. Du, B. Yang, X. Chen, H. Y. Zhu, Y. N. NuLi, C. S. Yang, *Biomaterials* **2014**, 35, 2120.
- [426] E. Jan, N. A. Kotov, *Nano Lett.* **2007**, 7, 1123.
- [427] Y. Bai, S. Ho, N. A. Kotov, *Nanoscale* **2012**, 4, 4393.
- [428] H. Zhang, P. R. Patel, Z. Xie, S. D. Swanson, X. Wang, N. A. Kotov, *ACS Nano* **2013**, 7, 7619.
- [429] A. Fabbro, M. Prato, L. Ballerini, *Adv. Drug Delivery Rev.* **2013**, 65, 2034.
- [430] E. W. Keefer, B. R. Botterman, M. I. Romero, A. F. Rossi, G. W. Gross, *Nat. Nanotechnol.* **2008**, 3, 434.
- [431] K. A. Ludwig, N. B. Langhals, M. D. Joseph, S. M. Richardson-Burns, J. L. Hendricks, D. R. Kipke, *J. Neural Eng.* **2011**, 8, 014001.
- [432] J. O. Winter, S. F. Cogan, J. F. Rizzo, *J. Biomed. Mater. Res., Part B* **2007**, 81B, 551.

- [433] K. C. Spencer, J. C. Sy, K. B. Ramadi, A. M. Graybiel, R. Langer, M. J. Cima, *Sci. Rep.* **2017**, *7*, 12812.
- [434] L. Rao, H. Zhou, T. Li, C. Li, Y. Y. Duan, *Acta Biomater.* **2012**, *8*, 2233.
- [435] Y. Lu, D. Wang, T. Li, X. Zhao, Y. Cao, H. Yang, Y. Y. Duan, *Biomaterials* **2009**, *30*, 4143.
- [436] Y. Zhong, R. V. Bellamkonda, *Brain Res.* **2007**, *1148*, 15.
- [437] S. Zhao, P. Tseng, J. Grasman, Y. Wang, W. Li, B. Napier, B. Yavuz, Y. Chen, L. Howell, J. Rincon, F. G. Omenetto, D. L. Kaplan, *Adv. Mater.* **2018**, *30*, e1800598.
- [438] L. Han, X. Lu, M. Wang, D. Gan, W. Deng, K. Wang, L. Fang, K. Liu, C. W. Chan, Y. Tang, L. T. Weng, H. Yuan, *Small* **2017**, *13*, 1601916.
- [439] N. Annabi, S. R. Shin, A. Tamayol, M. Miscuglio, M. A. Bakooshli, A. Assmann, P. Mostafalu, J. Y. Sun, S. Mithieux, L. Cheung, X. Tang, A. S. Weiss, A. Khademhosseini, *Adv. Mater.* **2016**, *28*, 40.
- [440] S. Ahadian, J. Ramón-Azcón, M. Estili, X. Liang, S. Ostrovidov, H. Shiku, M. Ramalingam, K. Nakajima, Y. Sakka, H. Bae, T. Matsue, A. Khademhosseini, *Sci. Rep.* **2014**, *4*, 4271.
- [441] S. R. Shin, S. M. Jung, M. Zalabany, K. Kim, P. Zorlutuna, S. B. Kim, M. Nikkhah, M. Khabiry, M. Azize, J. Kong, K. T. Wan, T. Palacios, M. R. Dokmeci, H. Bae, X. Tang, A. Khademhosseini, *ACS Nano* **2013**, *7*, 2369.
- [442] T. Dvir, B. P. Timko, M. D. Brigham, S. R. Naik, S. S. Karajanagi, O. Levy, H. Jin, K. K. Parker, R. Langer, D. S. Kohane, *Nat. Nanotechnol.* **2011**, *6*, 720.
- [443] J. Hur, K. Im, S. W. Kim, J. Kim, D. Y. Chung, T. H. Kim, K. H. Jo, J. H. Hahn, Z. Bao, S. Hwang, N. Park, *ACS Nano* **2014**, *8*, 10066.
- [444] H. Ding, M. Zhong, Y. J. Kim, P. Pholpabu, A. Balasubramanian, C. M. Hui, H. He, H. Yang, K. Matyjaszewski, C. J. Bettinger, *ACS Nano* **2014**, *8*, 4348.
- [445] S. Yang, L. Jang, S. Kim, J. Yang, K. Yang, S. W. Cho, J. Y. Lee, *Macromol. Biosci.* **2016**, *16*, 1653.
- [446] Y. Shi, C. Ma, L. Peng, G. Yu, *Adv. Funct. Mater.* **2015**, *25*, 1219.
- [447] J. Duan, X. Liang, J. Guo, K. Zhu, L. Zhang, *Adv. Mater.* **2016**, *28*, 8037.
- [448] G. P. Hao, F. Hippauf, M. Oschatz, F. M. Wisser, A. Leifert, W. Nickel, N. Mohamed-Noriega, Z. Zheng, S. Kaskel, *ACS Nano* **2014**, *8*, 7138.
- [449] T. Dai, X. Qing, Y. Lu, Y. Xia, *Polymer* **2009**, *50*, 5236.
- [450] T. Dai, X. Qing, H. Zhou, C. Shen, J. Wang, Y. Lu, *Synth. Met.* **2010**, *160*, 791.
- [451] S. Ghosh, O. Inganäs, *Adv. Mater.* **1999**, *11*, 1214.
- [452] V. R. Feig, H. Tran, M. Lee, Z. Bao, *Nat. Commun.* **2018**, *9*, 2740.
- [453] Y. Xu, X. Yang, A. K. Thomas, P. A. Patsis, T. Kurth, M. Kräter, K. Eckert, M. Bornhäuser, Y. Zhang, *ACS Appl. Mater. Interfaces* **2018**, *10*, 14418.
- [454] B. Yao, H. Wang, Q. Zhou, M. Wu, M. Zhang, C. Li, G. Shi, *Adv. Mater.* **2017**, *29*, 1700974.
- [455] Y. Lu, W. He, T. Cao, H. Guo, Y. Zhang, Q. Li, Z. Shao, Y. Cui, X. Zhang, *Sci. Rep.* **2014**, *4*, 5792.
- [456] Y. Wang, Y. Shi, L. Pan, Y. Ding, Y. Zhao, Y. Li, Y. Shi, G. Yu, *Nano Lett.* **2015**, *15*, 7736.
- [457] D. Mawad, E. Stewart, D. L. Officer, T. Romeo, P. Wagner, K. Wagner, G. G. Wallace, *Adv. Funct. Mater.* **2012**, *22*, 2692.
- [458] L. Pan, G. Yu, D. Zhai, H. R. Lee, W. Zhao, N. Liu, H. Wang, B. C.-K. Tee, Y. Shi, Y. Cui, Z. Bao, *Proc. Natl. Acad. Sci. USA* **2012**, *109*, 9287.
- [459] Y. Liu, J. Liu, S. Chen, T. Lei, Y. Kim, S. Niu, H. Wang, X. Wang, A. M. Foudeh, J. B.-H. Tok, Z. Bao, *Nat. Biomed. Eng.* **2019**, *3*, 58.
- [460] Y. Liu, A. F. McGuire, H.-Y. Lou, T. L. Li, J. B.-H. Tok, B. Cui, Z. Bao, *Proc. Natl. Acad. Sci. USA* **2018**, *115*, 11718.
- [461] P. Maiolino, M. Maggiali, G. Cannata, G. Metta, L. Natale, *IEEE Sens. J.* **2013**, *13*, 3910.
- [462] N. Wettels, V. J. Santos, R. S. Johansson, G. E. Loeb, *Adv. Rob.* **2008**, *22*, 829.
- [463] R. Koiva, M. Zenker, C. Schurmann, R. Haschke, H. J. Ritter, in *2013 IEEE/ASME Int. Conf. on Advanced Intelligent Mechatronics (AIM): Mechatronics for Human Wellbeing*, IEEE, Piscataway, NJ **2013**, pp. 1084–1089.
- [464] P. Mittendorfer, E. Yoshida, G. Cheng, *Adv. Robotics* **2015**, *29*, 51.